Development Of Flap Rudder System For Large Container Vessels

Akhil Karthika Ajith

Master Thesis

presented in partial fulfillment
of the requirements for the double degree:
“Advanced Master in Naval Architecture” conferred by University of Liege
"Master of Sciences in Applied Mechanics, specialization in Hydrodynamics, Energetics and Propulsion” conferred by Ecole Centrale de Nantes

developed at University of Rostock , Rostock
in the framework of the

“EMSHIP”
Erasmus Mundus Master Course
in “Integrated Advanced Ship Design”

EMJMD 159652 – Grant Agreement 2015-1687

Supervisor: Prof. Dr. Nikolai Kornev, University of Rostock, Rostock
Mr. Steve Leonard, IBMV Maritime Innovationsgesellschaft mbH

Reviewer: Jean-Baptiste Souppez, Southampton Solent University

Rostock, February 2018

DECLARATION OF AUTHORSHIP

I, Akhil Karthika Ajith

declare that this thesis and the work presented in it are my own and has been generated by me as the result of my own original research.

Development of Flap Rudder system for Large container vessels

I confirm that:

1. This work was done wholly or mainly while in candidature for a research degree at this University;

2. Where any part of this thesis has previously been submitted for a degree or any other qualification at this University or any other institution, this has been clearly stated;

3. Where I have consulted the published work of others, this is always clearly attributed;

4. Where I have quoted from the work of others, the source is always given. With the exception of such quotations, this thesis is entirely my own work;

5. I have acknowledged all main sources of help;

6. Where the thesis is based on work done by myself jointly with others, I have made clear exactly what was done by others and what I have contributed myself;

7. Either none of this work has been published before submission, or parts of this work have been published as:

8. I cede copyright of the thesis in favour of the University of Rostock;

Signed: …….....

Date: ……

CONTENTS

1. INTRODUCTION 11
1.1 Preface 11
1.2 Introduction to the Project 12
1.3 Aim and objective 13
2.THEORATICAL BACKGROUND 15
2.1 Rudder Design Criteria 15
2.2 Rudder Parameters 16
2.3 Flapped Rudders 23
2.4 Rudder Performance Prediction 24
2.5 Computation Fluid Mechanics 24
2.6 Turbulence and Turbulence Modelling 26
2.7 Boundary condition 30
2.8 Grid generation 31
3. TWO–DIMENSIONAL CFD ANALYSIS 33
3.1 Introduction 33
3.2 Flap Angle Mechanism 33
3.3 Inflow Angle Calculation 35
3.4 Pre Settings 37
3.5 Mesh Settings 38
3.6 Two Dimensional Analysis Result 41
3.7 Summary of Two Dimensional CFD Study 44
4.WAKE CALCULATION 46
5 THREE DIMENSIONAL CFD ANALYSIS 50
4.1 Introduction 50
3.2 Mesh setting 51
3, 3 Result 55
6.CONCLUSION AND RECOMMENDATIONS FOR FUTURE WORK 61
5.1 conclusion 61
5.2 Recommendation for Future Work 62
7.REFFERNCES 63
Appendix I 65
Appendix II 81

LIST OF FIGURES

Figure 1- Becker Flapped Rudder[6] 12
Figure 2-Rudder Propeller arrangement 16
Figure 3-Forces and Moments acting on rudder [14] 17
Figure 4 – Force and moment acting on rudder surface [14] 21
Figure 5-Flap Angle Mecchanism 34
Figure 6- Different flap ratios 35
Figure 7-Inflow angle calculation using actuator disc 36
Figure 8-Rudder boundary condition 38
Figure 9-Mesh convergence study 39
Figure 10 Meshed domain 40
Figure 11-section at upper side(+0.7R), rudder rotating towards port side at slow speed 41
Figure 12-section at lower side -0.7R,Rudder and flap rotating to port side at slow speed 42
Figure 13-section at lowerside -0.7R ,Rudder and flap rotating to stb side at slow speed 42
Figure 14-section at upperside +0.7 R ,rudder and flap rotating port side at cruise speed 43
Figure 15-section at lower side -0.7R ,rudder and flap rotating to port side at cruise speed . 43
Figure 16-section at lower side -0.7R ,rudder and flap rotating to stb at cruise speed 44

Figure 17 wake representation 47
Figure 18- Wake domain and model setup 48
Figure 19 - velocity and pressure distribution 48
Figure 20- wake cone volumetric source 49
Figure 21- propeller hub volumetric source 49
Figure 22- propeller hub volumetric source 49
Figure 23 – volumetric source for complete hull 49
Figure 24 - Rudder stb view 50
Figure 25- Rudder port view 50
Figure 26 - Bottom view 50
Figure 27- rudder top view 50
Figure 28 ship profile view 51
Figure 29-Ship aft view 51
Figure 30-ship forward view 51
Figure 31-Lift force comaprison for existing and optimum ratios 55
Figure 32-Drag force comparison for existing and optimum ratios 56
Figure 33- Vecter distribution of velocity at bulb 57
Figure 34-Flow seperation point at rudder bulb 57
Figure 35-top view of rudderbulb cavitation point 58
Figure 36-Lift force in different domain depth 58
Figure 37- Drag force in different domain depth 59
Figure 38- Lift force for new rudders geomtries 59
Figure 39-Drag force for new rudder geomeries 60
Figure 40-Mesh arrangment for 2D calculation 66
Figure 41 – Mesh setting at Leading edge 66
Figure 42-wall y+ value of Mesh settings 66
Figure 43 –Meshs setting at Rudder gap 67
Figure 44-Mesh setting at Rudder Flap 67
Figure 45- Volumeric sources used in flap and leading edge 67
Figure 46-vector distribution at 0 deg (k epsilon turbulent model) 68
Figure 47- vector distribution at 0 deg(k –omega turbulent model) 68
Figure 48- vector distribution at 0 deg (RST turbulent model) 68
Figure 49- vector distribution at 0 deg(spalart allmars turbulent model) 68
Figure 50- k epsilon turbulent model (vector disribution-15 deg) 69
Figure 51- k omega turbulent model (vector disribution-15 deg) 69
Figure 52- RST turbulent Model-(vector disribution-15 deg) 69
Figure 53- spalart allmars turbulent model-(vector disribution-15 deg) 69
Figure 54-k epsilon turbulent model (pressure distribution-15 deg) 70
Figure 55-k omega turbulent model (pressure distribution-15 deg) 70
Figure 56-RST turbulent model (pressure distribution-15 deg) 70
Figure 57-Spalart allmars turbulence model (pressure distribution-15 deg) 70
Figure 58-k epsilon turbulence model (pressure distribution-0deg) 71
Figure 59-k omega turbulence model (pressure distribution-0deg) 71
Figure 60-RST turbulent model (pressure distribution-0deg) 71
Figure 61-spalart allmars turbulence model (pressure distribution-0deg) 71
Figure 62- Ship profile mesh 72
Figure 63- volumetric source for wake field (top view) 72
Figure 64-volumetric source for wake field (profile view) 72
Figure 65- volumetric source for Rudder 72
Figure 66- volumeric source for Rudder bulb gap 73
Figure 67- volume source for Propelelr cylinder 73
Figure 68 volumetric source for flap 73

Figure 69- volumetric source for cylinder propeller 73
Figure 70-shear stress distribution at 18 degree rudder angle with reduced flap angle (slow speed) 74
Figure 71- shear stress distribution (Rudder angle 18deg flap 22.4 deg) 76
Figure 72- shear stress distribution (18 degree ruder angle 0 deg flap angle) 77
Figure 73-symmetric rudder with bulb 78
Figure 74-Symmetric rudder without bulb 78
Figure 75-Twist blended rudder 78
Figure 76- Twist plate rudder 78
Figure 77-shear stress distribution of existing rudder with slow speed 79
Figure 78-Shear stress distribution for newly developed symmetrical rudder (rotating toward port side–slow speed) 80
Figure 79-Turbulence models comparison 92

LIST OF TABLES

Table 1-Rudder Angle & Flap Angle combinatios 34
Table 2-Virtual Disc Details & Distributions 36
Table 3 Inflow angle calculation at 8 & 23 knot 37
Table 4-Point probe output -8 knot slow speed 37
Table 5-Point probe output -23knot cruise speed 37
Table 6- Defnition of the boundaries 7 38
Table 8-convergence study 38
Table 9-Default Mesh contols 39
Table 10-Mesh setting details for wake 47
Table 11-Boundary condition details 48
Table 12-Domain dimensions 51
Table 13 –Basuc Mesh details 52
Table 14- Region mesh setting details 52
Table 15-Domain boundary layer condition 53
Table 16-ship speed vs rpm 65
Table 17- Open water characteristics of ship at full scale 65
Table 18-Flap angle calculations 81
Table 19-2D rudder performance calculation at +0.7 R section (port side with slow speed) 84
Table 20-2D rudder performance calculation at -0.7 R section (stb side with slow speed) ... 85
Table 21-2D rudder performance calculation at -0.7 R section (port side with slow speed) .. 86
Table 22-2D rudder performance calculation at +0.7 R upper section (port side with cruise speed) 87
Table 23-2D rudder performance calculation at -0.7 R lower section (port side with cruise speed) 88
Table 24-2D rudder performance calculation at +0.7 R lower section (stb side with cruise speed) 89
Table 25-Turbulnce model comparison study 90
Table 26-3D CFD result for New geometries 93
Table 27-Hull force and turning moment at different water depth and drift angles 94

ABSTRACT

Feedback from the large container ships operators repeatedly suggest that these vessel tends to have maneuvering problems where typical shipyard supplied full spade rudders are fitted. This problem especially evident during Suez Canal transits where shallow water effects are also likely to be present. Problems reported included extreme difficulty in checking vessel yaw if it start to drift off course. The fitting of a flap rudder of suitable area will improve the slow speed yaw checking ability of such vessel however the standard flap arrangement used may result in excessive flap loading for very large flap rudders. Main idea of the theses to develop the existing standard design to be more suitable for installation in these type ships.

Investigate more optimal flap angle with respect to rudder angles. The existing flap actuation mechanism result in very aggressive flap angles at relatively low rudder angles. From previous CFD work it is known that this result in rudder stall starting at the flap trailing edge which spreads rapidly forwards as the rudder angle increases. More increase of flap angle as the rudder angle rotates would alleviate this situation. This work would be performed for varying operating conditions such as slow and cruise speed maneuvering. Initial calculation to be done in two dimesional CFD Solver, so would be relatively quick to implement. Final calculation would have to be made with 3D model and propeller present. The project aim to improve the performance of the standard Becker flap rudder redesigning its flap angle and rudder angle combinations.

GLOSSARY

Becker	Becker Marine Systems
EEDI	Energy efficiency design index
MEPC	Marine Environmental Protection Committee
CAD	Computer Aided Design
CFD	Computational Fluid Dynamics
PNA	Principle of Naval Architecture
DNV-GL	GL Germanischer Llyod
IMO	International Maritime Organisation
ITTC	International Towing Tank Conference
NACA	National Advisory Committee for Aeronautic
RANS	Reynolds-Averaged Navier-Stokes

1. INTRODUCTION

1.1 Preface

Marine control surface all have great influvence and are used in wild range of marine vehicle like ships as rudders for pitch contol and manoeuvering purposes. The purpose of the rudder to maintain the ship on a particular course and direction or enable the manoeuvre condition. The fundamental concept of a movable device to steer a ship has been in use since the ships were first operated. From the time of the early Egyptian vessel onwards, side mounted steering oar over the after quater was used for the steering. Side mounted steering concept continued until the twelth centuary when there was a major change in the concept from the side-steering oar to a stern mounted rudder using hinges and pintles. Introduction of the steering wheel and various discussion regarding the rudder operation are the main contribution of that time . Hutchinson[1] reports on discussion on maximum rudder operation, it was recommended that rule be prepare to limit rudder angle to 33°. Even after of so many years of discussions on maximum rudder angle remain ongoing. A cosiderabile amount of study was carried out on rudder and steering during the nineteenth centuary. Joessel[2] and Lumley[3] introduce notabile development in that era. Joessel carried out experiment on the plate rudder in the Loire river in 1873 and formulate emperical relationships for the torque on rectangular plates. In 1864 Lumely propsed concept of flapped rudders, that concept still exist where high lift forces are required to be developed. When reached twentieth centuary find a remarkabile increased in investigation into rudder performance prediction, major work include Denny[4], Bottomley[5]and others, specially with the invention of new propulsion system and the use of twin screws.

Now we reached twenty first centuary, with changing ship types, size and the speed and introduction of new rudder types also, and its the time to continuously review and update the design of the rudders. There is a growing interest in fuel efficiency of ships & water transportation sector because of high fuel price in the previous years, climate change and energy security issues. This is lead to a regulation governing the design efficiency of new ships called the Energy Efficiency Design Index (EEDI). The Marine Environmental Protection Committee (MEPC) of International Maritime Organization (IMO) currently set an initial bench mark for the same and currently engaged in a review of the 2020 target. Rudder and other devices are critically important in achieving fuel efficiency & controllability goal. So Rudder get a greatest attention in innovative maneuvering solutions.

1.2 Introduction to the Project

Becker Flap Rudder is one of the popular rudder type produce high lift force even at small angle of incidence due to the introduction of effective camber by the flap. Ship with large requirement of maneuverability and ships operators those who want to reduce fuel consumption normally prefer Becker Flap rudder (see figure 1).

Figure 1- Becker Flapped Rudder[6]

Feedback from the large container ships operators repeatedly suggest that these vessel tends to have slow speed maneuvering problems where typical shipyard supplied full spade rudders are fitted. This problem especially evident during Suez Canal transits where shallow water effects are also likely to be present. Problems reported included extreme difficulty in checking vessel yaw if it start to drift off course. The fitting of a flap rudder of suitable area will improve the slow speed yaw checking ability of such vessel however the standard flap arrangement used may result in excessive flap loading for very large flap rudders .

First systematic free-stream tests of flapped rudders were conducted 1968 by Kato and Motora [7] and 1972 by Kerwin *et al.* [8] in water, and Lutz *et al* [9] and more recently by Williamson [10] in wind tunnels. All of the tests were conducted at low Reynolds Numbers (Re) (apart from Lutz) and by using NACA profiles or similar section types. These profiles are however not suitable for high-lift rudders.

Since the advent of reliable numerical performance prediction of lifting surfaces with computational fluid dynamics (CFD), numerous studies have been carried out to predict the maneuverability performance of these rudders. CFD studies are cheaps compared to wind tunnel facility considering the number of trials. Date [11] tested high performance rudders in steady and periodic flow using systematic CFD studies. Some

years before Date, Chau [12] performed numerical free-stream rudder tests with different NACA section forms. Main idea of the theses to develop the existing standard design to be more suitable for installation in these type ships.

1.3 Aim and objective

IBMV is the sister company of Becker marine system founded in 1993 at Rostock, Germany. Main scope of work includes Hydrodynamics product development and optimization, act as a sales support of becker marine products and research & development wing of Becker marine system too. Mr. Willi Becker establish the Becker marine system in1946, Becker marine system has developed into a company known worldwide for its iterative ship maneuvering solutions as well as energy saving devices. With the innovation of Becker flap rudder, market leadership for high performance rudder was already reached the hights in the 1960s. As the technology leader, Becker is the standard for maneuvering solutions. Twisted rudders, spade rudder, maintenance free rudders and rudder bulb solution have been developed by Becker.

CFD is the use of computational techniques to solve numerically the equations defining fluid flow within and between bodies. Historically, the orgin of our ability to mathematically explain the detail flow around moving object such as ships came through the work of such legend as Newton, Eulers, Laplace, Navier and Stokes. Late 1950s progressively more complex theoretical method have been developed to analyse the performance of control surfaces and rudders. During the period of 1980-90 most of the comercial and Accadamic CFD codes are orginated. The equations solved in CFD solver are numerical approximations to mathematical model describing the physics of fluid flow. Therefore, always exists an inherant level of approximation to reality. When solve a flow around a rudder cause a small error in side force and steering torque due to the viscous effect and the accuracy level of physical model. For large ships, rudder drag is typically 2-3% of total resistance so accurate prediction of rudder drag is less importance. Main idea of the thesis to develop the existing standard design to be more suitable for operating in suez canal. To achive this goal Starccm+ Comercial CFD code was used, Main objective of studies includes the followings.

1. Investigate more optimal flap angle with respect to rudder angles. The existing flap actuation mechanism result in very aggressive flap angles at relatively low rudder angles. From previous CFD work it is known that this result in rudder stall starting at the flap trailing edge which spreads rapidly forwards as the rudder angle increases. More increase of flap angle as the rudder

angle rotates would alleviate this situation. This work would be performed for varying operating conditions such as slow and cruise speed maneuvering. Initial calculation to be done in Two Dimensional CFD Solver, so would be relatively quick to implement. Final calculation would have to be made with Three Dimensional model and propeller present.

2. Once the best flap ratios is known, the balance ratio of the rudder would be checked to minimize the maximum steering torque of the complete rudder. This CFD analysis would have to done with Three dimesional CFD model and propeller disc(actuator disc).

3. Investigate the existing problem when the container ship operated in suez canal operation and find technical solution to improve the maneuvering operation.

2.THEORATICAL BACKGROUND

2.1 Rudder Design Criteria

The rudder serves the twofold function of stabilizing a straight motion by fin effect and controlling the ship in steering and maneuvering. Rudder and other controlling devices are critically important features in achieving vessel controllability goal. Accordingly, the rudder receives the greatest attention in the section. At the concept design stage, the naval architect take the basis decision of a reasonable shaped rudder of the size and type commonly seen for ships of the anticipated class and service. During the initial design development of the hull form, decisions made regarding the shape of the underbody, shape of the section, distribution buoyancy, underwater profile. Propeller, rudder and thruster size and location can then be defined. All these item affect the controllability of the ship and are coupled to the hull underwater parameters towards the end of the preliminary design stage, the rudder stock location should be evaluate to see whether structure supports can be provided and whether steering gear can be arranged as normal in past practice ,otherwise special arrangement to be considered. From the focus of hydrodynamic point of view, the basis assumption of rudder design are summarized as follow.

(a) Type of rudder : All movable rudders are desirable for their ability to produce large turning forces for their size. selecting balance ratio according to block coefficient, Structural considerations, cost, the need for additional stabilizing side force provided by the horn, and the considerations may requires use of other type rudders.

(b) Location : The stern rudder are more effective than the bow rudder for maneuvering ahead. The main reason for this difference in effectiveness is the direction of drift angle, which makes a substantial contribution to the turning of the ship when rudder is located at the stern.

(c) Area : A suitable rudder area for a give hull form can be selected to satisfy desirable degrees of dynamic stability and maneuvering performance in calm water. The rudder area should reflect the fact that relatively large rudder provide superior performance under adverse conditions of wind and wave. The rudder area to be calculated and verified during the initial ship arrangement study (PNA). Det norke Veritas (DNV–GL) value for minimum rudder area are given below,

$$AR=\frac{T\times LBP}{100}\left[1+25\left(\frac{B}{LBP}\right)^2\right] \quad (1)$$

Where AR = Area of rudder

T = Draft

LBP = Length between perpendiculars

B = Beam

The formula applied only to rudder arrangement in which the rudder located directly behind the propeller.

(d) Height: Rudder height is generally limited by the stern shape and draft, rudder height to be increased as much as possible to get more efficient aspect ratios. The bottom of the rudder is arrange above the bottom of the keel for protection, more clearance in case where there is continuous operation with trim by the stern.

(e) Section shape : Thick streamlined sections are desirable due to these section have a relatively constant pressure. Structure point of view thick structure give more rigidity to rudder but they offer reasonable drag characteristics.

(f) Rate of swing: Size and the hydrodynamics efficiency of the rudder design based on the rate of swing also. The effect of an increased over the 2 1/3 deg/sec standard rate is high on fast and responsive vessels.

These parameters to be used to improve the controllability of the normal vessel.

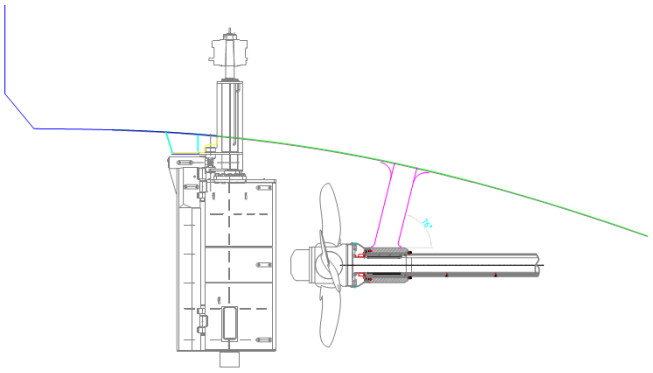

Figure 2-Rudder Propeller arrangement

2.2 Rudder Parameters

Rudders either cover the slipstream of the propeller of merchant vessels or facing the slower fluid stream close to the hull of a sailing boat. Most of the ships have the rudder positioned astern, either directly at the transom or behind the propeller shaft under stern of the ship. In both cases they are supposed to produce a force perpendicular to the longitudinal axis (mostly the symmetry axis or x-axis, defined in Figure 3). Since the centre of buoyancy of the ship is closer to amidships, forces generated at the rudder initiate a moment on the ship. This

moment is known as the turning moment. The stronger the force produced by the rudder the faster the ship can turn. This force is called lift or more correctly side force. In adition to the lift the rudder produces drag as an augment of the ship resistance. The effectiveness of the rudder is directly related to these forces. Both lift and drag are transferred by the rudder stock from the rudder to the ship structure. The stock is connected to a steering gear and bearings, which absorb the forces and dissipate them to the ship structure. The rudder stock has to withstand the bending moments produced by the rudder forces and the torque, which will be determined by the distance from the stock axis to the centre of pressure of the rudder. In the following the forces and moments will be explained in detail. The theory of the force generation from lifting surfaces is outlined in numerous fluid text books and is assumed to be given. A detailed explanation can be found from Milne-Thomson [13]

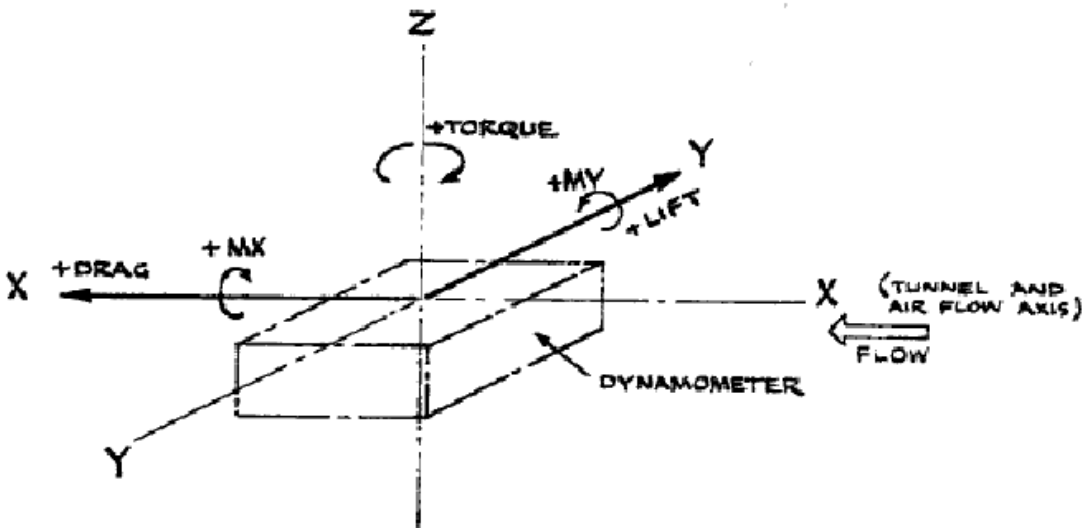

Figure 3-Forces and Moments acting on rudder [14]

2.2.1Lift

The lift arises from the centre of pressure of the rudder and is pointing in the direction perpendicular to the free stream direction. Symmetrical rudders have an idealised lift force of zero at zero rudder angle. With raising rudder angle the lift will increase until the flow around the rudder surface separates and the lift decreases over a certain level. The International Towing Tank Conference presented a standardisation to define forces and moments produced from lifting surfaces [15]. In there the rudder force parameters are normally expressed as non-dimensional parameters. This has the advantage to compare and validate the parameters from different ships or rudders better with each other. The non-dimensional lift acting on a rudder with finite span, e.g. a three-dimensional rudder

(known as wing in a lot of textbooks), is presented in Equation 2. The non-dimensional forces acting on a two-dimensional object, e.g. on a wing with infinite span, are normally presented by small letters. The non-dimensional lift in the two-dimensional domain, e.g. a rudder with infinite span (aerofoil), is shown in Equation 3.

$$C_L = \frac{L}{\frac{1}{2}\rho A_R U_\alpha^2} \quad (2)$$

$$C_l = \frac{l}{\frac{1}{2}\boldsymbol{\rho c} U_\alpha^2} \quad (3)$$

U_α is the free stream velocity, ρ is the density of the fluid, AR is the rudder plan area (bc) and α is the rudder incidence angle. L and l are the three-dimensional and two dimensional lift respectively acting on the rudder section and c denotes the chord of the rudder with infinite span.

2.2.2Rudder Drag

Compared to the lift, the drag force is in most cases undesired because it mainly increases the ship resistance. For merchant vessels the rudder accounts for roughly 5% of the total ship resistance. That is why this force indicates the efficiency of rudder. The drag, which is acting parallel to the free stream velocity U_α (y-axis), can be divided into partial drag components. The overall non-dimensional drag coefficient generated by the rudder can be expressed as in Equation 4 and 5 for the three dimensional (C_D) and two dimensional rudder (c_d) respectively.

$$C_D = \frac{D}{\frac{1}{2}\rho A_R U_\alpha^2} \quad (4)$$

$$C_d = \frac{d}{\frac{1}{2}\rho c U_\alpha^2} \quad (5)$$

where D and d are the three-dimensional dimensional and two-dimensional drag respectively.

The two-dimensional drag consists of the viscous pressure drag and the skin friction drag. Frictional drag results from viscous shearing stresses acting on the surface of the rudder body within the surface boundary layer during the movement of the rudder in the fluid. The

viscous shear stress (τ_w), in Equation 6, is governed by the viscosity of the fluid (μ) and the shear velocity ($\partial u/\partial y$) in the direction perpendicular to the surface of the body.

$$\tau_W = \mu \frac{\partial U}{\partial Y} \quad \textbf{(6)}$$

The non-dimensional two and three-dimensional skin friction drags are shown in Equation 7 and 8

$$C_F = \frac{\tau_W}{\frac{1}{2}\rho A_R U_\alpha^2} \quad \textbf{(7)}$$

$$C_f = \frac{\tau_w}{\frac{1}{2}\rho c U_\alpha^2} \quad \textbf{(8)}$$

Viscous pressure drag results due to the distortion of the fluid flow around the curved rudder surface and flow separation at the surface wall. Sometimes the pressure drag is also known as form drag because it depends on the shape or form of the body. Pressure drag arises from the pressure distribution around the rudder surface, where the local pressure is higher or lower than the ambient pressure. The viscous pressure drag coefficients, for both the three-dimensional and two-dimensional rudder, are given in Equation 9 and 10.

$$C_{VP} = \frac{D_{VP}}{\frac{1}{2}\rho A_R U_\alpha^2} \quad \textbf{(9)}$$

$$C_{vp} = \frac{d_{vp}}{\frac{1}{2}\rho c U_\alpha^2} \quad \textbf{(10)}$$

where D_{VP} is the three-dimensional viscous pressure force and d_{vp} the two-dimensional viscous pressure force. Three-dimensional rudders operating at an angle of incidence experience another drag component: the induced drag, which is also known as vortex drag or lift-induce drag. This drag parameter is defined as:

$$C_{ID} = \frac{D_I}{\frac{1}{2}\rho A_R U_\alpha^2} \quad \textbf{(11)}$$

where D_I is the three-dimensional induced drag force.

The fluid flow around a rudder body at an angle of attack produces a high pressure (pressure side) and a low pressure side (suction side). The pressure difference on both sides

causes the fluid to flow from the pressure side, around the rudder tip and root, towards the suction side. This spanwise flow of the three-dimensional rudder combines with the standard chordwise flow and results in a speed and direction change of the fluid flow. The flow starts to twist and produces vortices along the rudder tip, root and trailing edge which induces downwash behind the trailing edge due to the change of speed and the redirection of the flow downwards. This downwash results in an angular deflection and decreases the generated lift of the rudder compared to rudder section with the same angle of attack. The additional induced drag is equal to the product of the lift coefficient and the angle through which it is deflected. The angle deflection (ε) is defined as follows:

$$\varepsilon = \frac{C_L}{\pi AR} \tag{12}$$

Where AR is the aspect ratio of the rudder. Therefore the induced drag can be calculated from:

$$C_{ID} = \frac{C_L^2}{\pi AR} \tag{13}$$

The induced drag makes its possibile to calculate the total drag experienced by the rudder out of the two dimensional drag result.

$$C_D = c_d + k_i \frac{C_L^2}{\pi AR} \tag{14}$$

where k_i is rudder span efficiency factor and can be assumed to be 0.35-0.37 [14]. Knowing the lift curve slope (αi-2D) of the two-dimensional section (Equation 15), the lift coefficient of the three-dimensional rudder can be extrapolated (Equation 16) out of the two-dimensional results. That means that the rudder section generates lift corresponding to the generated lift of the rudder section of infinite span at an angle of incidence (α-ε).

$$\alpha_{i-2D} = \frac{dc_l}{da} \tag{15}$$

$$\mathrm{C_L} = \alpha_{\mathrm{i-2D}}(\alpha - \varepsilon) = \alpha_{\mathrm{i-2D}}\left(\alpha - \frac{57.3\mathrm{C_L}}{\pi \mathrm{AR}}\right) \tag{16}$$

$$\alpha_{i-3D} = \frac{dC_L}{d\alpha} = \frac{\alpha_{i-2D}}{\left(1 + \left(\frac{57.3\alpha_{i-2D}}{\pi AR}\right)\right)} \tag{17}$$

2.2.3 Resultant and normal force and moment

The total force on the rudder is called the resultant force, which can be calculated by adding the drag and lift force vectorially (see Equation 18). The normal force is acting perpendicular to symmetry axis of the ship and is important to estimate the turning moment produced by the rudder. Equation 18 and 21 give the definition of the normal force of the three-dimensional and two-dimensional rudder respectively. All forces can be found in Figure 4.

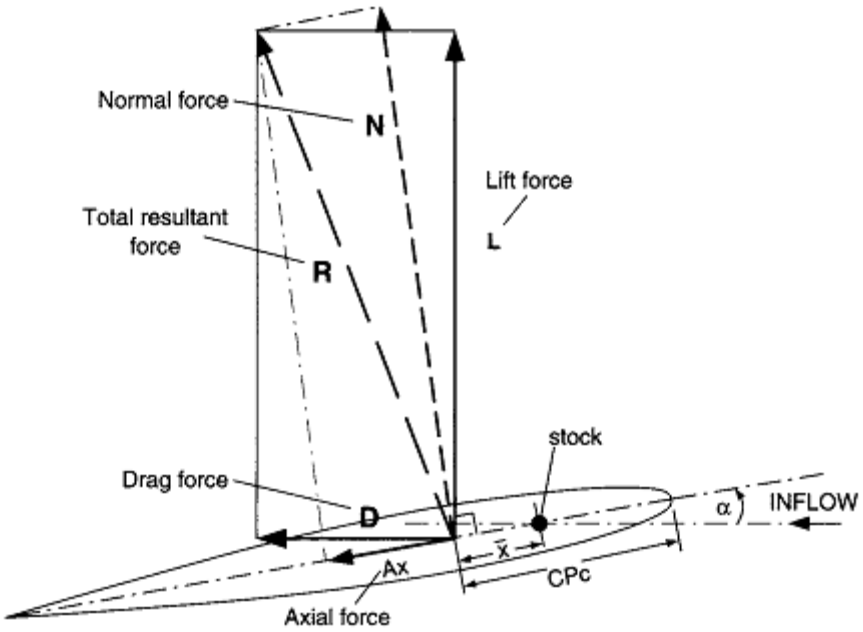

Figure 4 – Force and moment acting on rudder surface [14]

$$C_R = \sqrt{C_L^2 + C_D^2} \tag{18}$$

$$C_N = C_L Cos\,(\alpha) + C_D Sin(\alpha \tag{19}$$

$$c_r = \sqrt{c_l^2 + c_d^2} \tag{20}$$

$$c_n = c_l cos\,(\alpha) + c_d cos(\alpha) \tag{21}$$

The rudder moments are the moments generated by the forces on the rudder acting on the centre of pressure. The most important moment is the rudder torque about the rudder stock. The value of the torque normally defines the strength and the size of the stock.

Classification societies, e.g. DNV-GL[16] Section 14 B, proposed empirical formulae to estimate the rudder torque to ensure suitable stock design parameters in the early design stages. The moment about the symmetry axis, the x-axis, and the moment about the axis perpendicular to the symmetry axis, the y-axis, are completing the rudder moments. The non-dimensional moments for the three-dimensional rudder are shown in Equation 22 to 24.

$$C_{MZ} = \frac{M_Z}{\frac{1}{2}\rho A_R U_\alpha^2 c} \quad (22)$$

$$C_{MX} = \frac{M_X}{\frac{1}{2}\rho A_R U_\alpha^2 s} \quad (23)$$

$$C_{MY} = \frac{M_Y}{\frac{1}{2}\rho A_R U_\alpha^2 s} \quad (24)$$

where M_z, M_x and M_y are the three-dimensional moments about the stock axis, the x-axis and the y-axis respectively.

Equation 25 defines the spanwise moment (M_N) normal to the rudder body.

$$M_N = M_X cos\,(\alpha) + M_y sin(\alpha) \quad (25)$$

2.2.4 pressure and pressure coefficient

The centre of pressure is defined by the pressure distribution around the rudder section and rudder body. As described earlier is the determination of the centre of pressure important for the design of the rudder. The longitudinal centre of pressure parallel to the symmetry axis of the rudder is known as the chordwise centre of pressure (CPc) and the horizontal centre of pressure between the root and the tip of the rudder is the spanwise centre of pressure (CPs). The spanwise centre of pressure of three-dimensional rudders is defined at half of the span when the rudder section doesn't change from the root to the tip and the inflow is condition is the same at every point along the span. Otherwise both the chordwise and the spanwise centre of pressure will move slightly towards the leading edge or trailing edge and to the tip or root respectively at every angle of attack. Knowing

the distance of the rudder stock to the leading edge (W) and the distance from the rudder root to the measurement point of the rudder moments (R) both centre of pressures can be calculated [17]:

$$CP_C = \left(\frac{(M_Z)}{N} + w\right)\frac{100}{c} \quad (26)$$

$$CP_S = \left(\frac{M_N}{L} - R\right)\frac{100}{s} \quad (27)$$

The non-dimensional pressure around the rudder is shown in Equation 28.

$$C_P = \frac{P - P_0}{\frac{1}{2}\rho U_\alpha^2} \quad (28)$$

where p is the local pressure and p_0 is the ambient pressure at a point far upstream of the rudder.

2.3 Flapped Rudders

Flapped control surface, effectively work as a variable camber devices, can produce a significant amount of lift. Due to the efficient facility to produce high lift, they tend to use in the situation of lesser space, such as fin stabilizer, or for rudder to require to produce high manoeuvring. In 1862 Lumley [3] develop the concept of flap rudder for merchant and war ship. Lumley refer to the flap as the tail due to the symmetry to a fish.

Depending on the rudder size and the expected forces the flap is usually connected over two or three hinges with the main rudder part. The flap angle is varied due to a geometrical relationship. On the top of the flap a sliding piston, moving in a housing structure of the flap, is connected with a pivot to the rudder trunk which in turn accommodates the rudder stock. If the angle of the main rudder is varied over the stock the flap angle will be varied automatically. Compared to the standard NACA profiles the flapped rudders have their balance point, pivot point, further towards 50% chord, normally at 45% to 47% chord. Due to the position of the flapped rudder behind the propeller the rudder can cover a bigger area of the propeller race at higher angles of attack with this balance point. Hence the rudder body uses more accelerated flow from the propeller instead of the slower flow around the propeller slipstream. The moved balance point mainly governs the rudder design because at this point the rudder has to provide enough space to accommodate the rudder stock. Hence the thickest location of the rudder is at

the balance point. Based on Kato et al. [7] most flapped rudders have flap ratio of 25% and a flap angle to rudder angle ratio of two to achieve the best performance.

The flap design depends either on the main rudder design or on the designer's choice. Usually the flap will be formed out of straight plates to ease the construction and the manufacturing. The continuation of the main rudder contour shape is often very complicated because of the slender trailing edge form and the small change in curvature in the flap contour. Therefore the flap contour will mostly be simplified as a straight contour rather than curved. Flap rudders are very vulnarabile to damage and corossion due to the exposed operation of flap actuation mechanism. Due to the height request of manoeuvering performance , the flap mechanism is exposed to floating object and sand which causes erosion on the hinge parts.

2.4 Rudder Performance Prediction

Rudder test in water at different rudder angle and flap angle are difficult and rare in case. The empirical formula of the classification societies are rough order and specified only for well-known rudder type. Kato and Motora [7] present one of the first systematic set of open water test on flapped rudders. The rudder had NACA0020 section with effective aspect ratio of 2.0. The test were carried out in a reciprocating water channel at a Reynolds number of about $0.125*10^6$. Flap chord /total chord ratio C_f/C_i of 0.25 and 0.50 and 0.165 were tested and the lift and moment on the main rudder and flap were measured. It is concluded that rudder with flap ratio of 0.25 and flap angle /rudder angle ratio, β/α of 2, when the lift is almost doubled. Kerwin et al [8] carried out free stream test on a series of twelve flapped rudders in a water tunnel. Flap chord / total chord ratios of 0.2, 0.3, 0.4, 0.5, and 0.6.

Now day's wind tunnel and numerical prediction method are used for the rudder performance prediction. Numerical predictions concepts are explain below sections.

2.5 Computation Fluid Mechanics

CFD is the use of computational techniques to solve the numerical equations defining fluid flow around, within the body. As explained in introduction, the equations solved are numerical approximations to mathematical model describing the physics behind the fluid flow. A hierarchy of four CFD method are considered in order of increasing complexity are given below:

- Lifting line method,
- Surface panel or boundary element method ,

- Reynolds –averaged Navier-stokes method and
- Large Eddy simulation (LES) and Direct Numerical simulation (DNS) method.

First three method commonly used for the rudder and control surface design and all method vary complexity level. But now days LES and DNS are the most powerful computation tool to predict the performance and fluid flow behaviour, those tools requires high computational resources and required long computation time to solve the problem. The most challenging aspect of numerical analysis is to predict the interaction between a propeller and rudder as well as the secondary effect of hull and free surface.

Navier –Stokes method

Last few years before only start the rudder performance and flow prediction with the help of Navier stokes equation. The main reason for the delay was the limited availability of sufficient computational power and define the 3-D computation mesh around the rudder and a sufficiently large around the domain. The development of finite volume method, used by the most of the commercial and research flow solvers. The resulting equation express the exact conservation of the present flow properties within the control volume. The relationship between physical conservation and the governing equations forms one of the main significance of the finite volume method.

RANS equation

Complete Navier –Stokes equation govern both laminar and turbulent flow they are not suitable for the direct computation of turbulent flows. A complete time dependent solution of the exact Navier-Stokes equations for high –Reynolds number flows in complex geometries is always difficult to solve. Two alternative method to solve the problem like to transform the Navier –Stokes equation in such way that the small-scale turbulent fluctuation do not have to be directly stimulated; Reynolds averaging and filtering. By adding extra term in the governing equation that need to model represented by number of equations for all unknowns known as closures.

The Reynolds-averaged Navier stokes equations represent the transport equation for the mean flow quantities, with all the scale of the turbulence modelled. These approach of permitting a solution for the mean flow variables greatly reduce the computational task. If the flow defined as steady, the governing equations will not contain time derivative and the steady state solution provide swiftly and economically. For all the analysis of this thesis used the concept of steady state due to the time limitation. For the transient situation, since the time step will be determined by the global unsteadiness in the mean flow rather than by the turbulence. The Reynolds –averaged approach is generally used for practical engineering calculations. The method of

averaging the behaviour of turbulence was first proposed by Reynolds [18]. In this case, the flow variables are resolved into,

$$\boldsymbol{u = U + u'} \qquad \boldsymbol{v = V + v'} \qquad \boldsymbol{w = W + w'} \qquad \boldsymbol{p = P + p'} \qquad \textbf{(29)}$$

Where (u', v', w') ^{T} and p are the unsteady time varying flow about slowly varying mean flow (U, V, W) ^{T} and P. On the substitution into the complete Navier –Stokes equation, and the following time averaging, the unsteady RANS equation are obtained. The averaged form of the continuity equation is given below

$$\frac{\boldsymbol{\partial U}}{\boldsymbol{\partial X}} + \frac{\boldsymbol{\partial V}}{\boldsymbol{\partial Y}} + \frac{\boldsymbol{\partial W}}{\boldsymbol{\partial Z}} = \boldsymbol{0} \qquad \textbf{(30)}$$

The time averaged Navier stokes momentum equation are given by

$$\frac{\boldsymbol{\partial U}}{\boldsymbol{\partial t}} + \boldsymbol{U}\frac{\boldsymbol{\partial U}}{\boldsymbol{\partial x}} + \boldsymbol{V}\frac{\boldsymbol{\partial U}}{\boldsymbol{\partial y}} + \boldsymbol{W}\frac{\boldsymbol{\partial U}}{\boldsymbol{\partial z}} = \frac{\boldsymbol{-1}}{\boldsymbol{\rho}}\frac{\boldsymbol{\partial p}}{\boldsymbol{\partial z}} + \boldsymbol{v}\left(\frac{\boldsymbol{\partial^2 W}}{\boldsymbol{\partial x^2}} + \frac{\boldsymbol{\partial^2 W}}{\boldsymbol{\partial y^2}} + \frac{\boldsymbol{\partial^2 W}}{\boldsymbol{\partial z^2}}\right) - \left(\frac{\boldsymbol{\partial u'\, w'}}{\boldsymbol{\partial x}} + \frac{\boldsymbol{\partial u'\, w'}}{\boldsymbol{\partial y}}\frac{\boldsymbol{\partial u'\, w'}}{\boldsymbol{\partial z}}\right) \qquad \textbf{(31)}$$

2.6 Turbulence and Turbulence Modelling

Reynolds averaging of the complete Navier–Stokes equations gives rise to six additional independent stresses. A process of closure is required to express the stress in terms of known values. These procedure, known as the turbulence modelling. Unfortunate fact that none of the single turbulent model is universally accepted as being superior for all cases of problems. The selection of turbulent model will depend on consideration such as the physics en-compassed in the flow, the established practise for the case of problem, the level of accuracy required, and the amount of time available. A number of turbulence model developed over the years, all varying their complexity and preference to certain situations.

Turbulence models can be roughly divided into four main categories: algebraic (Zero equation), one equation, two equation and stress transport models. In below describe some of the turbulence model commonly used for industrial problems.

2.6.1The Spalart-Allmaras Model

The Spalart–Allmaras model described as one equation model that solve the modeled transport equation for the kinematic eddy viscosity. The Spalart Allmaras model was designed especially for the aerospace applications involving the wall bounded flows and gives good result for boundary layer subjected to adverse pressure gradient. Now a days these model popular in turbomachinery application too.

Spalart Allmaras model effectively a low Reynolds number model, requiring the viscous affecting region of the boundary layer to be properly resolved. This might be the best choice for relatively crude simulation on coarse meshes where accurate turbulence computation are not critical. Near wall gradient of the transported variables in the models are much smaller than the gradient of the transport variable in the other well-known models. This is might be a problem when use non layered meshes used near wall may lead to the numerical errors.

Wilcox [19] presents free shear flow spreading rate for the model. While accepting result are received for wake, mixing layer and radial jet flows, the predicted spreading rate for plane and round jet are inaccurate. Based on this experiment, Wilcox concluded that the model is not suitable for jet like shear flow regions and flow involving complex recirculating and body force(buoyancy) than two equation model force such as K-Epsilon and K- Omega or Reynolds Stress Transport.

Three variant of the model are available in the STAR-CCM+

- Standard Spalart Allmaras
- High Reynolds Number Spalart Allmaras
- Spalart Allmaras detached eddy model

Standard is a low Reynolds number model, it is applied without wall function. This model can be used with all y+ wall treatment for all simulations. High Reynold number version only suited to coarse, wall function type meshes where y+ wall above 30. If viscous damping functions adversely affect result, then this model to be selected for flow solving. This problem is likely to be present if y+ values are in the intermediate range of 10-30.

2.6.2 Standard k-ε turbulence model

The k-ε turbulence model compute the Reynold stress based on the Boussinesq [20] eddy hypothesis for Newtonian fluid, whereby the Reynold stress are related to the mean rate of deformation, turbulent kinetic energy and turbulent viscosity within the fluid domain. K Epsilon turbulence model is a two equation model that solve transport equation for the turbulent kinetic energy and the dissipation rate ε. The transport equation are of the form suggested by Jones and Launder [21], with coefficients suggested by Launder and Sharma[22] Various K-Epsilon model have been used for several decade , and its widely used in the industrial applications.

Two equation models predict an unexpectedly large growth of turbulent kinetic energy in stagnation point flows. This growth can have an adverse effect on the rest of the flow solution. The following wall treatement are availabile as appropiate to the specific K-Epsilon model:

- High Y+ Wall Treatment
- Low Y+ Wall treatment

- All Y+ wall treatment
- Two layer wall treatment
- Elliptic blending wall treatment

Low-Reynolds number and two layer approches are newly modified to use in this model for solving the viscous sublayers. The standard k-ε turbulence model perform well in variety of applications, a number of weakness associated within the standard k-ε turbulence model are outline below,

- Flow separation is poorly predicted from the surface under the action of adverse pressure gradient. The real flow much closer to separation or more separation than the computed flow.
- The turbulent kinetic energy is over predicted in region of impingement and reattachment, leading to poor prediction of boundary layer development around the leading edge of control surface especially rudders and fins.
- Flow recovery following the reattachment of a separation zone is often poorly predicted as a result of the implementation of wall function within the standard k-epsilon turbulence model.
- Prediction of highly swirling flows is poor, such as separated region of slow flow recirculating and vortex shedding.
- Unable to capture the laminar and transitional flows, when doing the performance prediction of rudder are often operating at transitional Reynolds numbers and can have up to 50% laminar flow.

2.6.3 K- Omega Turbulence models

The k-omega model is a two equation model that is an alternative to the K-Epsilon model. The transport equation that are solved are for the turbulent kinetic energy k and the specific dissipation rate ω, that is the dissipation rate per unit turbulence kinetic energy ($\omega \sim \varepsilon/k$). One dominant advantage of the k-Omega model over the K-Epsilon is its improved performance for the boundary layer under the adverse pressure gradient. This model can applied throughout the boundary layer, including the viscous dominant region, without further modification. The standard K-Omega model can be used in this mode without requiring the computation of wall distance. The standard k-omega model developed from the Wilcox k-ω model [23], which incorporates modifications for low Reynolds number effect, compressibility, and shear flow spreading. The Wilcox model always reduce the disadvantage of k –epsilon model such as free shear flow spread rates that are in close agreement with measurement for far wakes, mixing layer, and plane, round, and radial jet, and applicable to wall bounded flows and shear flows.

2.6.4 The shear-stress transport (SST) k-ωModel

A variation of the standard k-ω model called the SST K-ω model, The shear- stress transport (SST) K-ω Model was developed by Menter [24] to effectively bled the robust and accurate formulation of the k-ω in the near wall region with the free stream independence of the k-ε model in the far field. To achieve this, the k-ε model is converted into a k-ω formulations. The SST k-ω model is similar to the standard k-ω model, but need to do the following refinement.

- Turbulence model like k-w and the transformed k-ε model are both multiplied by a blending function and both model are added together. This Blending function near the wall activates the standard k-ω model, and zero away from the surface, which activate the transformed k-ε model as well.
- The SST model incorporates a damped cross diffusion derivatives terms in the ω equations.
- The modelling constants are different.
- The definition of the turbulent viscosity is modified to account for the transport of the turbulent shear flow.

SST k-ω model more accurate and reliable than the standard k-ω model for flow seperation and reatatchement prediction. Due the more convenient prediction of these model and reliability and accuracy in adverse pressure gradient flow around the rudder, these model used for all the 2D & 3D analysis of these master thesis.

2.6.5 Reynolds stress transport Models

These model commonly known as second moment closure models, solve transport equation for all component of the specific Reynolds stress tensor, $\mathbf{R=-T_t/\rho = v'v'}$. These models used to analyse the effect such as anisotropy due to strong swirling motion, streamline curvature, rapid change in strain and secondary flows in ducts. The RST model carries high computational overhead due to the additional solving of equation than K-Epsilon model (Seven equation in three dimensions solved instead of two equation of K-Epsilon model).

Comparison between above described model will explain in the chapter of two dimensional CFD analysis.

2.7 Boundary condition

Turbulence model and mesh setting didn't give the solution for the flow, to get the correct solution from the governing equation, necessary to define the initial boundary condition for the dependent variables that describe the problem to be solved. The correct choice of boundary condition leads to the correct solution of the problem. The use of unrealistic and wrong boundary condition can lead to the incorrect flow solution or solver diverge rapidly. Most frequently used linear boundary condition are, the Dirichlet (value specified) and Neumann condition (gradient of value specified) [25]. Normal boundary condition used for rudder problems are:

2.7.1 Inlet

The inlet boundary condition is a form of Dirichlet boundary condition. The dependent variable of U, V, W, K, and ε are prescribed in the boundary condition. The pressure is not set for an incompressible flows, as it is extrapolated from the downstream. Sometimes the definition of the turbulent quantity in the inlet boundary condition are quite difficult. If the computation are to be compared with the experiment data, the inlet turbulent quantities of ε and k should be set according to the measured value from the experiment.

2.7.2 Wall

The wall boundary condition requires that the velocity on the wall satisfy the no slip condition. Also the non-zero value of the ε and zero value k also lead the same situation. Wall boundary can either defined by slip or no-slip wall. The non-slip neglect the wall friction, so that the tangential component of the velocity not zero at this stationary wall. Different to slip walls no-slip walls assume a tangential wall velocity of zero, i.e. skin friction is created. The development of the boundary layer is associated with the no-slip wall. In there the fluid velocity increases gradually with the distance from the surface wall. The properties of the turbulent fluid flow within the boundary layer can be described by the non-dimensional vertical distance from the wall (Y^+).

$$Y^+ = \frac{y_p}{u}\sqrt{\frac{\tau_w}{\rho}} \qquad (32)$$

Where y_p is dimensional vertical distance from the wall ϑ is kinematic viscosity.

Flows in the region of y+ < 11.63 are taken to be laminar [14]. In there the shear stress is completely viscous. For y+ ≥ 11.63 the boundary layer flow is considered to be turbulent. The explicit value of 11.63 is the intersection of the linear profile in the laminar region and the log-region. Thumb rules recommends to choose the non-dimensional wall distance

between 30 < y+ < 500, so that the flow gradient can be resolved more accurately. This wall function is considered to be not valid in areas of stagnation, separation and reattachment.

2.7.3 Pressure outlet

Pressure outlet defines the fluid exit in the domain. The pressure is specified explicitly as a static pressure (in many cases the atmospheric pressure). This boundary should be set as far away as possible form the model in the domain. Otherwise the solution demands reverse flow across the outlet, which can cause solving problems.

2.8 Grid generation

The geometry, resolution and quality of the grid have a great influence on the numerical results. Therefore the grid generation is an important part of obtaining an accurate solution. The computational grid is defined by a finite number of cell points within the domain at which the numerical solution to the characteristic equations of flow is obtained. Commercial CFD package are offering a number of different mesh types to the user. The main difference between them is the way to connect the different elements in the domain. Structured mesh is defined by regular cell connectivity. The main advantage of this mesh is the possibility to control the density of the grid directly but this can often consume a lot of time and can be difficult. Unstructured meshes define the density on specific zones, which makes it possible to generate a fine mesh even around complicated geometries. It is characterized by the irregular connectivity of the mesh points. The third mesh type, the hybrid mesh, combines structured and unstructured mesh. All mesh types showed good performance for numerical prediction of lifting devices.

2.9 Research Metodology

As explain in introduction , the aim of th eproject was to improve the flap rudder performance from the existing becker flap rudder design. The research was divided into Two main parts: two-dimensional CFD study and the three-dimensional CFD study. Two-dimensional studies excluded three-dimensional flow effects, i.e. propeller flow, and simplify the flow problem as being free stream to allow for two-dimensional analysis. The RANS solver showed high reliability for numerical marine application and was used in combination with the commercial CFD software package of STAR-CCM+, which was provided by the ibmv rostock. The performance and the behaviour of the current Becker flapped rudder design were studied first before the flap angle was varied. Throughout the study the main focus remained on the lift and drag generation on diffrent flap and rudder angle combinations.

The design of a rudder section can be varied at numerous points to increase the ability of developing lift at a certain angle of attack. The previous researches showed that it makes sense to fix some design parameters of the section to save some valuable project time. In the following some flow and rudder parameter are defined:

- Only Becker twisted unsymmetrical rudder were investigated in this work
- Find the relationship between rudder angle and flap angle and iterate more flap angle ratios.
- Rudder performance improvement was focused on the flap & rudder angle combinations.
- The balance point was fixed at 47% of chord from the leading edge and the flap ratio was retained at 0.25
- Due to the complexity of the full scale rudder flow behind the propeller and the hull the flow was simplified to be uniform, symmetric and steady
- Flap angle was governed by the mechanical linkage system between the flap axis and the pivot point of the sliding piston
- The Rudder angle was varied between zero and a maximum of 35 degree
- Rudder performance was mainly tested in slow speed (8 knot) cruise speed (23 knot) at shallow water condition.

In the two & three-dimensional CFD study primary focused were as follows,

- Run Becker at different flap ratios and find out the flapped rudder optimum flap ratios using the two-dimension CFD solver.
- Optimum and existing flap ratios analyse and compare using the three-dimensional CFD solver
- Using three dimensional CFD solver find out the current flow problem effect in the rudder for different boundary condition like depth and inlet velocity, develop new rudder geometry for the existing operating conditions.
- Compare the results for different case study.

3. TWO–DIMENSIONAL CFD ANALYSIS

3.1 Introduction

Intial step of the master thesis is the Two Dimensional CFD analysis of becker flapped rudder flap angle ratios. To predict the flap angle mechanism need to find the operation mechanism behind the flap angle and rudder angle. After finding the different flap Angle ratios, these ratio tested using the CFD package of STAR-CCM+ with the help of Computer Aided Design (CAD) for the becker flap rudder uses throughout all analysis for this master thesis. Existing flap actuation mechanism result in very aggressive flap angles at relatively low rudder angles, from previous CFD work it is known that this result in rudder stall starting at the flap trailing edge which spreads rapidly forwards as the rudder angle increases. More increase of flap angle as the rudder angle rotates would alleviate this situation. This work would be performed for varying operating conditions such as slow and cruise speed maneuvering. This chapter is rather focused on getting positive trends in the lift and drag curves than on determining the exact separation point due to the earlier described weaknesses of RANS in estimating separated flow.

3.2 Flap Angle Mechanism

Operation phyiscs behind the Flap Actuation mechanism is different from the other patented rudder model. Rudder is roating based on the rudder stock and flap roate along with rudder with dependednt rotaion mechanism axis so Flap angle **β** is relatively depend on Rudder angle **α.** Fixed length between Rudder rotation axis and Flap rotation axis is **a ,**and distance between fixed pivot point in header box and rudder axis is **b.** Using the Trignometric laws of cosine and sins used to determin the relatuion between the rudder angle and flap angle. So Ratio between **a/b** decide the flap angle for new ratios, for the exisiting rudder a/b ratio 1.5 was used.

Different flap angle combination find using changing the a/b ratio (1.5 to 1.7) and these ratio tested using Two Dimensional analysis at different speed condition like 23 knot cruise speed and 8 knot slow speed. Different flap angle ratio combinations used for the Two Dimensional analysis are given below (detail calculation provided in APPENDIX II-Table 18).

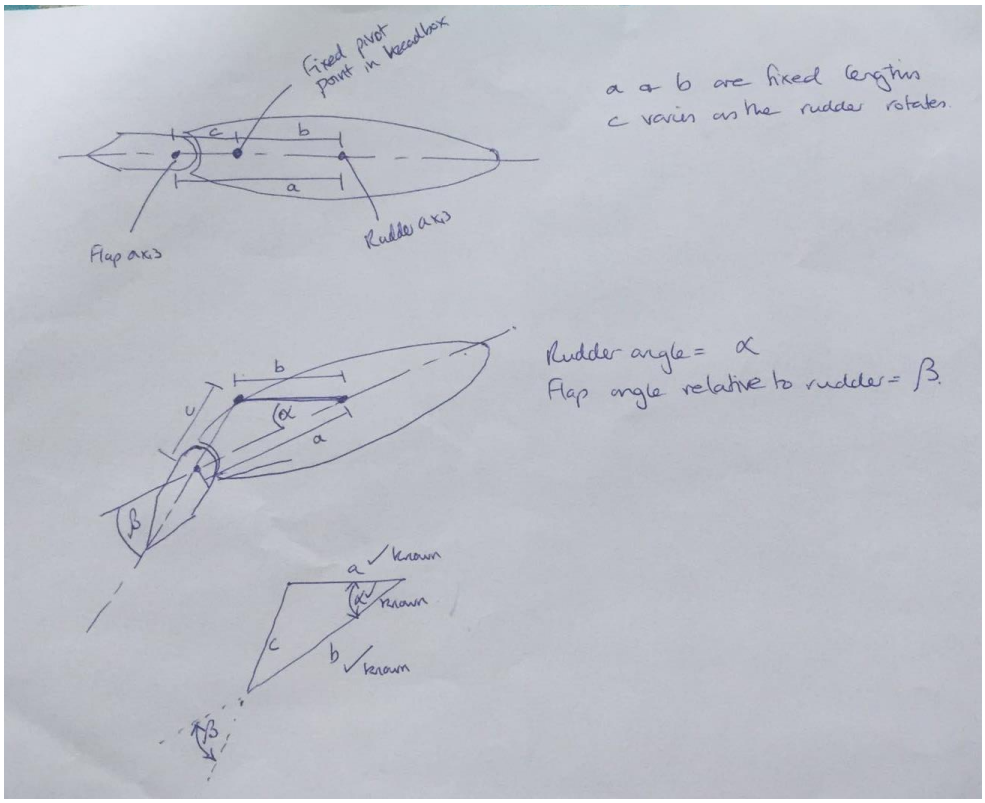

Figure 5-Flap Angle Mecchanism

Table 1-Rudder Angle & Flap Angle combinatios

existing ratio (a/b=1.5)														
Rudder Angle	**0**	2	4	6	8	10	12	14	16	18	20	22	24	26
Flap Angle (β)	**0.0**	3.99	7.90	11.68	15.27	18.63	21.72	24.55	27.10	29.38	31.40	33.18	34.74	36.10
Ratio A (a/b =1.55)														
Rudder Angle	**0.0**	2.00	4.00	6.00	8.00	10.00	12.00	14.00	16.00	18.00	20.00	22.00	24.00	26.00
Flap Angle (β)	**0.0**	3.63	7.20	10.66	13.96	17.08	19.98	22.65	25.09	27.29	29.27	31.03	32.58	33.95
Ratio B (a/b =1.6)														
Rudder Angle	**0.0**	2.00	4.00	6.00	8.00	10.00	12.00	14.00	16.00	18.00	20.00	22.00	24.00	26.00
Flap Angle (β)	**0.0**	3.33	6.60	9.79	12.86	15.76	18.49	21.02	23.34	25.46	27.38	29.11	30.65	32.01
Ratio C (a/b =1.65)														
Rudder Angle	**0.0**	2.00	4.00	6.00	8.00	10.00	12.00	14.00	16.00	18.00	20.00	22.00	24.00	26.00
Flap Angle (β)	0.0	3.07	6.10	9.06	11.91	14.63	17.20	19.59	21.81	23.85	25.71	27.40	28.91	30.27
Ratio D (a/b =1.7)														
Rudder Angle	**0.0**	2.00	4.00	6.00	8.00	10.00	12.00	14.00	16.00	18.00	20.00	22.00	24.00	26.00
Flap Angle (β)	**0.0**	2.85	5.67	8.43	11.09	13.65	16.07	18.34	20.46	22.42	24.22	25.86	27.35	28.68

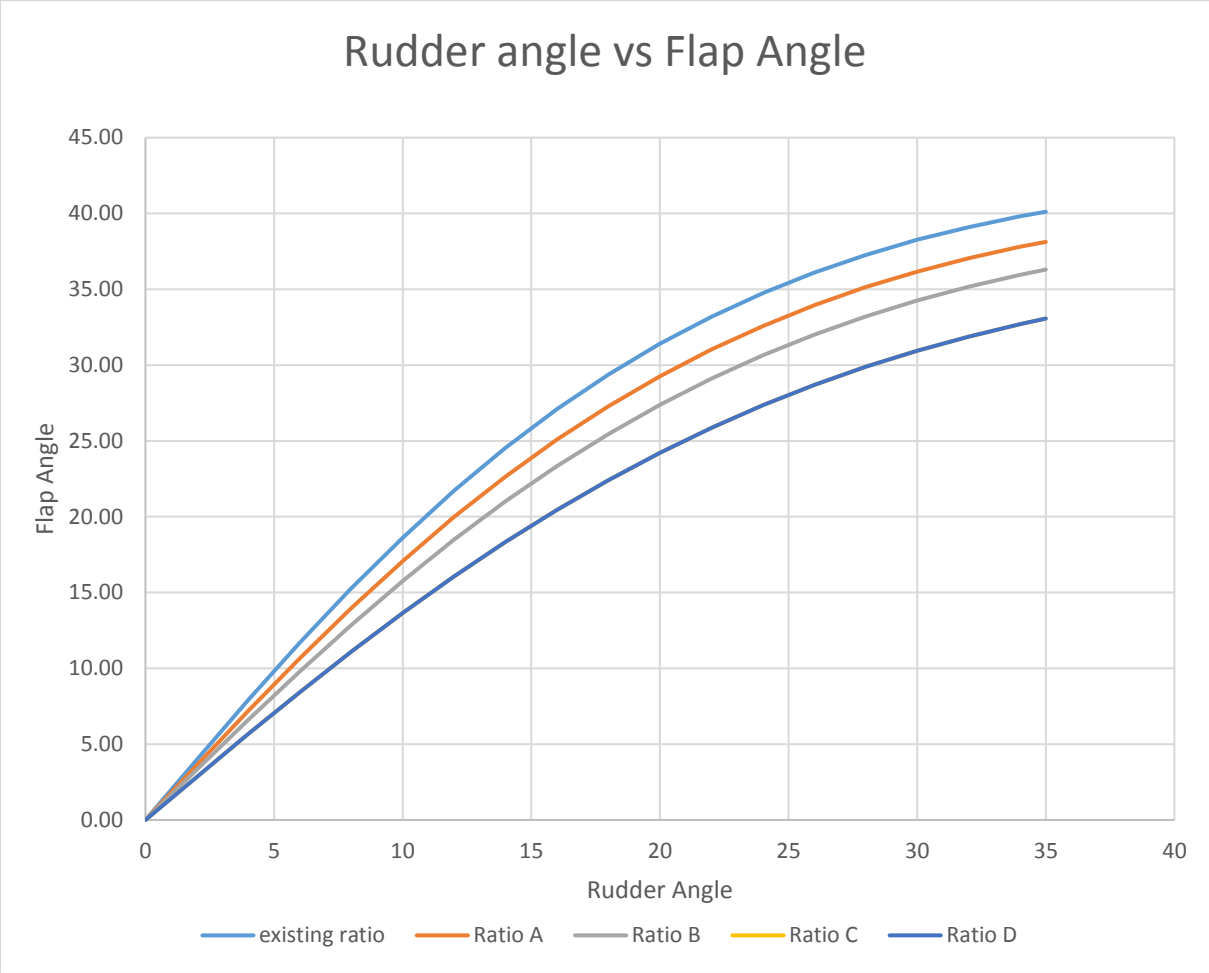

Figure 6- Different flap ratios

3.3 Inflow Angle Calculation

When a ship moving ahead the flow passing throught the propeller is excited and rotated. The swir and the acceleration induced in the flow by the propelelr alters the speed and incident of the flow arriving at the rudder situating aft of the propeller. This phenomena control the force and moment developed by the rudder. These force are crucial in predicting the overall performance of manoeuvering. In Two Dimensional analysis done without the help of propeller and actuator disc, for these analysis inlet flow considerd as straight but in real ship operation condition flow from propeller coming as a certian angle due to the propeller geometry. Inlet flow angle is important to predict the forces acting on tudder as well as to predcit the performance of manoeuvering So to compute the exact inflow angle new analsis done with the help of a virtual propeller. Actuator disc (virtual propeller) inner and outer radius and thickness inserted in the star-ccm+ platform as a actuator disc characteristics. Open water test value corrected for full scale filed as table in the starccm+ and used that excel file for the input of actuator disc. The main selction of parameters are give in below in table .

Table 2-Virtual Disc Details & Distributions

Propeller curve	OPEN WATER RESULT FULL SCALE
Disc Geometry	As per the Propeller geometry
Thrust and torque Distribution	Radial Distribution option(same Distribution)
Thrust and Torque distribution	Goldstein´s Optimum Distribution
Inflow specification	As per the propeller geometry
Propeller handeness option	Right handed
Operation point input option	Rotation rate (N)
Rotation Rate	0.47 rps (Low speed)

To calculate the inflow angle two point probe arranged in the +0.7 R,-0.7R radius of the Propeller. Point probe in up and down direction calculate the velocity vector in x,y,z direction and calculate the inflow angle from vector property.

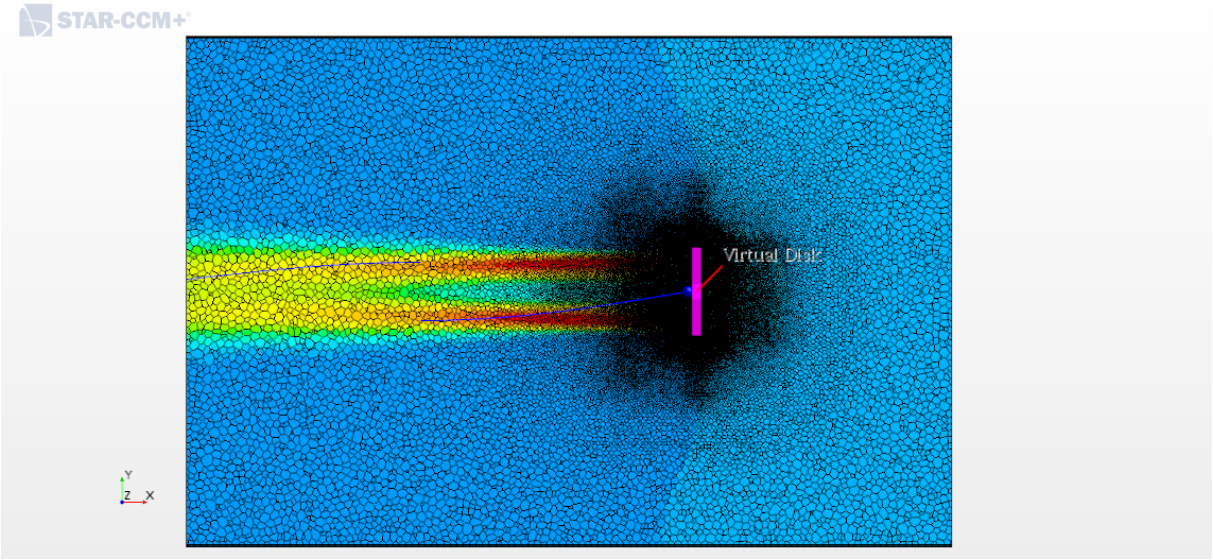

Figure 7-Inflow angle calculation using actuator disc

3.3.1 Final Inflow Angle

All wake input value consider from the Model test result at Draught condition 14.5m, Head wind 0m/s. For slow speed condition wake and RPM information are not avilabile in the Model test result report so that data interpolate linearly(data provided in the Annex1). Advance coeffient value also consider from the Model test result. Final selection of inflow angle and the input from the two probs are given below in tables where x,y,z cordinate represent the position of each point probes.

Table 3 Inflow angle calculation at 8 & 23 knot

Advance velocity calculation at 8 knot		
Inlet Velocity ,V	8	kt
Inlet velocity (m/s)	4.1152	m/S
Wake fraction ,W	0.27	
velocity of advance ,V_A	3.004	m/S
Advance coefficient, J	0.62	
Propeller Diameter ,D	10.3	m/S
N(RPS) @8 knot	0.47	RPS
Inflow angle	10.2	Deg
Advance velocity calculation at 23 knot		
Inlet Velocity ,V	23	kt
Inlet velocity (m/s)	11.8312	m/S
Wake fraction ,W	0.233	
velocity of advance ,V_A	9.075	m/S
Advance coefficient, J	0.642	
Propeller Diameter ,D	10.3	m/S
N(RPS) @23 knot	1.372	RPS
Inflow angle	10.2	Deg

Table 4-Point probe output -8 knot slow speed

slow speed case,8 knot speed								
Probe	**Velocity[i] (m/s)**	**Velocity[j] (m/s)**	**Velocity[k] (m/s)**	**Flow angle (radian)**	**X (m)**	**Y (m)**	**Z (m)**	**Flow Angle (Deg)**
ProbeA (+0.7R)	-4.302	0.77	0.298	0.17	-1	0	-3.6	10.19
probe B	-4.302	-0.77	-0.301	-0.17	-1	0	3.6	-10.16

Table 5-Point probe output -23knot cruise speed

High speed ,23 knot								
Probe	**Velocity[i] (m/s)**	**Velocity[j] (m/s)**	**Velocity[k] (m/s)**	**Flow angle (radian)**	**X (m)**	**Y (m)**	**Z (m)**	**Flow Angle (Deg)**
Probe A(-0.7R)	-12.99	2.34	0.90	0.17	-1	0	-3.6	10.22
probe B	-12.99	-2.33	-0.91	-0.17	-1	0	3.6	-10.18

3.4 Pre Settings

Domain size and the location of Rudder immersed in the fluid to be fixed Before starting the mesh preparation and computation. The domain size and the first mesh were produced and choosen based on the comparison with similar studies [26][27] and with the help of CFD team

from IBMV Maritime Innovationsgesellschaft mbH (IBMV). The boundary locations based on the chord length of the rudder profile(c). The defnition of boundaries and their location are defined in table 7.

Table 6- Defnition of the boundaries 7

Line	Boundary condition	Location from Model
AD	Inlet	4.6c
BC	Pressure outlet	6c
AB	wall	3c
CD	wall	3c
Model	wall	-

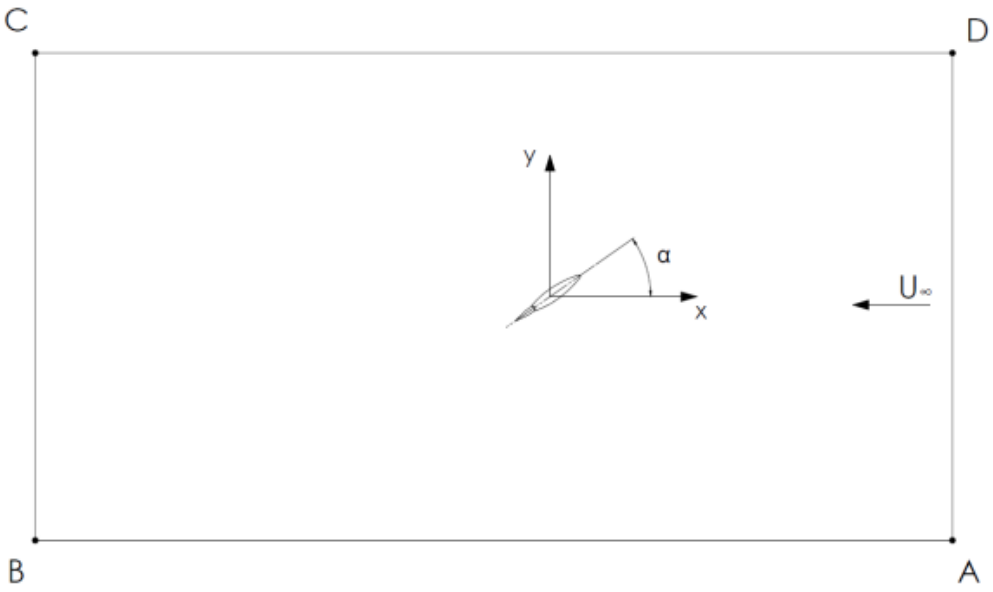

Figure 8-Rudder boundary condition

The outerwall AB and CD were defind as slip walls and the model surface set as no-slip wall.

3.5 Mesh Settings

The intial backgroud mesh was generated with STAR-CCM+ standerd mesher. Convergence study of mesh size shows that cell number between 50000 and 80000 have almost similar result, so Mesh base size 0.9m selected for the setting to reduce the computation effort and to save time .

Table 8-convergence study

SI No	Base Size(m)	Number of cells	Lift (N)	Drag (N)
1	1.5	30478	21967.39	639.28
2	1.4	31990	21963.54	639.90

3	1.3	34730	21963.60	635.44
4	1.2	37596	21349.78	622.05
5	1.1	41337	20726.65	608.81
6	1.0	45548	20668.97	604.70
7	0.9	51983	20640.70	601.57
8	0,8	58703	20636.15	598.82
9	0,7	68991	20615.49	596.95
10	0,6	84574	20609.88	594.98

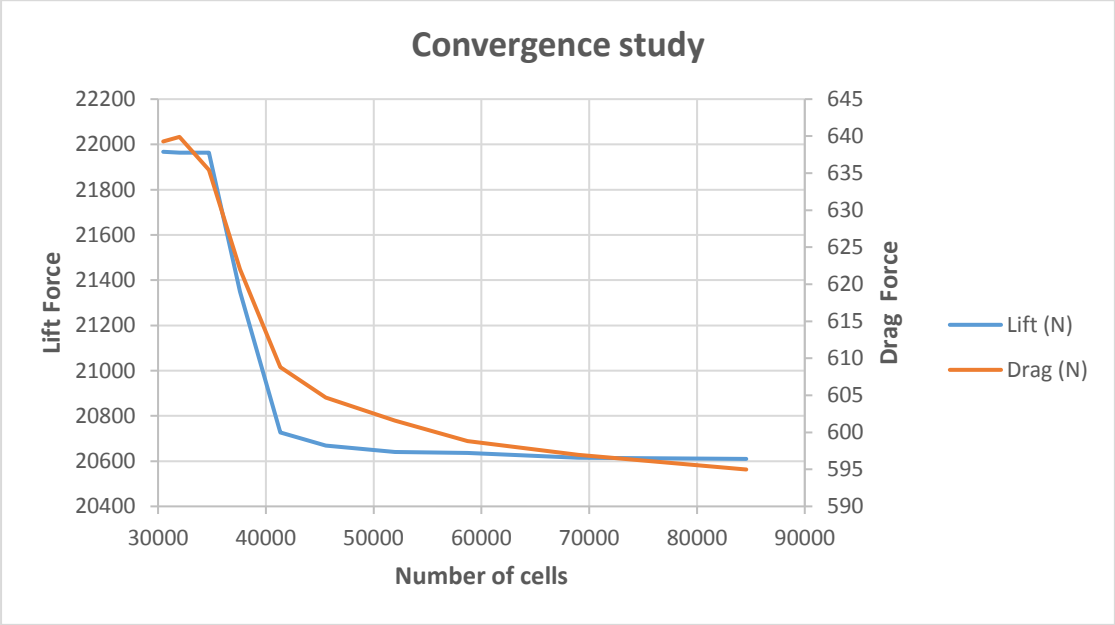

Figure 9-Mesh convergence study

Two dimension analysis done for two horizontal section at +0,7R and -0,7R, major part of propeller thrust act on this portion of the rudder that's why select these location for the analysis. From the domain exact location of this point subtracted and start the meshing procedure, Automated Mesh (2D) & Badge for 2D meshing tools used for this purpose. polygonal meshes and prism Layer Meshes used as a Meshes , and for the default controls base size used as per the convergence study. Detail Default controls are given below in table.

Table 9-Default Mesh contols

Base Size	O,9m
Target surface size	100%
Minimum Surface Size	25%
Surface curvature	36,0 pts/circle
Surface growth rate	1,05
Number of prism layers	7

Prism layer streching	1,25
Prism layer thickness	50.0 mm

Coupled flow with k-omega turbulence model as the models for the flow analysis of the case, All case run the iteration with steady case with All Y^+ wall treatment. In initial condition velocity provided from the above calculation shown in the table (Annex I-Table 17) with assumed wake field from the model test result. Temporary storage retained option to be activated from the expert option from the solver tab to maintain the pressure correction in CFD analysis. Maximum steps for stopping criteria selected as 6000 and after that one enable automatically. The whole meshed domain shown in below figure and some further screenshots are shown in Figure 40 to 45 in the Appendix I.

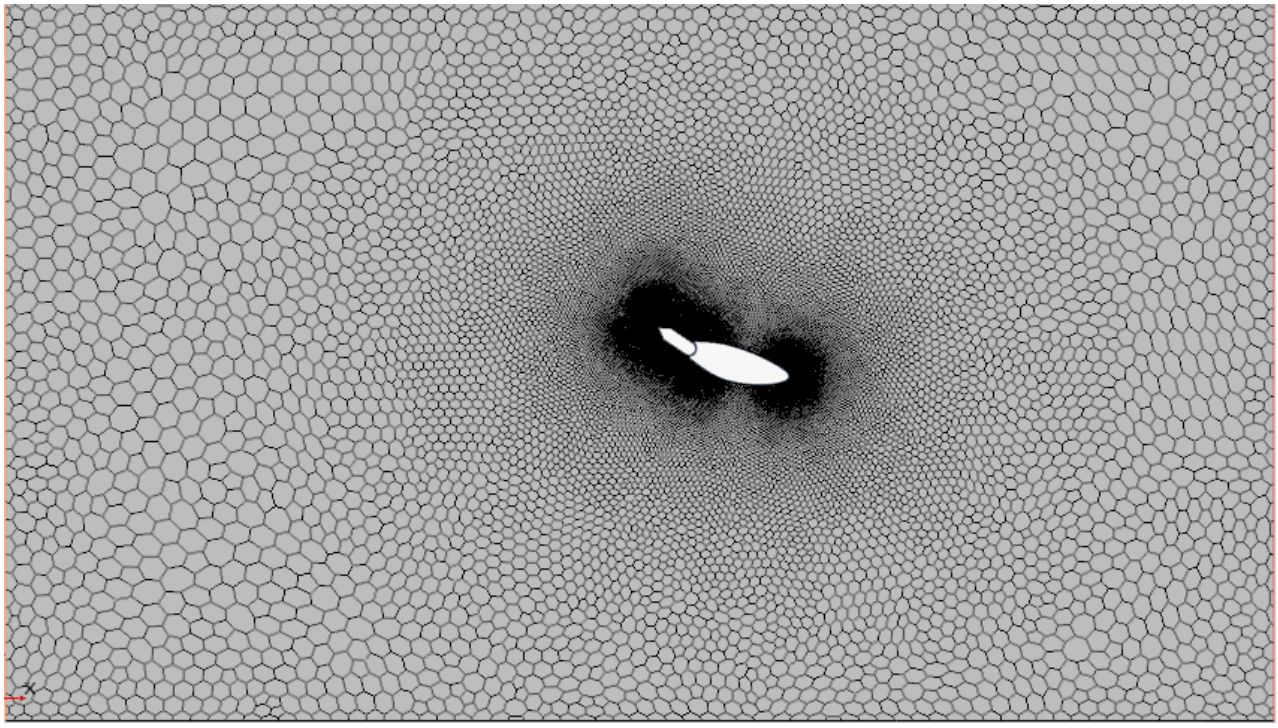

Figure 10 Meshed domain

Inlet velocity at the inlet was fixed on 3.004 m/s for slow speed condition and 9.075m/s for cruise speed condition with coresponding to Re= $2.6674*10^4$, $8.0583*10^4$ respectievely. The fluid density and dynamic viscosity were to set 1004.0 kg/m^3 and $8.8871*10^{-4}$ pa-s respectively. Courant Number fixed as five. Stoping criteria of solution was set to 6000 iteration. With provided computer of the ibmv average computaion time was 20 minutes.

3.6 Two Dimensional Analysis Result

The main analysis of the two-dimesional CFD iteration conducted at section +0.7 R and -0.7 R (3.605 m) from propeller centre. Existing flap and rudder angle ratios and newly obtained ratios (Ratio A,B,C,CD) based on a/b ratio are solved using two dimesion CFD solver, K-ω SST turbulence model used for the flow prediction. And these flow prediction conducted for two operating condition such as slow speed (8 knot), cruise spped (23 knot) conditions.

When the rudder and flap rotating to port side existing rudder stall at 12 deg and ratio C&D stall at 18 deg. When rudder rotating to port side upperside of the rudder fill with adverse pressure gradient due to the propeller flow interference.

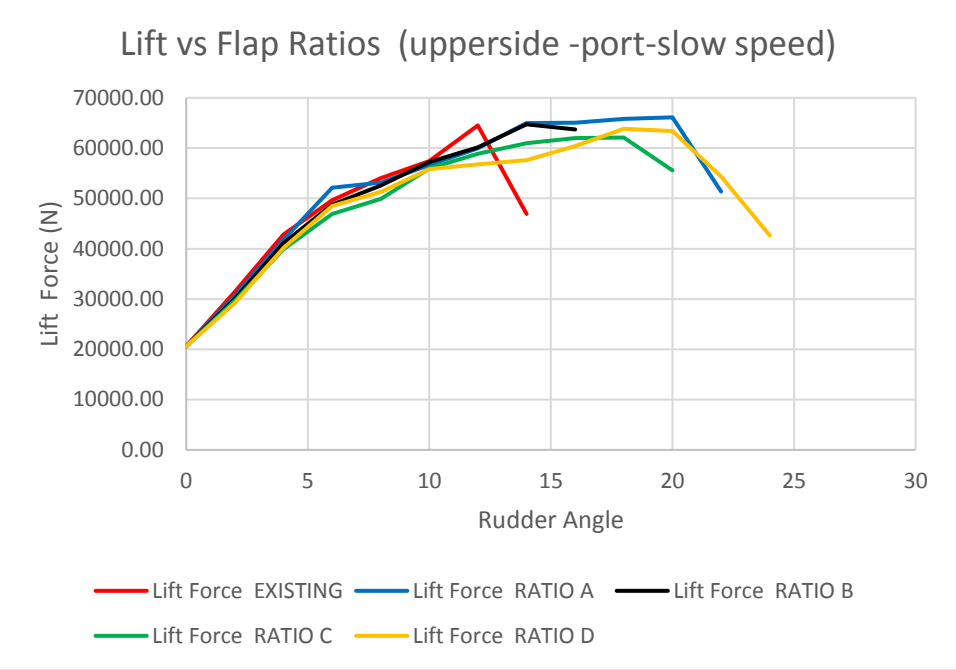

Figure 11-section at upper side(+0.7R), rudder rotating towards port side at slow speed

When the rudder and flap rotating to both port side stall happend at 12 deg ruder angle but the improved new flap ratio D was stall at 20 deg rudder angle. Ratio D present a good manoeuvering performance and dely the stall around 8 deg rudder angle. When analysing the velocity vector and pressure distribution for two dimension flow ,flow seperation start the mid of the suction side of the rudder just before the flap geometry (reffer figure 51 in the turbulence model comparison). When we comparing the vector and pressure distribution for zero rudder angle and 15 deg rudder angle towards port side, at zero degree flow seperation start near flap trailing edge. When we increasing the Rudder angle flow seperation shifted to more forward in the rudder suction side region. Due to unsymmetric nature of the rudder and suction side of the ruddder have more change in curvature than pressure side so when the flow hit the leading edge

a big adverse pressure gradient distributed in the pressure side and leading edge of the rudder too. Result of side force and rudder at diffrent sections are given below in figures 12 to 16

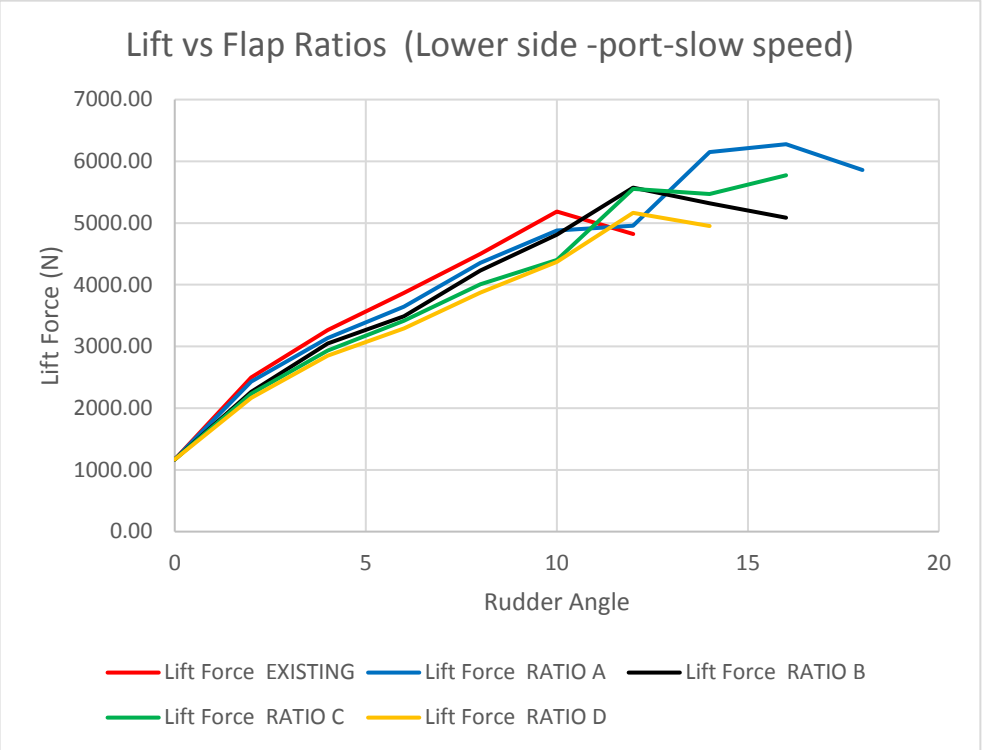

Figure 12-section at lower side -0.7R,Rudder and flap rotating to port side at slow speed

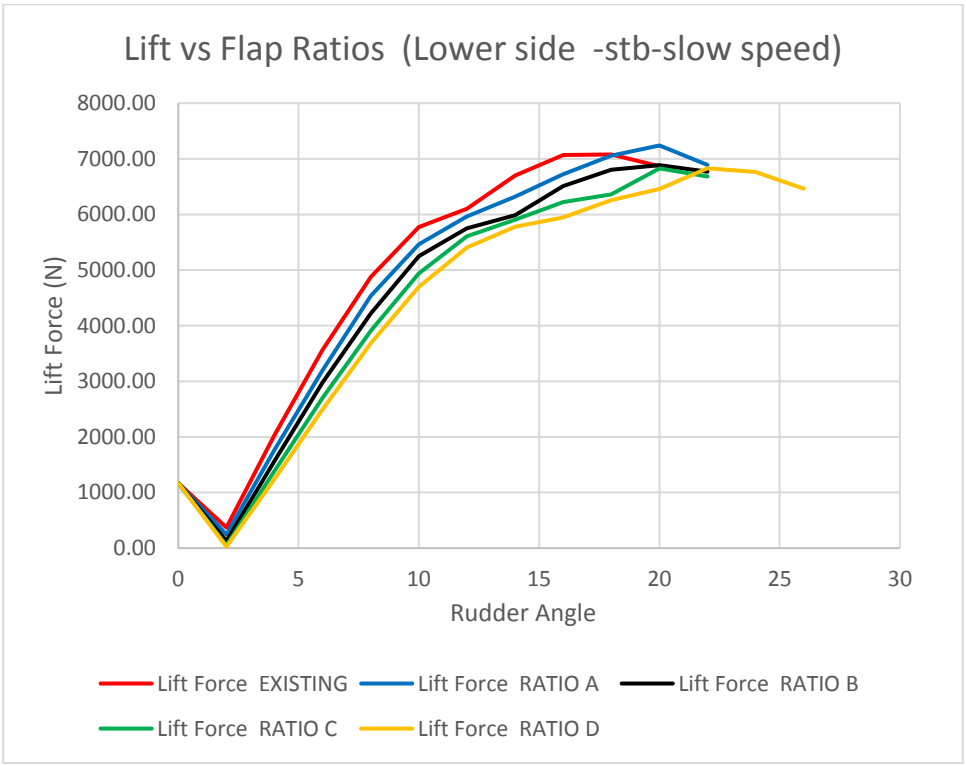

Figure 13-section at lowerside -0.7R ,Rudder and flap rotating to stb side at slow speed

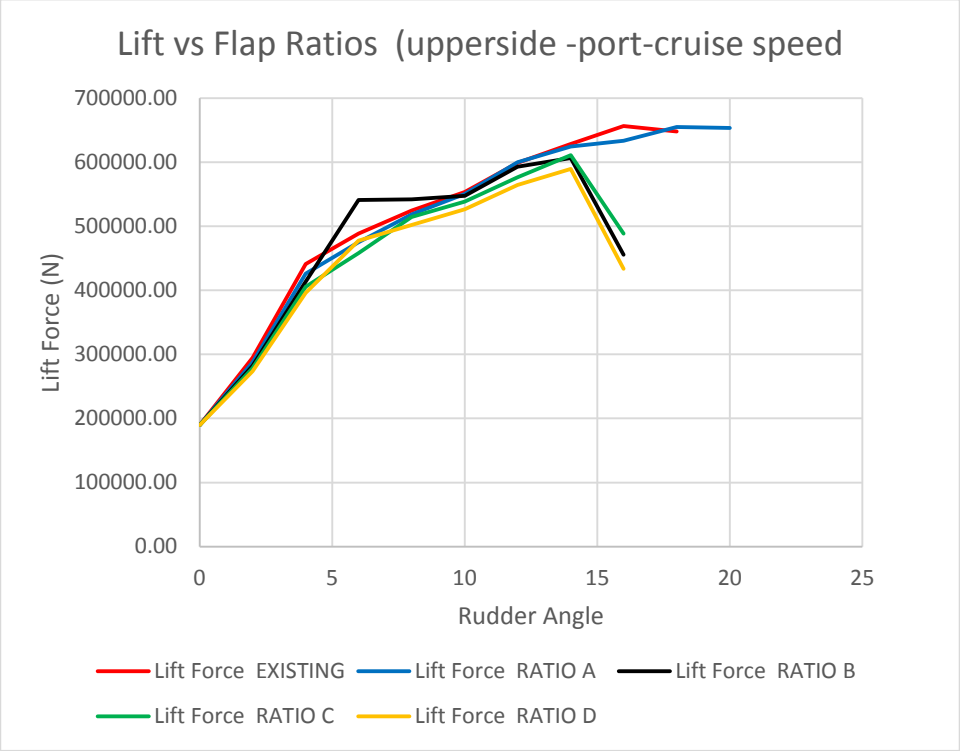

Figure 14-section at upperside +0.7 R ,rudder and flap rotating port side at cruise speed

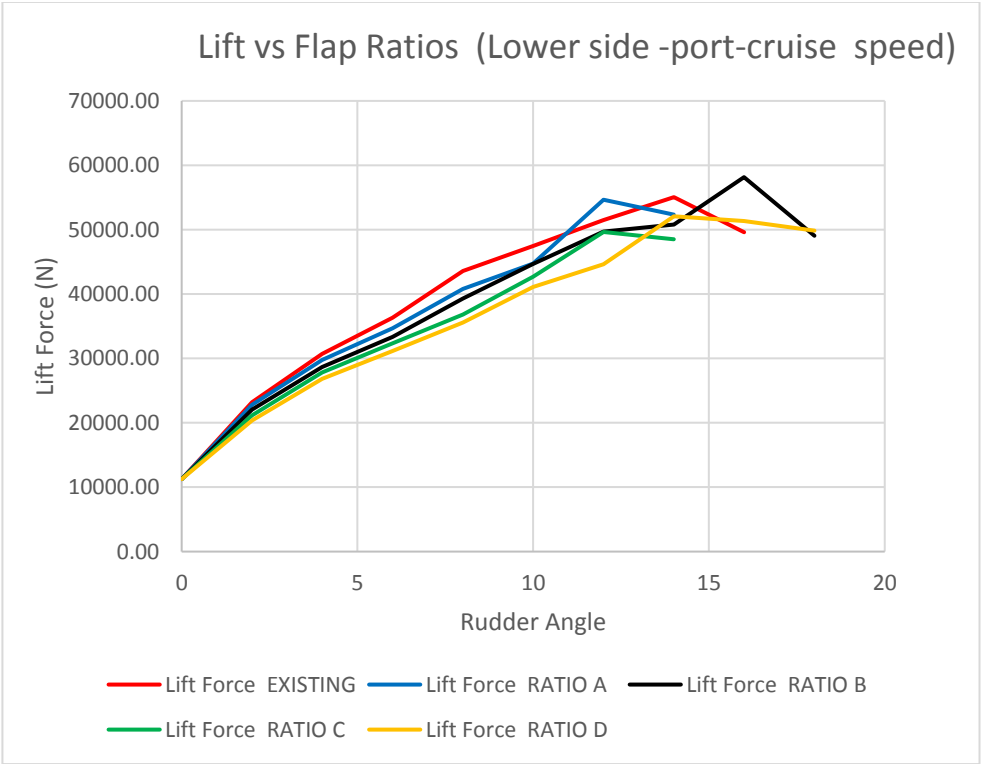

Figure 15-section at lower side -0.7R ,rudder and flap rotating to port side at cruise speed

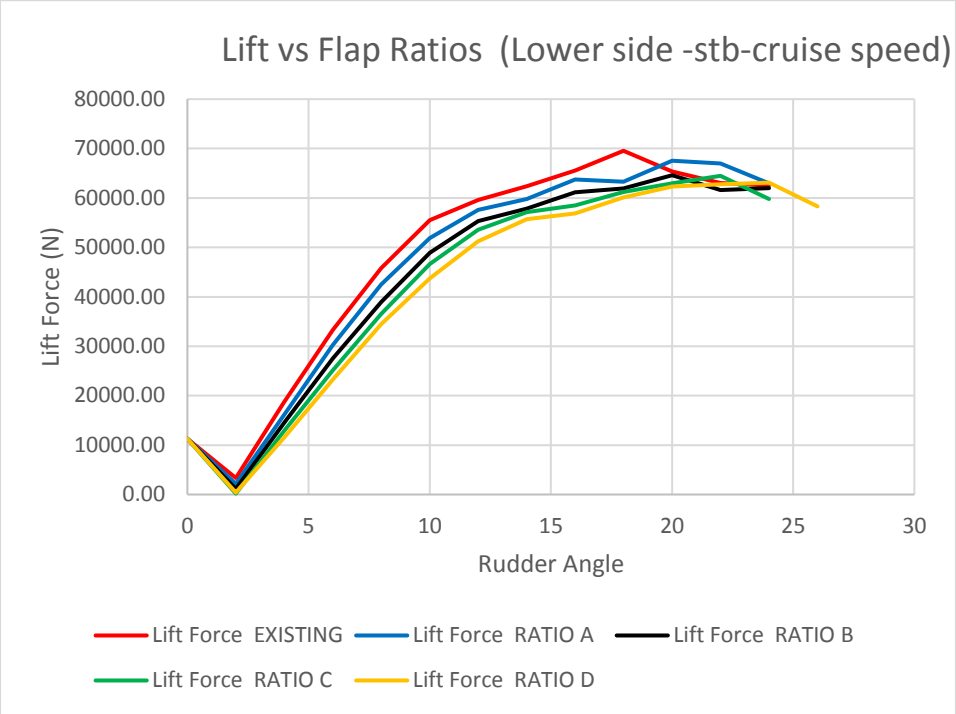

Figure 16-section at lower side -0.7R ,rudder and flap rotating to stb at cruise speed

when the ship referrence speed in increased to cruise speed the rpm of the propeller shifted to 26 rpm to 80 rpm so it will automatically increase the advance coeffiecent of the propeller. Normally propeller with high advance ration make high acceleration on rudder leading edge lead to the early flow seperation of flow happend in this case. In cruise speed condition almost all new flap ratios showing same side force or lesser side force than exisitng ratios, ratio D meet always a better or maintain the same side force in cruise condition due to this property of the flap angle ratio, Ratio D selected as the optimum flap angle ration to compare with existing ration in three dimensional CFD cases.

3.7 Summary of Two Dimensional CFD Study

From the two dimensional CFD study get a intital idea about the flow physics behind the becker flap rudder. Analysis result prove that when increasing the a/b ratio the performance of the rudder also inccrease if the flow seperation start from the leading edge of flap or near region. That means need to increase the fixed ditance ‘b’ between rudder stoke axis and pivote point for the flap actuation mechanism. In practical sense for the current becker flap ruddder maximum possibile changing distcane is around 150mm when considering the safety requirment and operation requirment. When do a new design from the scrach these conceptis useful to improve the high maneuvering capability of rudder.

Turbulent models comparison study also done in this section, detial value of analysis are given in the Annex II (Table 25, Figure 79). Four well known models are seleted for these analysis three RANS model such as spalart Allmaras, k-omega SST, K-Epsilon turbulence model and use one another model based on the scond moment closure model such as Reynolds stress transport model (RST). Except spalart allmaras model all other models showing almost similar result, splart-Allmaras model is the simple on eequation model all others are in the class of higher order models and these model work in low reynolds flow case only and efficient to solve viscous effeting region. Rudder related flow are more turnulent so the force and moment prediction of spalart allamaras are unrealistic in nature. 15 deg and 0 deg flow analysis for vector and pressure distributions are plotted in the ANNEX I (Fig 46-61), pressure distribution in the spalart allmars model shows the inactivity in nature in the figure (diffent from other model).

K-Epsilon, K-Omega model are two equation model predict almost similar result but k-epsilon model weak in the prediction of flow separation and reattchment. Turbulent Kinetic energy of the flow also over predicted by the k-epsilon model. In two dimension analysis rotation of the flow didint count but in three dimesional anlysis region of slow flow rotating and recirculating and vortex shedding but k-epsilon model are very poor to predict the same. K-Omega SST model devloped from the drw back of k-epsilon model, so this model perform well and close to reality. RST model always higher in the prediction but it consist of seven equation in three dimensionally required alot of computaion power(1.5 times greater than k-omega SST model) to solve the fluid flow equation. Considering the holistic approch of performance and cost k-w SST model was good for rudder performance prediction compared to RST model.

4.WAKE CALCULATION

The classical Kelvin wake comprises surface gravity wave and is developed by a ship moving in calm water of infinite depth. The disturbance created by the ship in a reference frame attached to it is stationary and it shows that wake pattern and amplitude are also stationary in is reference frame wake has a half angle about 19.47 º.

Most features of gravity wave treated using the idea of wave speed and group velocity: the group velocity represents the velocity of wave packet and the phase velocity is the speed of crest within the packet. The wave at a point within the wake are controlled by their propagation speed and their stationarity in the reference frame of the ship. when the water is very deep , waves traveling at high speed can propagate on the surface. The group speed is typically half of the wave speed. In contrast, at large wavelength in shallow water both group velocity and phase velocity approach the same values. This implies that there are two regions when the ship is slowly moving at a speed less than wave speed and Group velocity, transverse waves can propagate at the ships speed and the wake will be resemble the kelvin wake. There will be divergent and transverse wave system intersecting in cusps region. When the ship is moving at a speed greater than the maximum, transverse wave cannot propagate only divergent wave present in the wake field. In this regime, the wake half angle $\beta_{max,}$ will be determined by the maximum group velocity, C_{gmax} ,and the ship speed, According to :

$$\boldsymbol{sin\beta_{max} = \frac{C_{gmax}}{U}} \quad \textbf{(33)}$$

The dispersion relationship for a wave in shallow water permit the phase speed ,c, and the group velocity ,Cg to be find. The dispersion relation is given by

$$\boldsymbol{\omega^2 = gktanh(hk)} \quad \textbf{(34)}$$

Where **ώ** angular velocity is the acceleration due to gravity, k is the angular wave number, h is the water depth , when in deep water hyperbolic term can be neglected except when k is small. The phase and group velocity can be derived directly from the dispersion relation as below.

$$\boldsymbol{C(K) = \frac{\omega}{K} = \frac{\sqrt{gtanh(hk)}}{k}} \quad \textbf{(35)}$$

$$\boldsymbol{C_g(k) = \frac{dw}{dk} = \frac{C}{2}\left(1 + \frac{hk}{sinh(hk)cosh(hk)}\right)} \quad \textbf{(36)}$$

When **hk** is very large, the group speed half of the phase velocity. When **hk** is small the group velocity approaches the phase speed the phase constains is simply:

$$\boldsymbol{c = UCOS\,\theta} \qquad \textbf{(37)}$$

Where $\boldsymbol{\theta}$ is the angle between the group velocity and ship velocity vector.

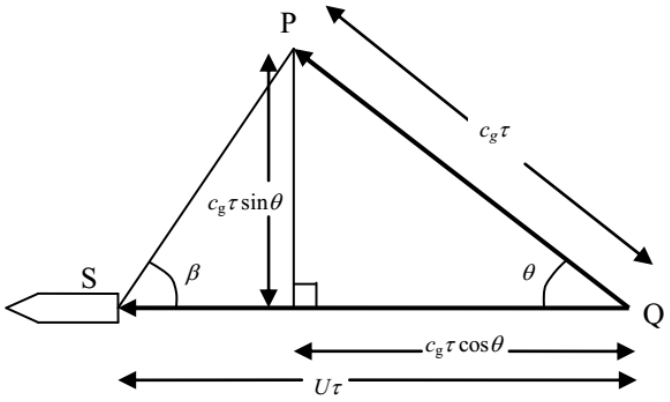

Figure 17 wake representation

Wake result from the model test result is enough to-do the two dimensional analysis of flap rudder, for Three dimensional analysis case exact wake requirement is required so new wake calculated for two cases operation like slow and cruise speed condition.

Table 10-Mesh setting details for wake

Base size	30.9m
No of prism layers	8
Prism layer streching	1.8
Prism layer thickness	450mm
Surface growth rate	1.3m
Surface curvature pts/circle	36
Mesh models	Prism Layer meshes
	Surface remesher
	Trimmer messhes
Prism layer thickeness	250mmn
Volume mesh cells	3012754

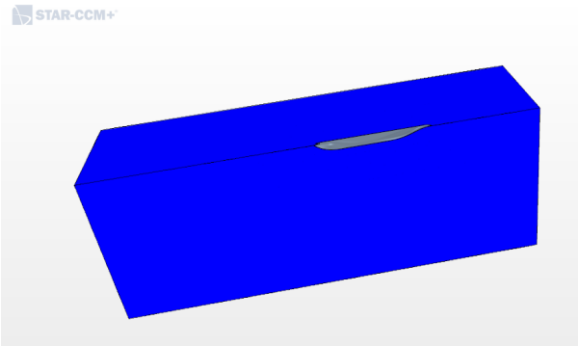

Figure 18- Wake domain and model setup

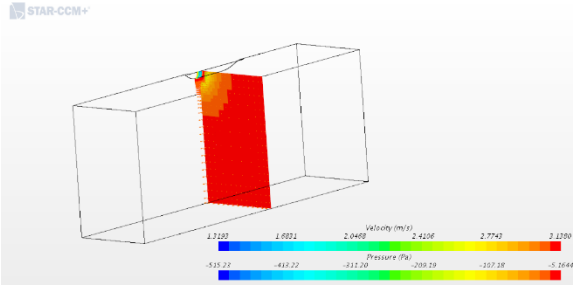

Figure 19 - velocity and pressure distribution

Table 11-Boundary condition details

REGION	Boundary condition
Free surface	Symmetry condition
Inlet	Velocity inlet
Midship	Symmetry plane
Outerwall	wall
Outlet	Pressure outet
Ship hull	Wall (Rough wall surface specification)

no slip condition selected for the shear stress specification and the following scalar values specified for the wall surface specification

E = 9.0 (The log law offset)

Kappa = 0.42 (von karaman constant)

Wall roughness parameters

B = 0 (coefficient B in roughness function)

C = 0.253 (coefficient C in roughness function)

Rplus smooth = 2.25

Rplus Rough = 90.0

Half of the hull consider for the wake calculation, Velocity input considered two condition as before slow and cruise speed condition and final result of wake calculation reflected for the complete hull with the help of java script. To verify the result of iteration pressure and velocity

distribution checked for the inlet boundary and satisfy the initial conditions. Depth and mesh setting fort the wake calculation same as the real domain used for the Three Dimensional calculation in later stage. Turbulent kinetic energy and specific dissipation and velocity in in x,y,z direction extracted from the this process.Wake calulated for three ship operating condition like,

1) shallow water with tangitial velocity
2) Intermediate water depth
3) Deep water depth

In Shalow water case additional volume source used fort he domain to increse the number of verical cells in z direction (suez canal depth is considerd for the size oft he domain), all wake calculation done wthout any appendages and in full scale condition.

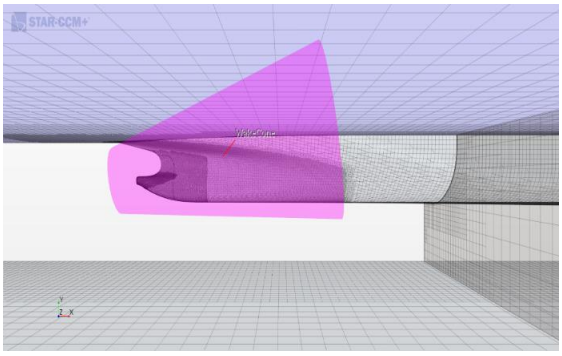

Figure 20- wake cone volumetric source

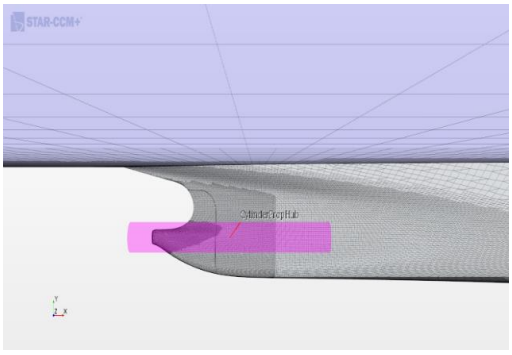

Figure 21- propeller hub volumetric source

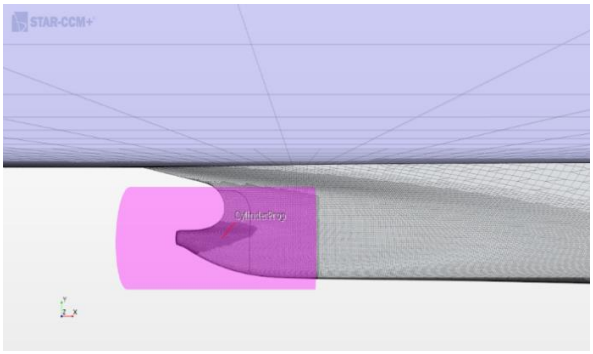

Figure 22- propeller hub volumetric source

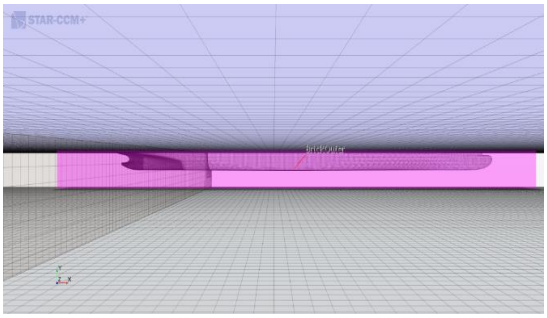

Figure 23 – volumetric source for complete hull

5 THREE DIMENSIONAL CFD ANALYSIS

4.1 Introduction

Three dimensional calculation of rudder done with the help of Actuator disc and ship hull with wake. Wake input fröm the previous calculation filed as a table in the Star directary and inserted in the inlet boundary condition. Existing and optimum flap ratio compared in the resepected calculation based on CFD flow analysis.

First step of the three dimensional calculation was the preparation of rudder geometry for the meshing, its done with the help of solid works and surface repair option from star ccm+ . Surface repair include the process of removing of unnecessary part of Geometry and filling of holes and scraps too. There is gap in between rudder and Flap, to manage the flow seperation in that region required alot of cells so to avoide and control the Number of cells extended the rudder portion to forward and do a curve fitting in that region.

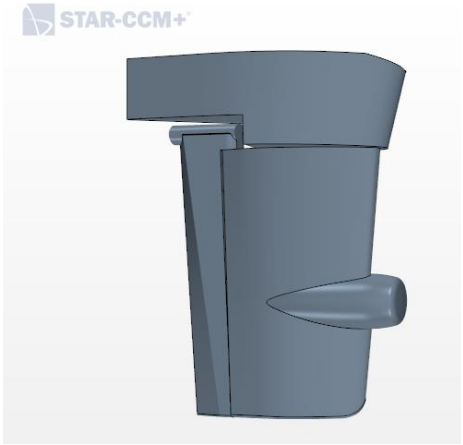

Figure 24 - Rudder stb view

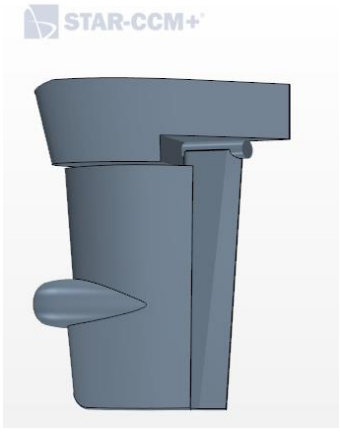

Figure 25- Rudder port view

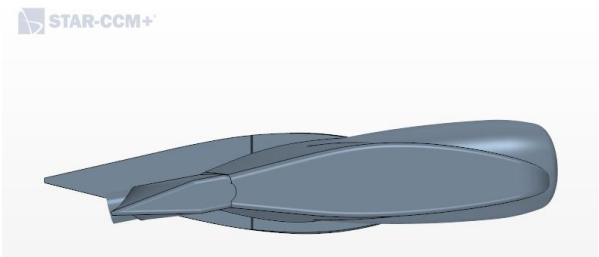

Figure 26 - Bottom view

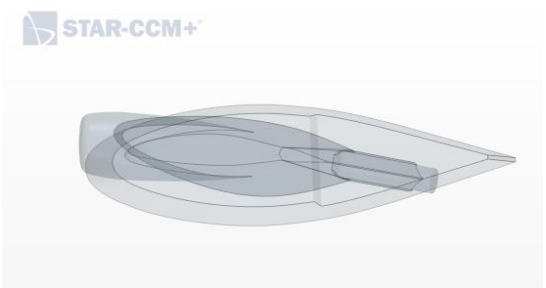

Figure 27- rudder top view

Modified rudder geometry and Ship model (CAD Geometry) uploaded in starccm+ using the option " import surface mesh". Then Local cordinate system created for the Rudder, Flap sytem and the propeller for the roation purpose based on the geometry. Then Fluid domain is created for the ship hull and geometry, size of the domain selected as below from the main cordinate system .

Table 12-Domain dimensions

	Corner 1	Corner 2
x	-800 m	101.25m
y	-14.5m	14.5m
z	-400 m	400 m

Wake calculated at the point of 101.25 from the transom stern of the ship, so ship hull is substacted at the point of wake calculation.

Figure 28 ship profile view

Figure 29-Ship aft view

Figure 30-ship forward view

3.2 Mesh setting

Two type of mesh setting available in the star software one is Region based and the next one is part based meshing, region based mesh setting was used in the complete CFD work . To make regions each surface of the rudder selected and "split by patch" used for the creation of separate

part and after the creation separate part those part assign to regions. Region based meshing helping to identify the flow characteristics for the complicated geometry like rudder through custom mesh setting used in the regions. Polyhedral mesher, prism Layer Mesher, Surface mesher are the default meshing model selected for the 3D analysis other parameters selcted for the mesh settings are given below.

Table 13 –Basuc Mesh details

Base Size	30.3 m
Number of prism layers	6
Prism layer streching	1.7
Prism layer thickness	90.0 mm
Surface curvature	36.0 pts /circle
Surface growth rate	1.3
Surface size	
Relative /Absolute	Relative to the base
Size method	Min and target

Base size is selected based on the propeller diameter, normally 3 times of the propeller size is used as a base size. All other value selected based on the refference file and reccomendation from ibmv proffestional engineers. Main Region mesh setting are give below,

Table 14- Region mesh setting details

Region	Surface size(% of base size)		Shear stress specification	Tangetial velocity specification	Wall surface specifcation	Customize prism mesh	Boundary condition	Surface curvature
	Target size	Minimu size						
Flap bottom	0.3	0.04	No slip	Fixed	smooth	Default value	Wall	Default value
Flap Link	0.3	0.04	No slip	Fixed	smooth	Default value	Wall	Default value
Flap Linkage	0.05	0.04	No slip	Fixed	smooth	Default value	Wall	Default value
Flap main	0.3	0.04	No slip	Fixed	smooth	Default value	Wall	Default value
Flap TE	0.05	0.04	No slip	Fixed	smooth	Default value	Wall	Default value
Rudder Bottom	0.3	0.03	No slip	Fixed	smooth	Default value	Wall	72 pts/circle
Rudder Bulb	0.3	0.04	No slip	Fixed	smooth	Default value	Wall	72 pts/circle
Rudder Main	0.3	0.04	No slip	Fixed	smooth	Default value	Wall	72 pts/circle

Rudder TE	0.1	0.04	No slip	Fixed	smooth	Default value	Wall	Default value
Rudder Top	0.3	0.04	No slip	Fixed	smooth	Default value	Wall	Default value
Headbox Bottom	0.5	0.15	No slip	Fixed	smooth	Default value	Wall	Default value
Headbox main	0.5	0.15	No slip	Fixed	smooth	Default value	Wall	Default value
Headbox TE	0.075	0.05	No slip	Fixed	smooth	Default value	Wall	Default value
Hul Aft with Nozzle	0.35	0.15	No slip	Fixed	smooth	Default value	Wall	Default value
Hull Main	2.5	0.75	No slip	Fixed	smooth	Default value	Wall	Default value

Domain Boundary conditions are given below,

Table 15-Domain boundary layer condition

Region	Turbulence specification	Velocity specification	Boundary condition	Speciific Dissipiation rate	Turbulent kinetic energy	Velocity
Inlet	K+omega	Componets	Velocity inlet	Table(x,y,z)	Table(x,y,z)	Table(x,y,z)
Outlet	Intensity+viscosity ratio	-	Pressure outlet	-	-	-
Freesurface	-		Symmeetry plan		-	-
Wall	-	Vector	Wall	-	-	-4.1152,0,0 m/s

To get fine mesh density in a specified zone for both surface and volume meshes different type of volumetric mesh controls are used in the starccm+ iteration. Volumetric sources details are provided in the Annex I [image 67-73] volumetric refinement zone defind using volumetric shapes and geometry part. For geometry parts,the control takes its defnition from the root description only. Volumetric control geometry and specific cell size selected bases on the flow characteristic of rudder and hull interaction. Volumetric control can overlap and extend outside the region boundary defnition. Volumetric contols can also overlap from one region to another, but the effect is only included if the region belong to same mesh continues as the volumetic controls. If Two or more volummeric controls overlap, the samllest user defined cell size take priority. Polyhedral mesh and surface remeser meshing model option to be implimented for volumetric sources used in this analysis.

Open water characterstics from the self propulsion test result [17] file as a table and utalised for the virtual disc data for propeller Thrust, Torque , Advance coeffient and propeller efficency

.Body Force propeller method used to specify the propeller characeristics ,the method models the flow field intraction of the hull of a ship and the propeller. The flow induced by the propeller depend on the flow arounf the ship hull or wake. It can be clearly advantage to use Body force method regarding the mesh size and so reducing the computational cost over performing the fully resolved geometry of the propeller .this method is very useful if we are not intrested in analyzing the flow field around the propeller but more importantly need the correct propulsion specification.

The body force propeller method uses the following approches

- Specification of an operating point, for example, the rotation speed.
- Definitions of a virtual disc regarding the position and direction in which thrust is produced.
- Specification of a propeller performance curve.
- Specification of an inflow velocity plane that yield an average velocity and density for propeller inflow.

As a result ,the radially varying distributuion of the axial and tangential forces of the modeled propeller acting on the flow is calculated. The integration of these force over the disc gives the thrust and torque of the propeller. Disc geomery and orientation of propeller selected as per the propeller Geometry. Two RPM conditions selected for the operation 26rpm for low speed 80 rpm for cruise speed(value selected from open water characteristic test). The radial thrust and torque disdtributions are calculated by using Golstein optimum distribution.

RANS turbulence models provide closure relation for the Reynolds–Averaged Navier-stokes equations. That govern the transport of the mean fow quanties. The k-omega model that solves transport equations for the turbulent kinetic energy $\boldsymbol{k}$ and the specific disspiation rate $\boldsymbol{\omega}$ the dissipation rate per unit turbulence kinetic energy $(\boldsymbol{\omega\alpha\varepsilon/k})$ in order to determind the turbulent edy viscosity. One severe advantage of the k–omega model over the K-Epsilon model is the improved performance for boundary layers under adverse pressure gradients. So SST(Menter) k-Omega turbulence selected for the analysis. The standerd k-omega model is in the orginal form is sensitive to the levels of the turbulence in the free stream. Menter´s [24] SST K-Omega model uses the insensitivity to free-stram conditions of the k –Epsilon model in the far field , while retaining the advantage of the K-Omega modle near walls. Both k-Omega turbulence models are availabile with all three wall treatment High Y^+, low Y^+,and all Y^+. For most of the application , the recommended choice of models is the SST K-Omega model combined with the all Y+wall treatment so for the three dimensional rudder analysis also same recommended model to be used. Spseudo-time marching approch is used for the calculation of coupled flow for conservation of mometum,mass and energy. One advantage of the couple solver is that CPU

time scales linearly with cell counting. With the coupled flow solver, the conservation equation, momentum, energy, and speciers are solved in a coupled manner, they are solved simultaneously as a vector of equations. The velociy field obtained from the momentum equations. From the continuity equation, the pressure is calculated and the density is evaulated from the equation of state. The coupled system of equations is solved by either implicit or the explicit time –integration scheme. For all analysis coupled flow with implicit integration with 2 order discretization was used.

3, 3 Result

Three dimensional analysis done for two cases like existing and optimum flap ratios, output from Two dimensional CFD analysis indicate that optimum ratios have better manuevering performance than existing rudder but Three Dimension analysis with the help real condition like ship hull, wake shows that both case almost sililar performance and new ratios have a little bit high performanec than existing one.

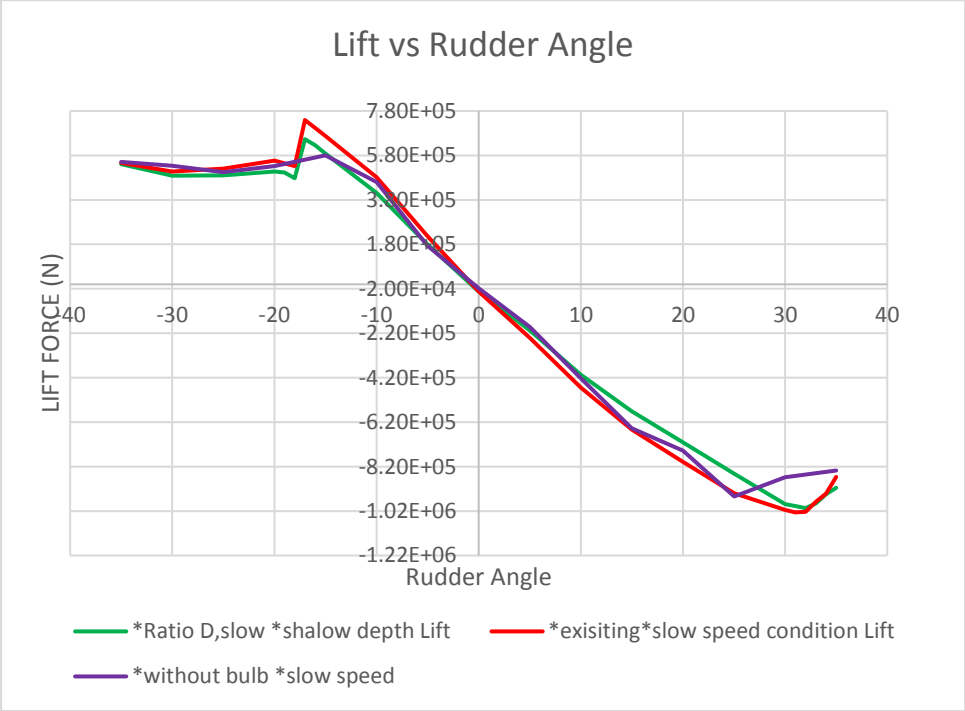

Figure 31-Lift force comaprison for existing and optimum ratios

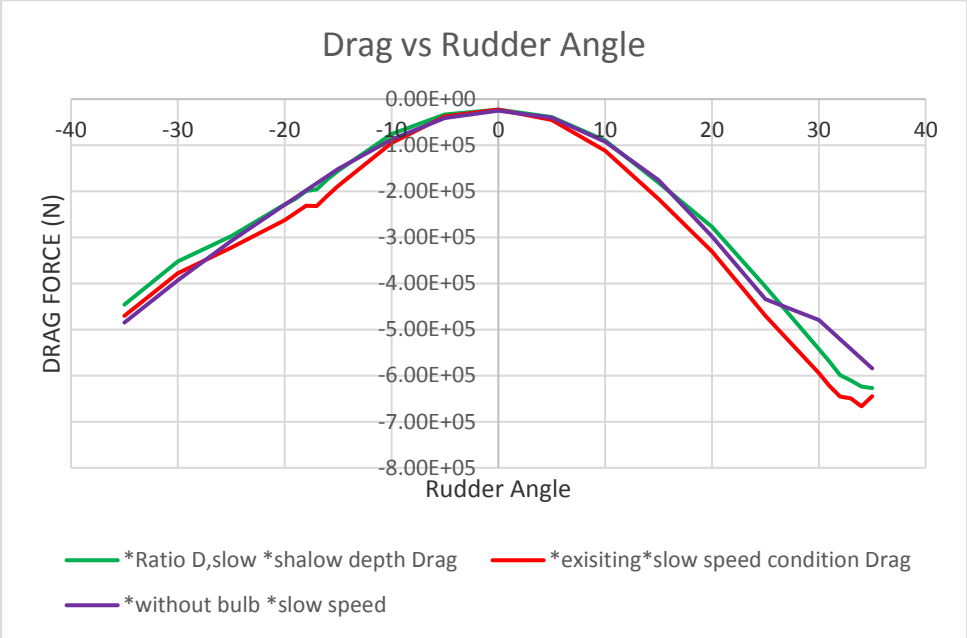

Figure 32-Drag force comparison for existing and optimum ratios

When the rudder rotating to port side and stall beyond 17 degree rudder angle, from the post processing of flow analysis understand that there is early flow seperation start form the Leading edge of rudder. Inteference of bulb in that location also create unwanted disturbance in that location the same case analysis done with abscense of rudder bulb also.

A detail analysis stall rudder angle is done when the rudder and flap is rotating to the port side to improve the flap characterstics in stall to reduce the flap angle at a constant intervel of 2 degree, post processing of these flow analysis prove that flow seperation start from the Leading edge of rudder (shear stress analysis given in the Annex I-Figure 70).

To cross check tha analysis the same situation replicate with max flap angle (22.4 degree) and zero flap angle with below cases(Annex I-figure 71,72).

- Flap angle Max/Min with normal condition (Suez canal depth)
- Flap angle max /minimum without bulb
- Flap angle max/min with 20 m domain depth
- Flap angle max/min with 600 m depth

Rudeer with 18 degree zero degree flap angle case shows severe flow seperation from the Leading edge of the rudder due to the hull characteristics and propeller load influvence. For the same case without bulb also showing flow seperation start from the Leading edge of the rudder. Intial working plan to develop or improve the flap agle but for this condition it doesn't make any influvence due to the early flow seperation from the leading edge and the twisting geomerty of the rudder.

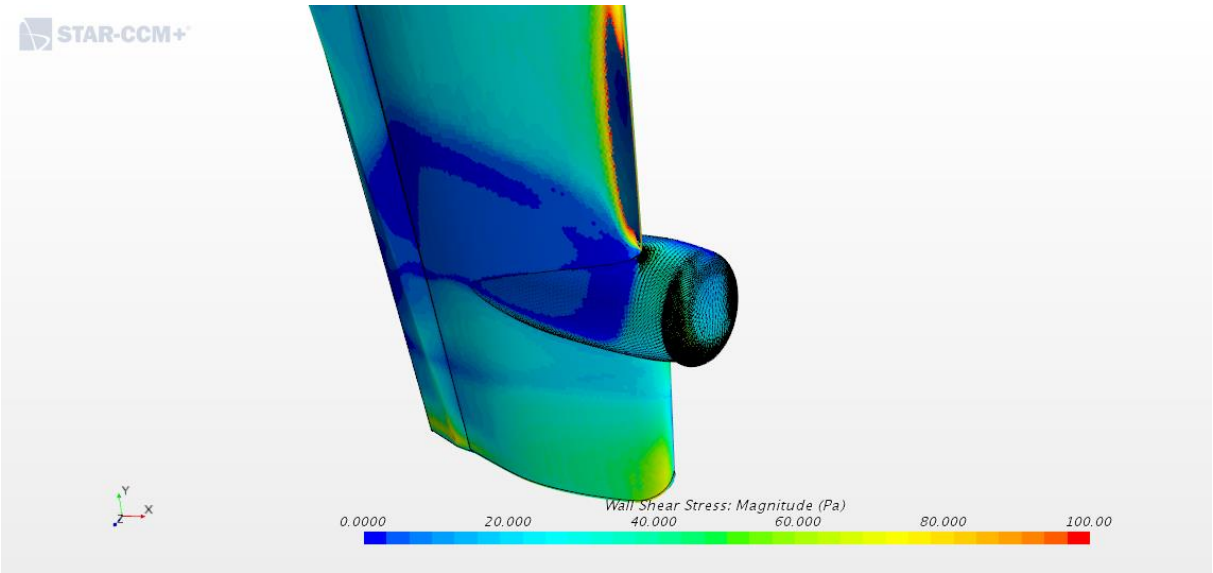

Figure 33- Vecter distribution of velocity at bulb

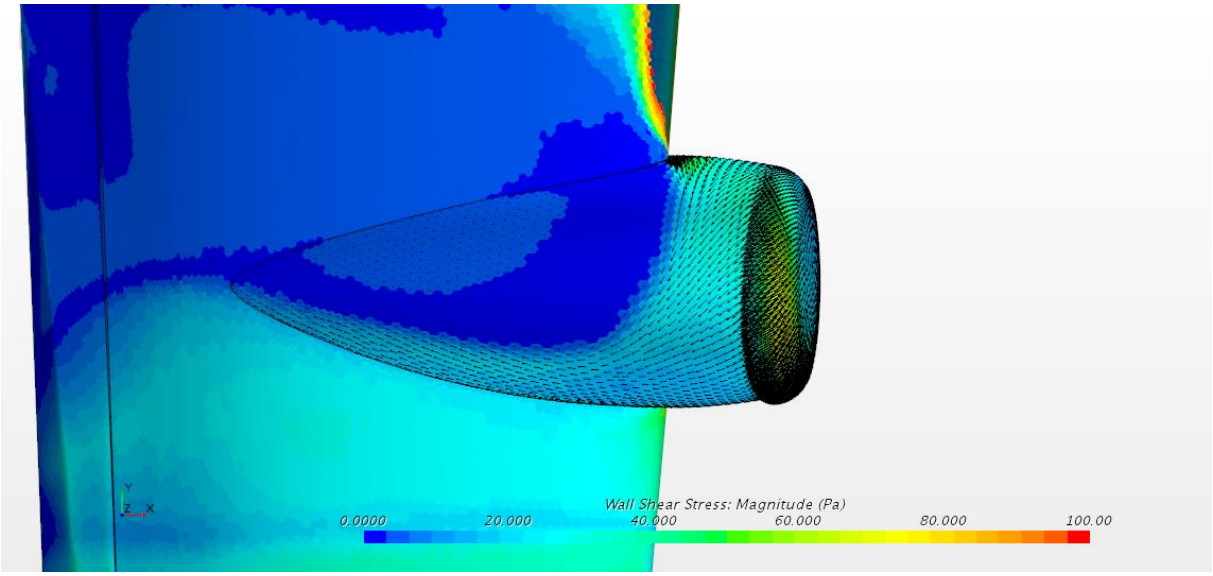

Figure 34-Flow seperation point at rudder bulb

Image for the bulb velocity vector shows that there is a possibilty of cavitation at the intersection point of leading edge and bulb at top portion, and same point is the location of flow seperation for all cases also.

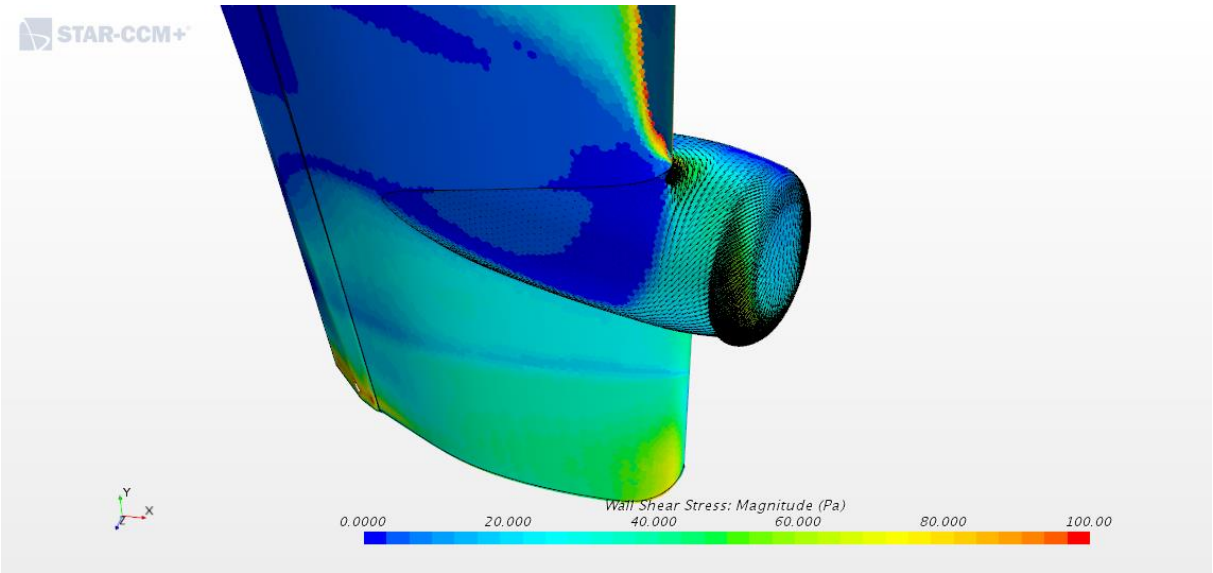

Figure 35-top view of rudderbulb cavitation point

3.3.1 Analysis for different water depth

Domain depth is changed in this case form Suez canal to 300 m (intermediate)600 m m depth(deep water) it shows that shallow water rudder exhibit lack of maneuvering ability and in intermediate and deep water exhibit almost same characters. For shallow water case hull force is dominating 2 to 3 times rather than deep water (separate maneuvering CFD analysis report for the same ship hull refer for the ship hull force and turning moment at different drift angle and ship radius /LBP ratios –Annex II-Table 27)

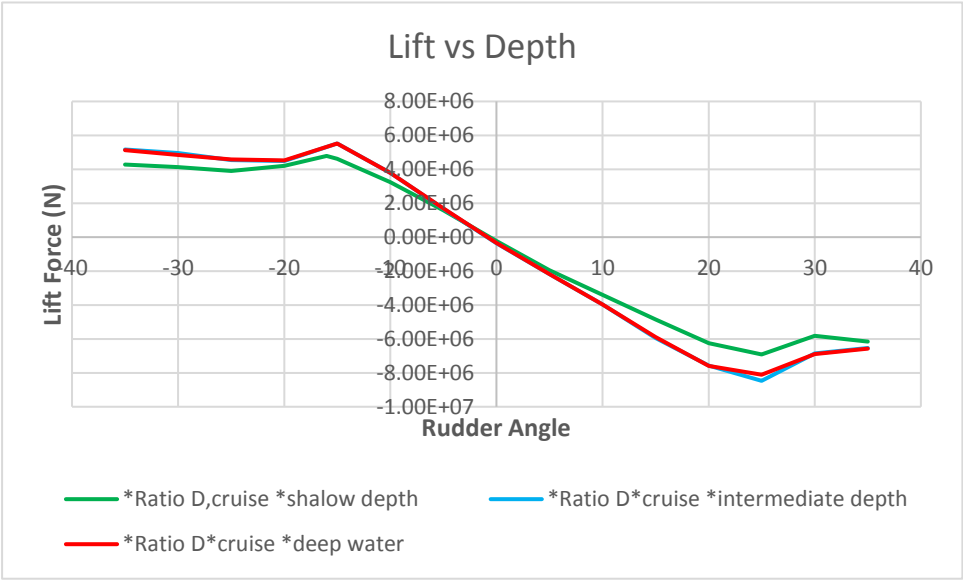

Figure 36-Lift force in different domain depth

Early flow seperation happen Due to the severe problem of rudder geometry in the leading edge side so to optain good performance change the different rudder geomerty in trail error condition. New geometry used in the optimisiation are given below(AnnexI -Figure 73-76) ,

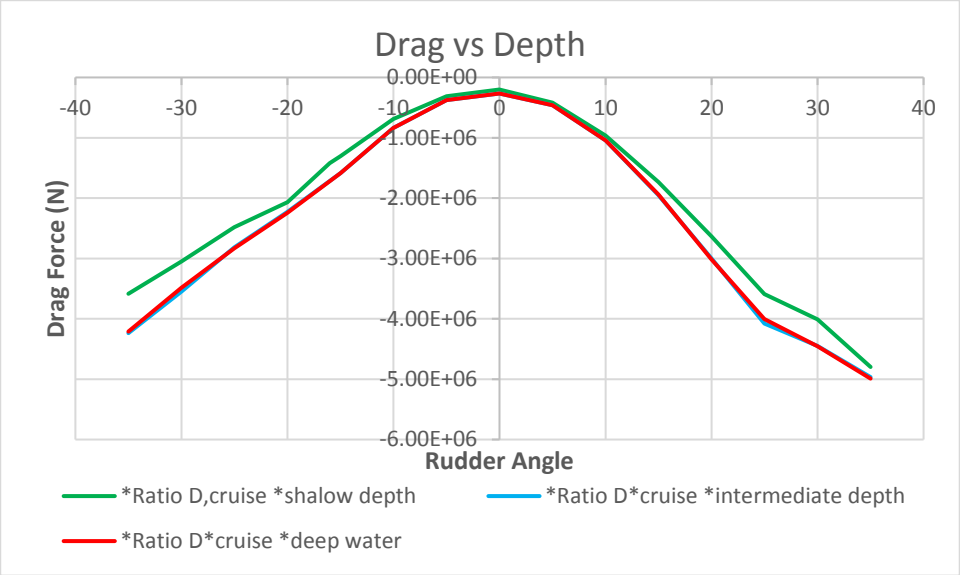

Figure 37- Drag force in different domain depth

- Symmetrical rudder
- Symmetrical rudder without bulb
- Blended trailing edge rudder
- Twisted rudder with holding plate

Result of iteration for different case like cruse speed and slow speed at shalow water condition are given below.

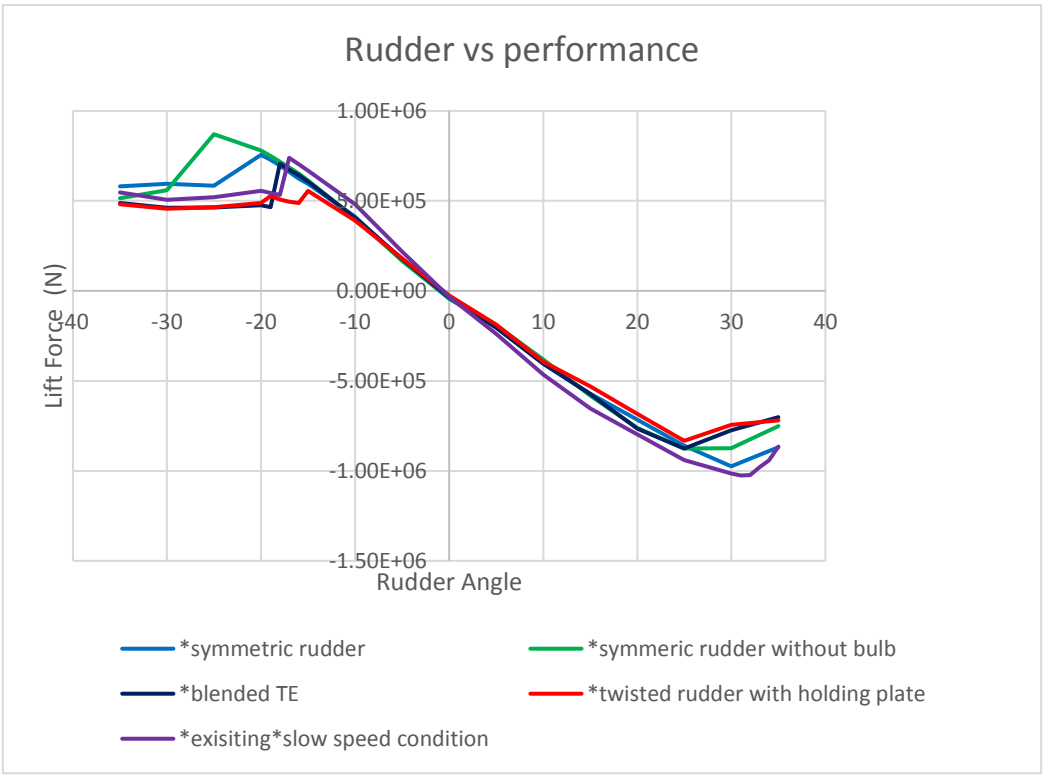

Figure 38- Lift force for new rudders geomtries

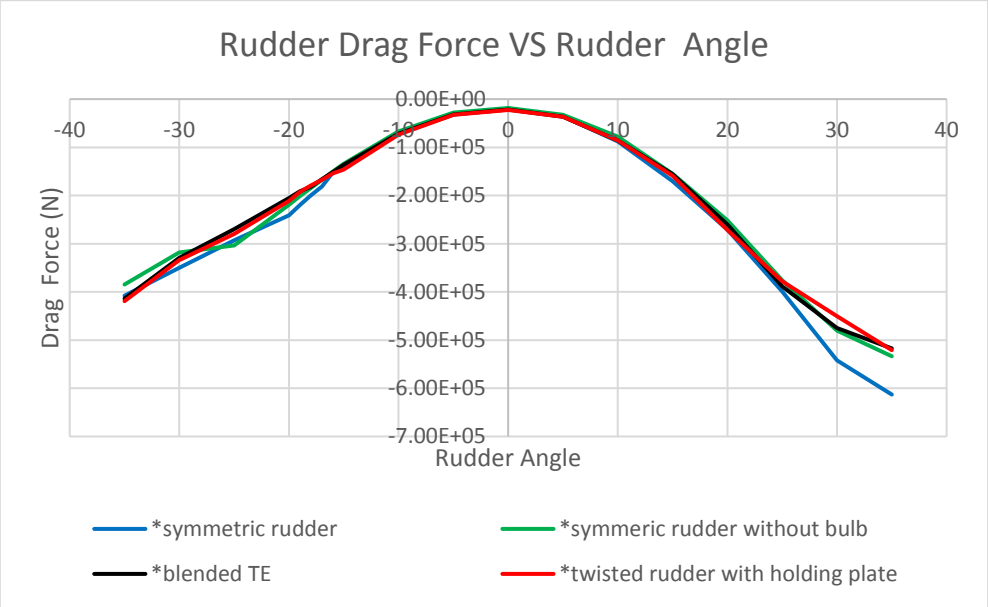

Figure 39-Drag force for new rudder geomeries

Symmetrical rudder without bulb showing good performance in shallow water case due to the absence of rudder bulb and twisted geometry and the flow around the four case investigated and flow seperation for symmetic rudder start at the flap side. So further reduced flap angle ratios will increase the rudder performance as well.

6.CONCLUSION AND RECOMMENDATIONS FOR FUTURE WORK

5.1 conclusion

Numerical method were used successfully to predict the performance of high lift Becker rudder at different rudder angle and flap angle combinations. Optimum rudder angle find from the existing rudder was performed well in Suez Canal condition at slow speed. The two dimensional CFD section study was using approximately 55000 grid nodes and the critical solver parameters have been identified. But when we comparing the two dimensional result with three dimensional CFD Section, there is big difference between them. Inaccurate prediction of the k-ε and k-ω SST turbulence model where found to be close to stall indicating over predicting of both model. This is the problem of all turbulence models. However the k-ω SST& Reynolds stress transport model seem to be predict the flow separation close to the real problem, but when we compare the computation coast k-ω SST model are relatively less price and showcase better flow separation prediction too.

In three dimension analysis used 5.5 million grid nodes to solve the flow around the rudder so the result almost meet the real analysis, in two dimension CFD analysis two section of the rudder only consider for the scope of work. But when the Becker twisted unsymmetrical rudder operated in shallow water for a large containership, the flow separation start from the rudder bulb. Rudder bulb act as strong separation point and the starting point of the twisted region also act as the separation point. Acceleration in rudder bulb create big interaction from propeller so big ship with high speed normally create a cavitation in that point. Hull force in shallow water is three times more than of the Deepwater so rudder side force can't provide a larger force than hull and it's the reason for lack of manoeuvring problem in shallow water. Normally in channels and near port assistance tug is available to manoeuvre the vessel to manage the lack of operation but all the shallow water assisting tug or another facilities are not available. One of the best solution is the reduction propeller RPM in this condition reduce the rudder interaction and avoid the unnecessary fuel consumption also.

Rudder bulb retrofit reduce the Hub vortex losses as well as the propeller rotation losses, but it will reduce the rudder performance in shallow water too. So the retrofit of rudder bulb need to balance both manoeuvring performance and reduction of losses like hub vortex and propeller rotation loses. More over ship manoeuvring is more prior importance than the fuel consumption reduction.

5.2 Recommendation for Future Work

Based on the result and experience obtained in the present project the folowing recommendations should be considerd with a view to continue the work and improve the method.

- All three dimensional analysis is done with the help of virtual disc with steady state so need to do a transient case with help of real propeller to sort out the more flow problems.
- Flap actuation mechanism may lead to accident due to the continuous expose operation, and also flap angles are fixed in nature, so need to find out an optimum flap angle for each rudder angle and to develop an independent hydraulic system for flap so this one operate independently from rudder. New independent hydraulic system with flap help to operate the small manoeuvring operation without moving rudder so this case reduce the operation cost of the vessel also.

7.REFFERNCES

[1] Hutchinson, *W. A Treatise on Naval Architecture,* 4th edition, 1794. New Impression 1969. The Conway Maritime Press, London.

[2] Joessel, Rapport sur des experiences relatives aux gouvernails. *Memorial du Genie Maritime,* Rapport 9, 1873.

[3] Lumley, H. On the steering of ships. *Transactions of the Royal Institution of Naval Arcbitects,* Vol. 5, 1864, pp. 128-134

[4]Denny, M.E. The design of balanced rudders of the spade type. *Transactions of the Royal Institution of Naval Architects,* Vol. 63, 1921, pp. 117-130.

[5] Bottomley, G.H. Manoeuvring of ships. Part II - Unbalanced rudders of twin screw ships. *Transactions of the Institute of Engineers and Shipbuilders in Scotland,* Vol. 67, 1923/24, pp. 509-559

[6] http://www.bpress.cn/im/tag/Becker-Marine-Systems/ [Accessed on11/01/2018]

[7] H. Kato and S. Motora, "Studies on Rudders with Flap", Journal of Society of Naval Architects, Japan, Vol. 124, 1968, pp. 93-104

[8] J. E. Kerwin, P. Mandel and S. D. Lewis, "An experimental study of a series of flapped rudders", Journal of Ship Research, Society of Naval Architects and Marine Engineers, December 1972, pp. 221-239.

[9] T. Lutz, A. Wolf and W. Würz, "Design and Verification of an Airfoil with Trailing-Edge Flap and Unsteady Wind-Tunnel Tests", UPWIND WP1B3 Technical Report, 2011

[10] G. A. Williamson, "Experimental Wind Tunnel Study of Airfoils with Large Flap Deflections at Low Reynolds Numbers", PhD Master of Science, University of Illinois, 2012

[11] J. C. Date, "Performance Prediction of High Lift Rudders operating under Steady and Periodic Flow Conditions", PhD thesis, Department of Ship Science, Faculty of Engineering, University of Southampton, May 2001

[12] S.-W. Chau, "Numerical Investigation of Free-Stream Rudder Characteristics Using A Multi-Block Finite Volume Method", PhD thesis, Institut für Schiffbau der Universität Hamburg, July 1997

[13] L. M. Milne-Thomson, "Theoretical Hydrodynamics", Dover Publications, New York, 1968, ISBN: 0-486-68970-0.

[14] A. F. Molland, S. R. Turnock, "Marine Rudders and Control Surfaces",Butterworth-Heinemann, 2007, ISBN 978-0-75-066944-3.

[15] B. Johnson, D. Clarke, C. Podenzana-Bonvino and K. Hasegawa,"International Towing Tank Conference ITTC Symbols and Terminology List,Prepared by the 22nd ITTC Symbols and Terminology Group", August 1999.

[16] DNV-GL, “Rules and Classification and Construction Part I”, Hamburg, 2013

[17] A. F. Molland, S. R. Turnock, „Wind Tunnel Investigation of the Influence of Propeller Loading on Ship Rudder Performance“, Ship Science Report No. 46,University of Southampton, March 1991.

[18] Reynolds, O. On the dynamical theory of incompressible viscous fluids and the determination of the criterion. Philosophical Transactions of the Royal Society, Series A, Vol. 186, 1895, pp. 123-164.

[19] Wilcox, D.C.1998. ‘Turbulnce modeling for CFD’. 2nd edition ,DCW Industries ,Inc.

[20] Boussinesq, J. Essai Sur La Theorie Des Eaux Courantes. Mem. Present'es Acad. Sci., Vol. 25, 1877.

[21]]Jones, W.P., and Launder, B.E. 1972. “The Prediction of Laminarization with a Two-Equation Model of Turbulence”, Int. J. Heat and Mass Transfer, 15, pp. 301-314.

[22] Launder, B.E., and Sharma, B.I. 1974. “Application of the Energy Dissipation Model of Turbulence to the Calculation of Flow Near a Spinning Disc”, Letter in Heat and Mass Transfer, vol. 1, no. 2, pp 131-138.

[23] Wilcox, D.C. 1998. “Turbulence Modeling for CFD”, 2nd edition, DCW Industries, Inc.

[24] Menter, F. R., "Two-Equation Eddy-Viscosity Turbulence Models for Engineering Applications," **AIAA Journal**, Vol. 32, No. 8, August 1994, pp. 1598-1605.

[25] Anderson, J.D. Computatioal Fluid Dynamics. The Basics with Applications.McGraw-Hill International Editions, New York, 1995.

[26] A. Stuck, S. R. Turnock and N. Bressloff, “An Evaluation of the RANS Method for the Prediction of Steady Ship Rudder Performance Compared to WindTunnel Measurements”, Ship Science Report No. 130, University of Southampton, January 2004.

[27] D. C. Eleni, T. I. Athanasios and M. P. Dionissios, “Evaluation of the turbulence models for the simulation of the flow over a National Advisory Committee for Aeronautics (NACA) 0012 airfoil”, Journal of Mechanical Engineering Research, Vol. 4(3) pp. 100-111, March 2012.

Appendix I

Table 16-ship speed vs rpm

Ship speed(Kt)	RPM
12	40.9
16	54.5
19	65.2
20	68.8
21	72.5
22	76.2
23	80
24	83.9
25	88.2

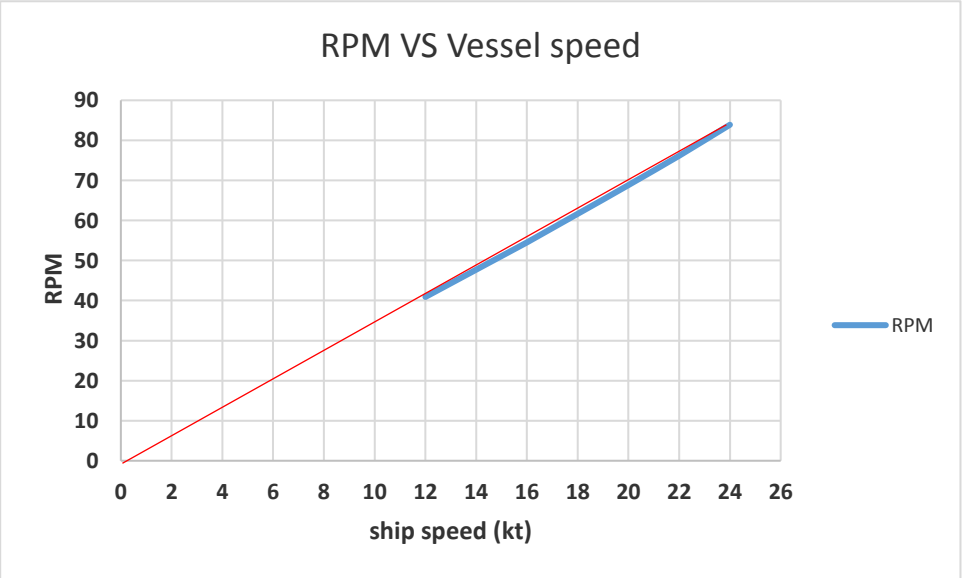

Table 17- Open water characteristics of ship at full scale

J	KT	KQ	ETA
0	0.4999	0.06541	0
0.05	0.4774	0.06267	0.061
0.1	0.4549	0.05993	0.121
0.15	0.4321	0.05718	0.18
0.2	0.4091	0.05442	0.239
0.25	0.3858	0.05166	0.297
0.3	0.3623	0.0489	0.354
0.35	0.3386	0.04614	0.409
0.4	0.3149	0.0434	0.462
0.45	0.2909	0.04064	0.513
0.5	0.2669	0.03785	0.561
0.55	0.2427	0.03504	0.606
0.6	0.2185	0.03218	0.648
0.65	0.1942	0.02924	0.687
0.7	0.1695	0.02622	0.72
0.75	0.1446	0.02309	0.748
0.8	0.1194	0.01985	0.766
0.85	0.0939	0.01648	0.77
0.9	0.0679	0.01298	0.749
0.95	0.0417	0.00938	0.673
1	0.0153	0.00569	0.427

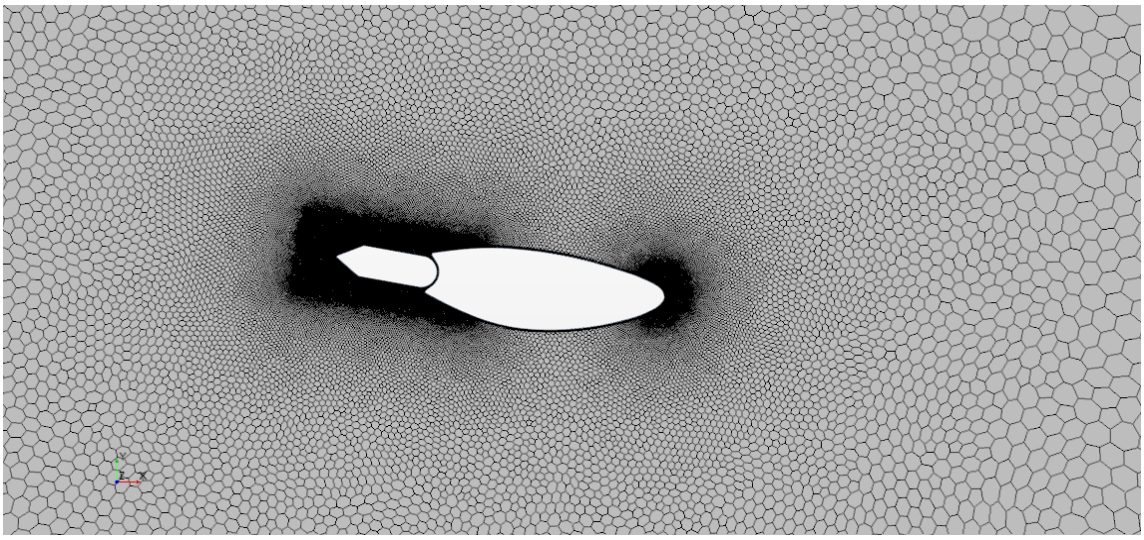

Figure 40-Mesh arrangment for 2D calculation

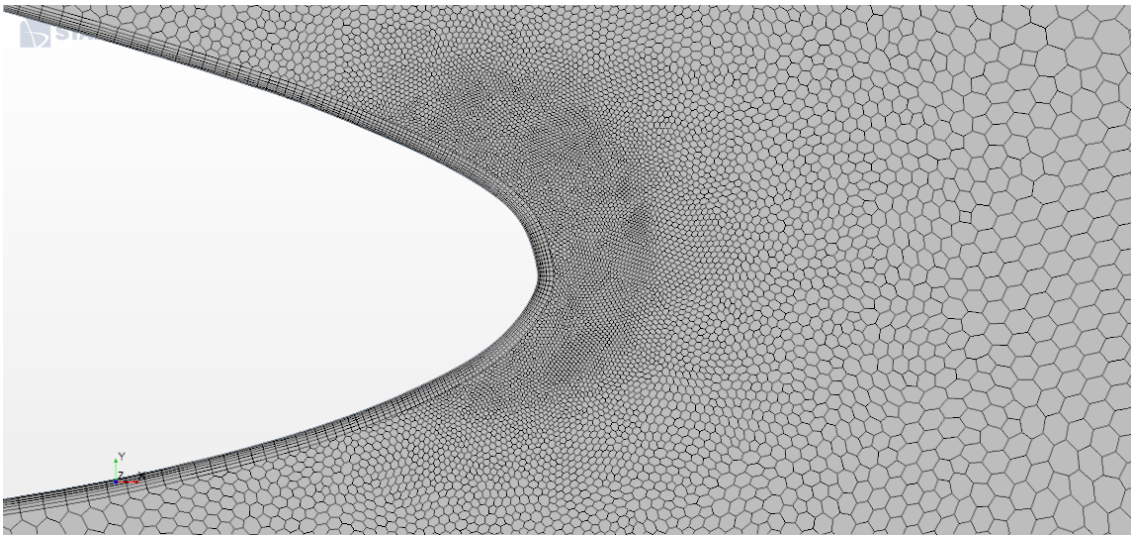

Figure 41 – Mesh setting at Leading edge

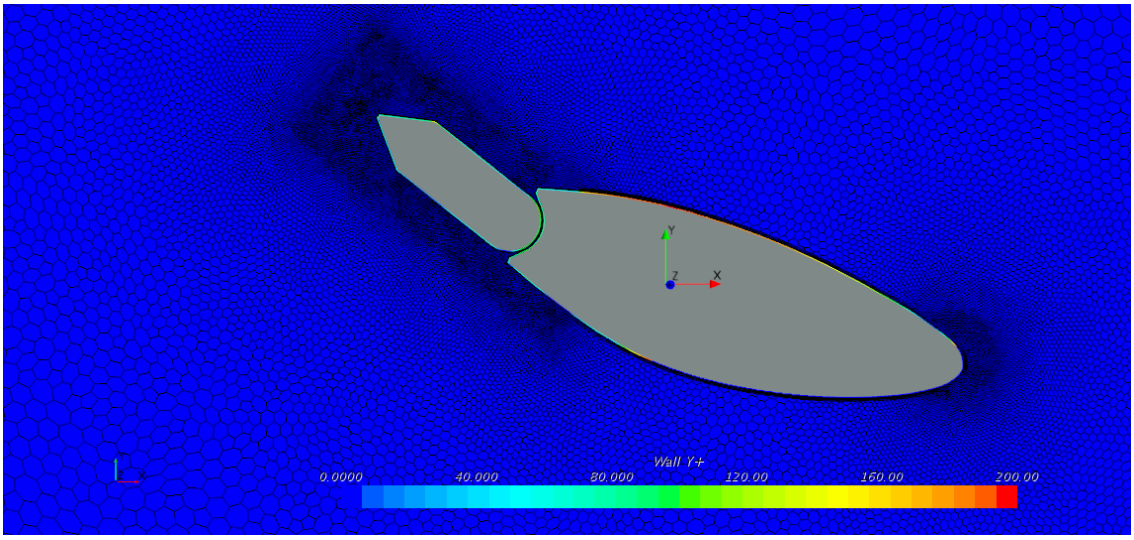

Figure 42-wall y+ value of Mesh settings

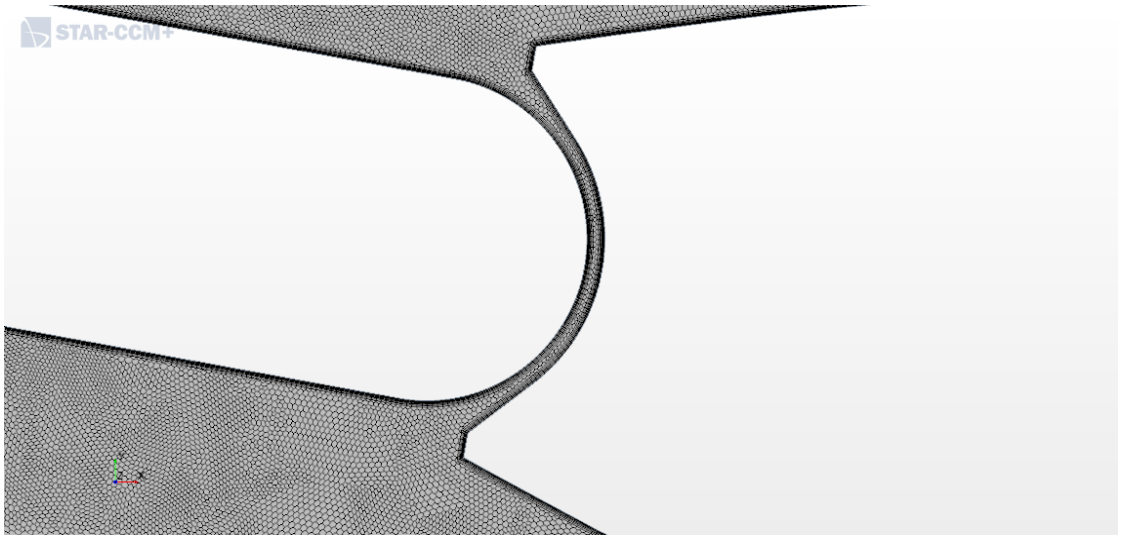

Figure 43 –Meshs setting at Rudder gap

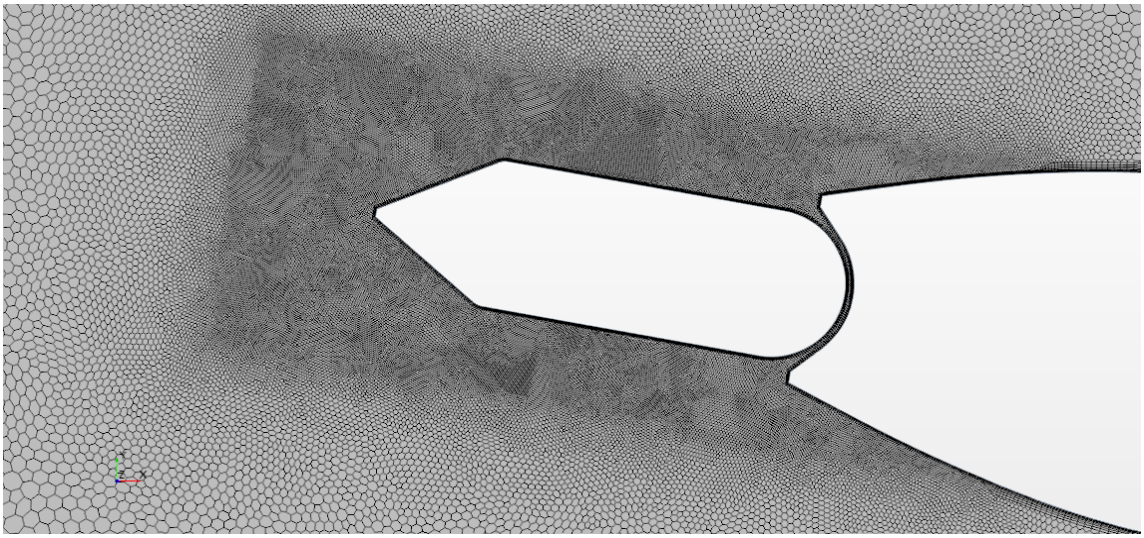

Figure 44-Mesh setting at Rudder Flap

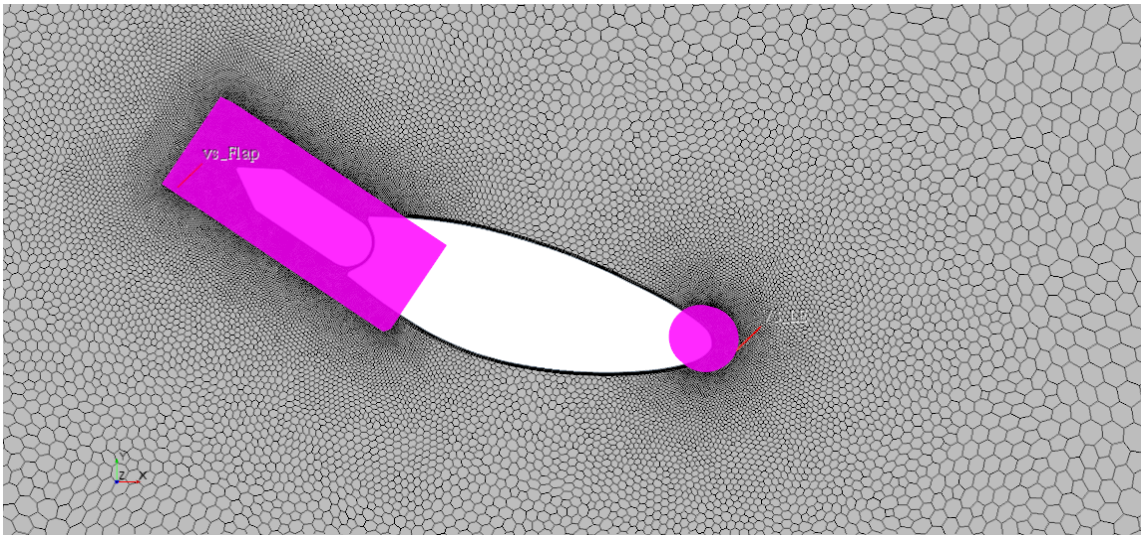

Figure 45- Volumeric sources used in flap and leading edge

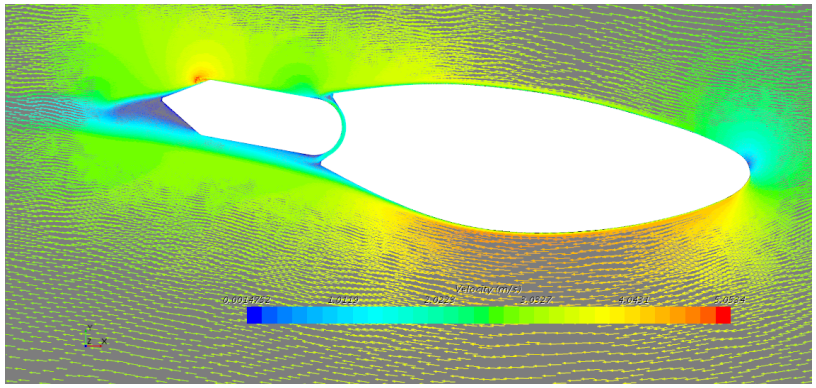

Figure 46-vector distribution at 0 deg (k epsilon turbulent model)

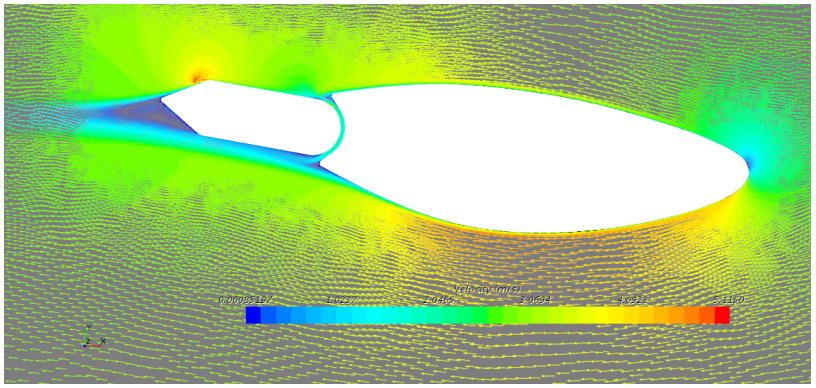

Figure 47- vector distribution at 0 deg(k –omega turbulent model)

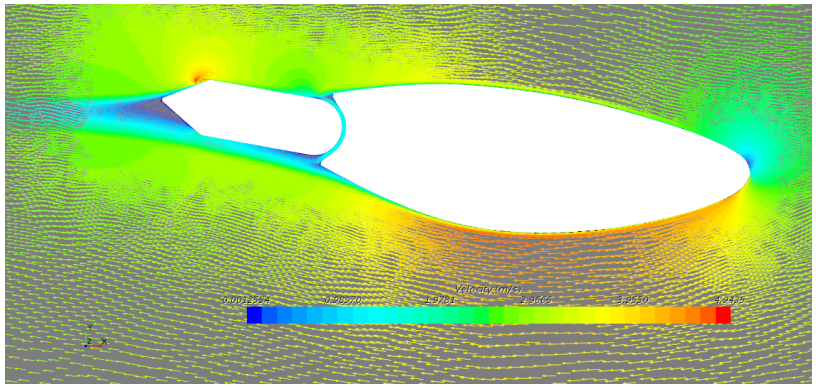

Figure 48- vector distribution at 0 deg (RST turbulent model)

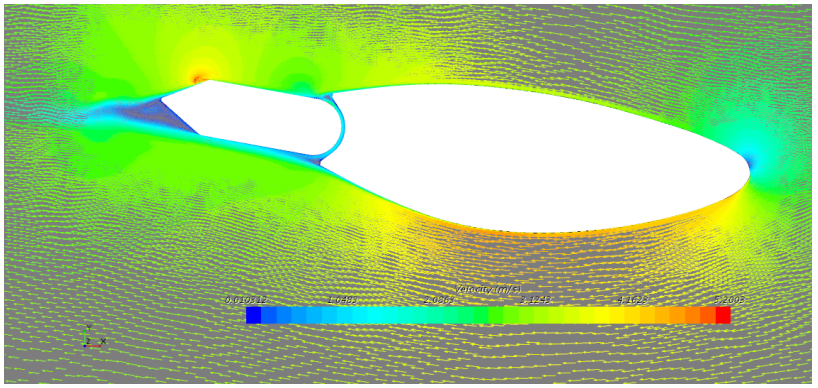

Figure 49- vector distribution at 0 deg(spalart allmars turbulent model)

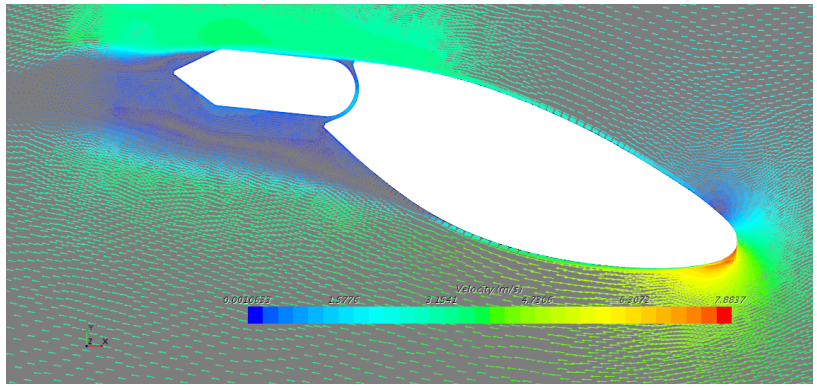

Figure 50- k epsilon turbulent model (vector disribution-15 deg)

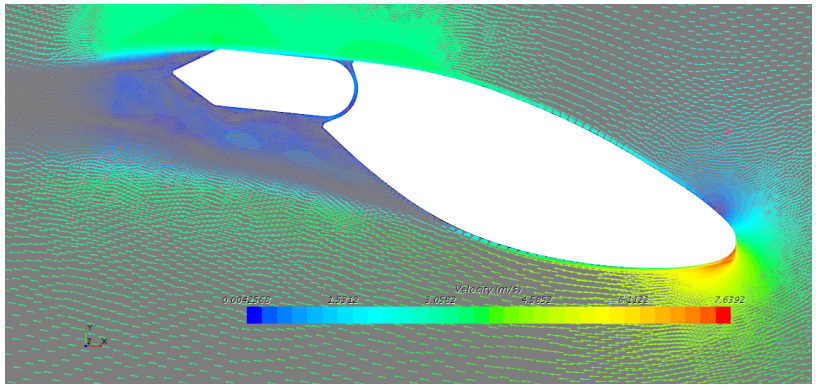

Figure 51- k omega turbulent model (vector disribution-15 deg)

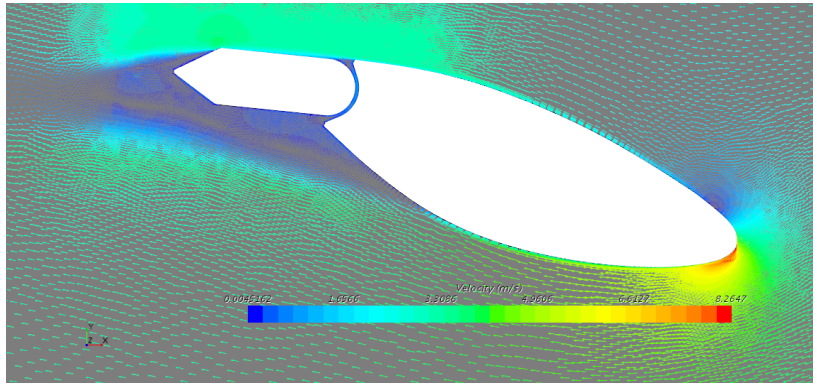

Figure 52- RST turbulent Model-(vector disribution-15 deg)

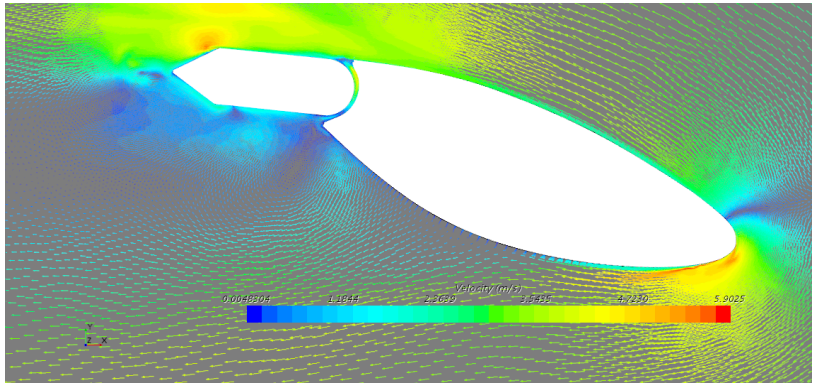

Figure 53- spalart allmars turbulent model-(vector disribution-15 deg)

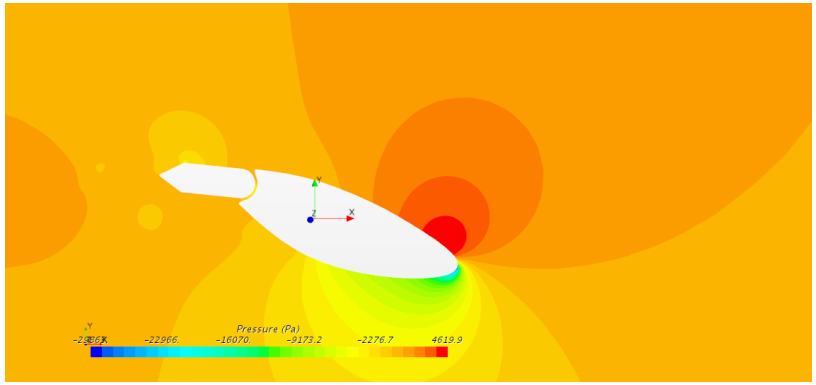

Figure 54-k epsilon turbulent model (pressure distribution-15 deg)

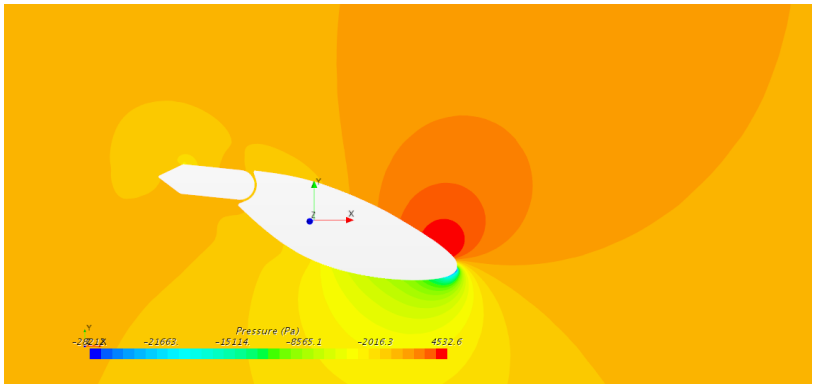

Figure 55-k omega turbulent model (pressure distribution-15 deg)

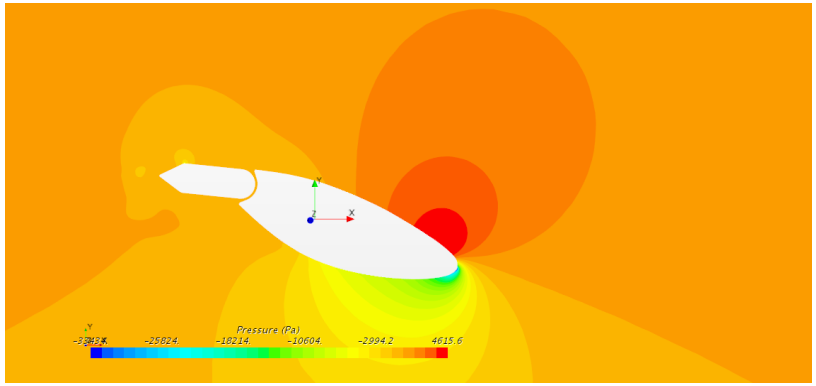

Figure 56-RST turbulent model (pressure distribution-15 deg)

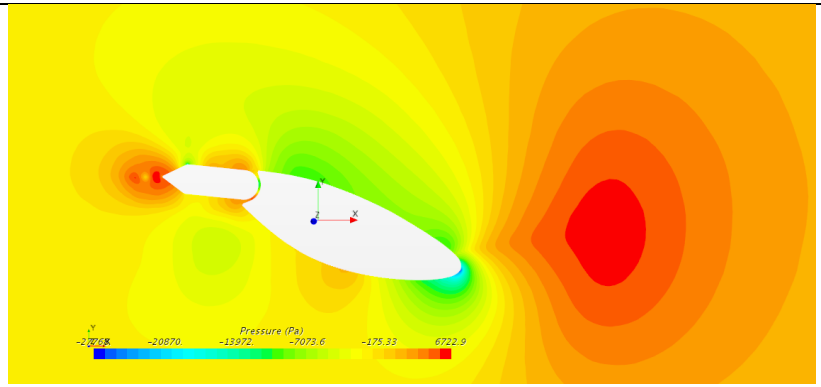

Figure 57-Spalart allmars turbulence model (pressure distribution-15 deg)

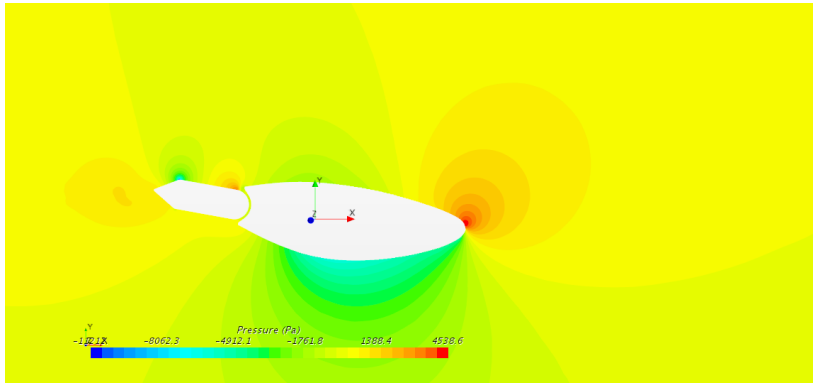

Figure 58-k epsilon turbulence model (pressure distribution-0deg)

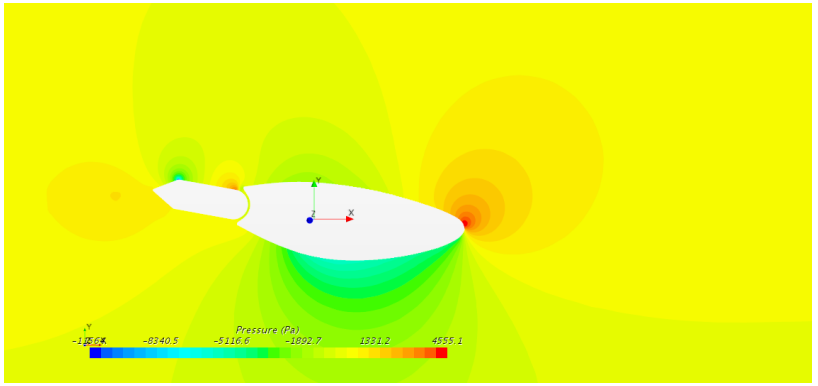

Figure 59-k omega turbulence model (pressure distribution-0deg)

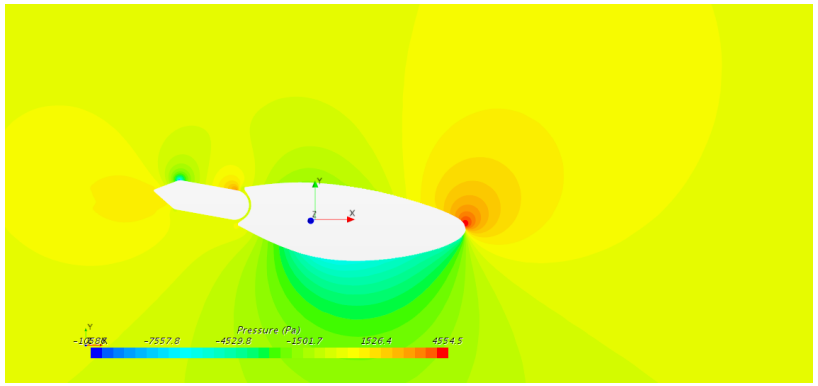

Figure 60-RST turbulent model (pressure distribution-0deg)

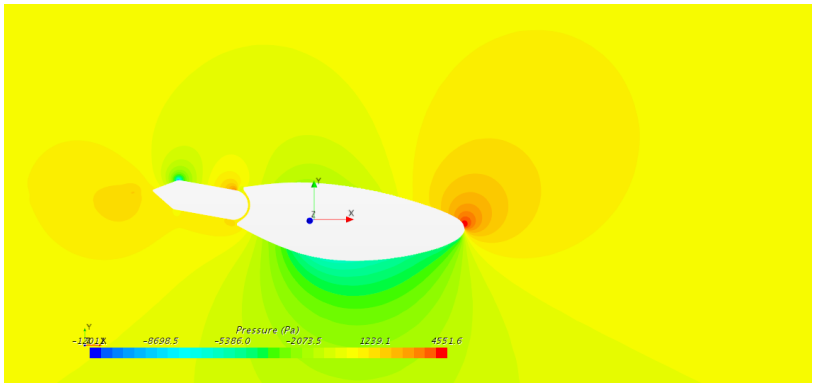

Figure 61-spalart allmars turbulence model (pressure distribution-0deg)

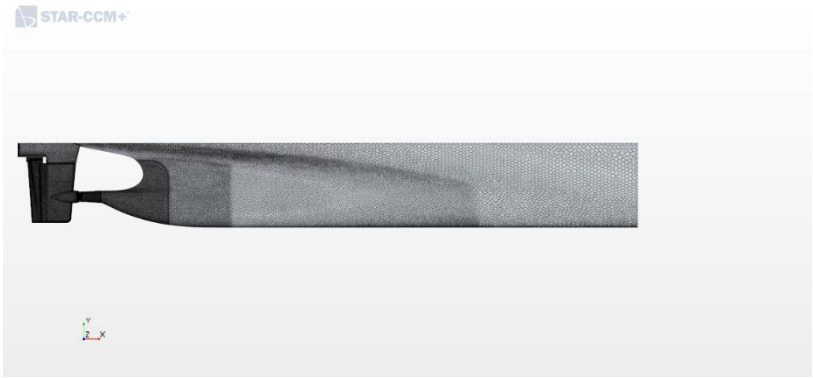

Figure 62- Ship profile mesh

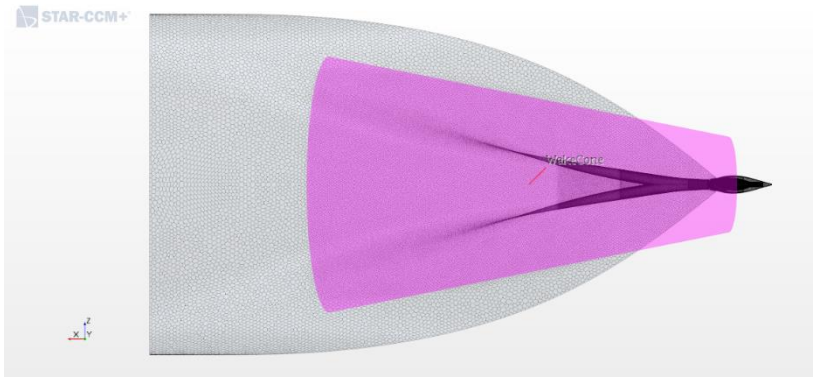

Figure 63- volumetric source for wake field (top view)

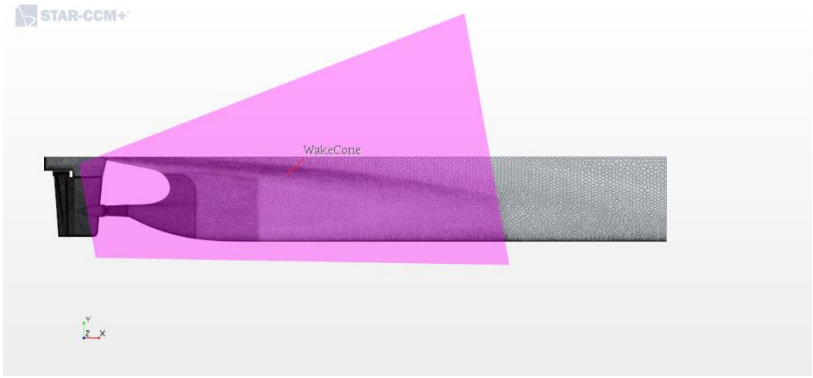

Figure 64-volumetric source for wake field (profile view)

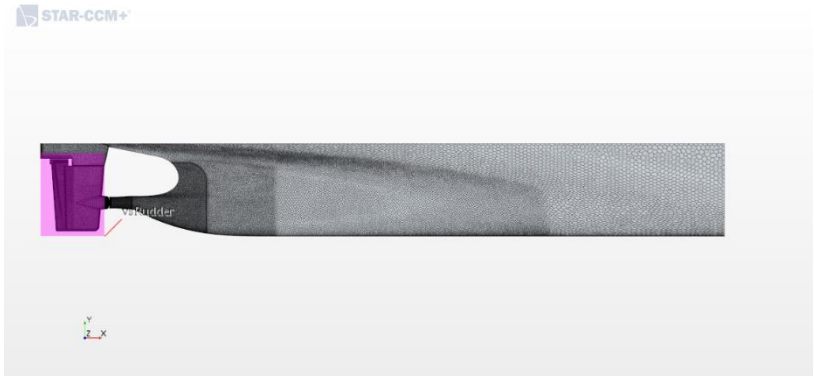

Figure 65- volumetric source for Rudder

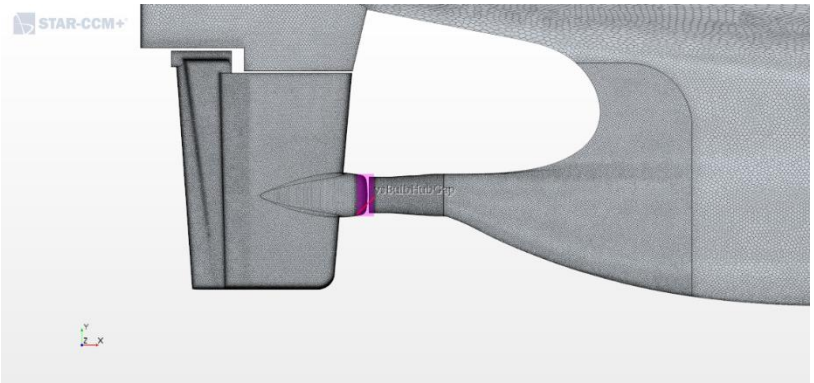

Figure 66- volumeric source for Rudder bulb gap

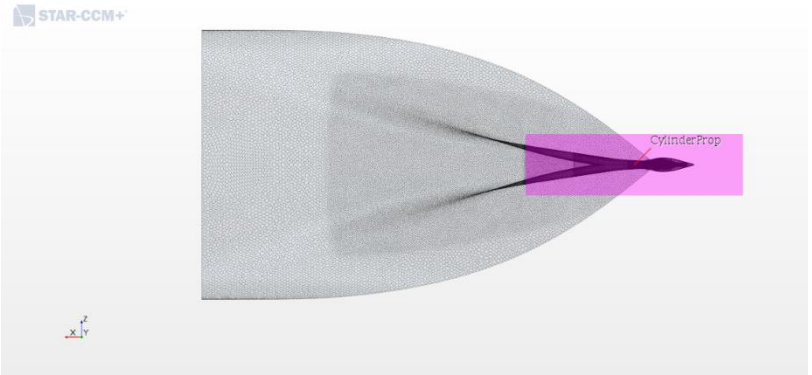

Figure 67- volume source for Propelelr cylinder

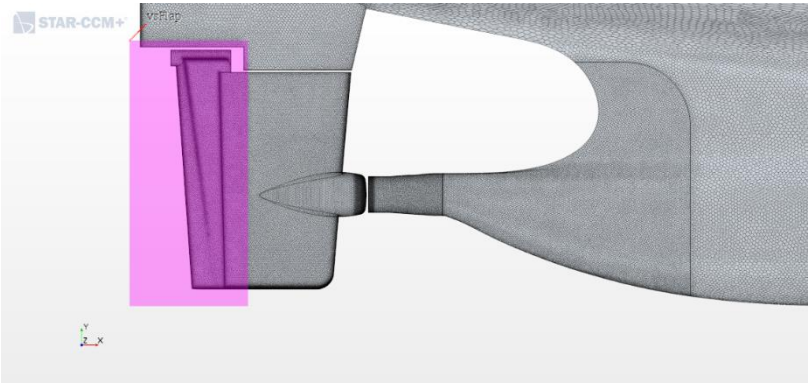

Figure 68 volumetric source for flap

Figure 69- volumetric source for cylinder propeller

Figure 70-shear stress distribution at 18 degree rudder angle with reduced flap angle (slow speed)

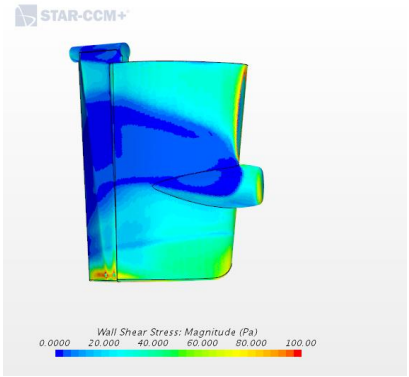

Flap angle 22.4 deg

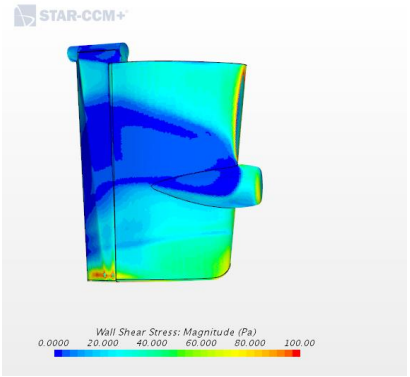

Flap angle 20.4 deg

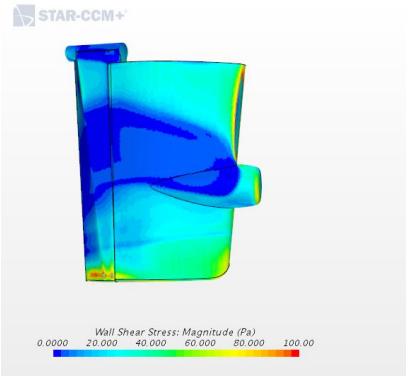

Flap angle 18.4 deg

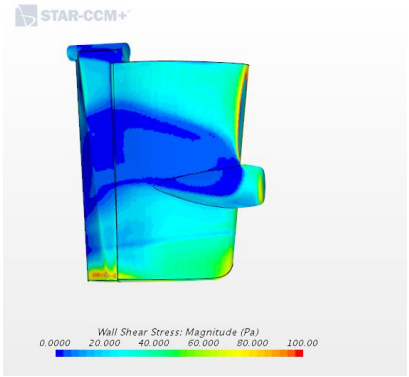

Flap angle 16.4 deg

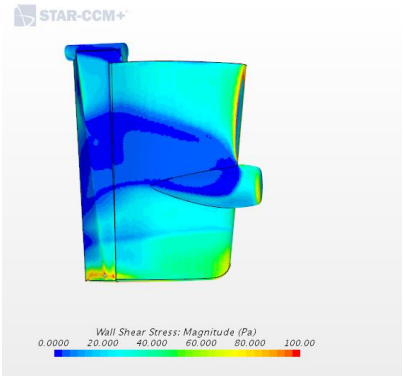

Flap angle 14.4 deg

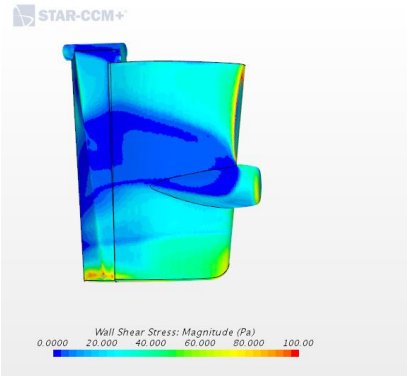

Flap angle 12.4 deg

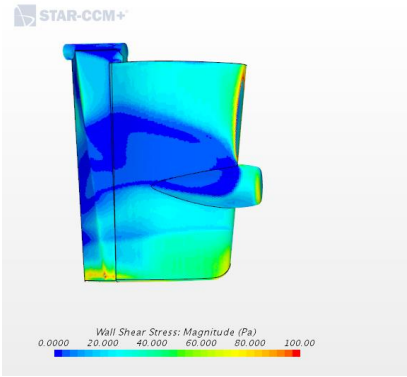 Flap angle 10.4 deg	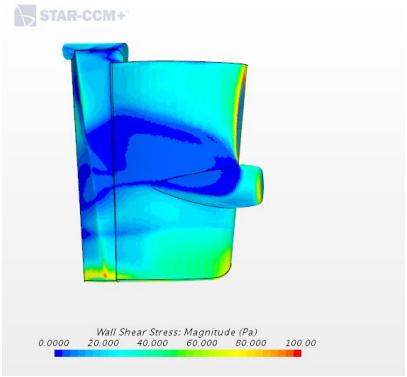 Flap angle 8.4 deg	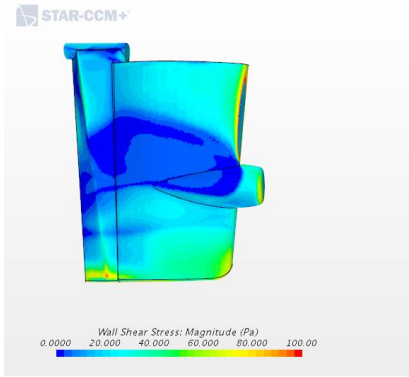 Flap angle 6.4 deg
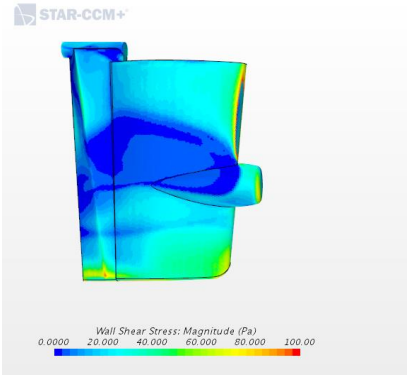 Flap angle 4.4 deg	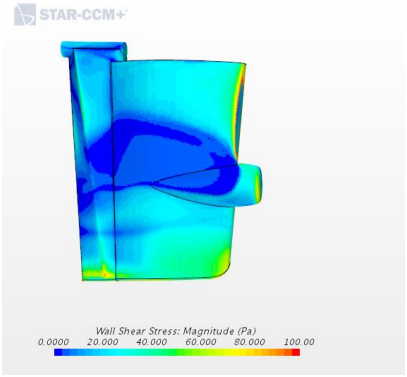 Flap angle 2.4 deg	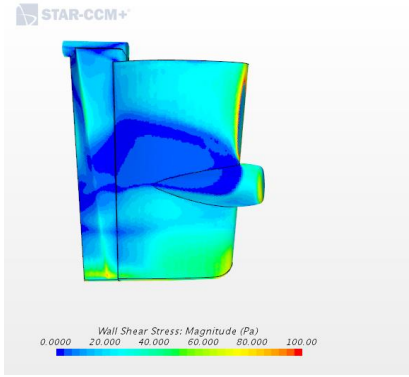 Flap angle 0 deg

Figure 71- shear stress distribution (Rudder angle 18deg flap 22.4 deg)

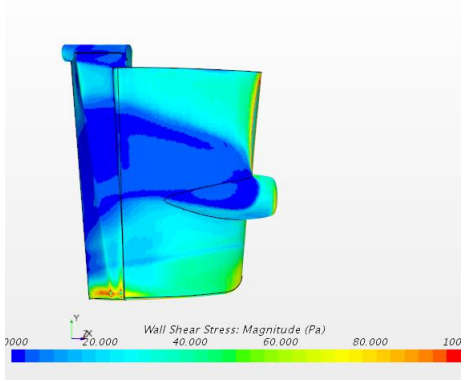

Normal domain condition

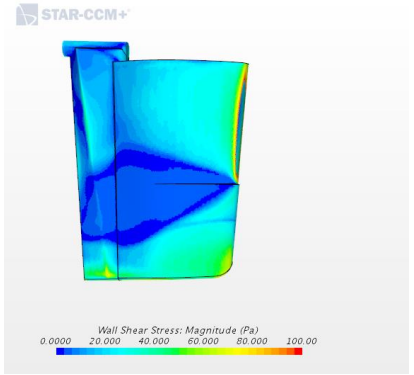

Rudder without bulb

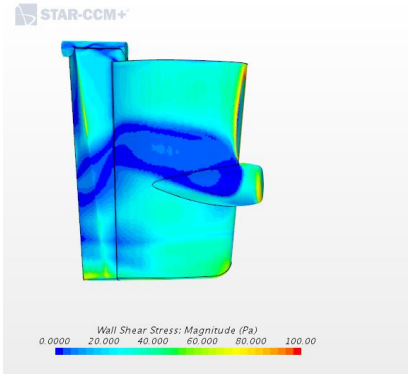

Reduced water depth condition (20 m)

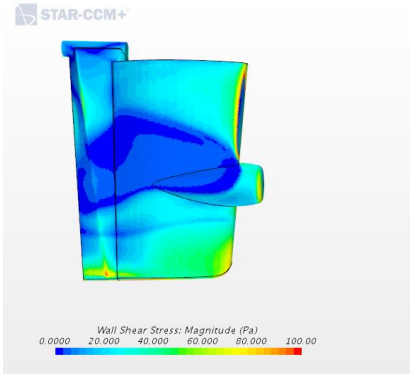

Increased water depth (600 m)

Figure 72- shear stress distribution (18 degree ruder angle 0 deg flap angle)

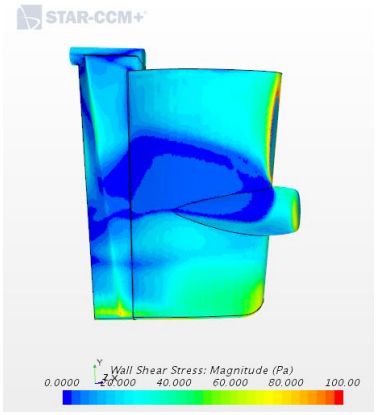

Normal domain condition

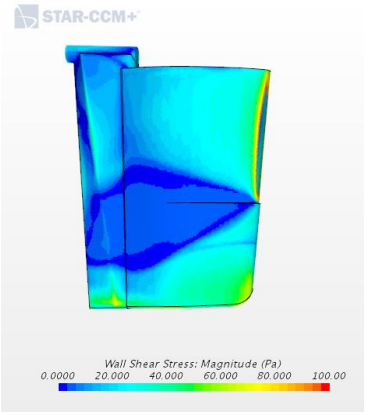

Rudder without Bulb

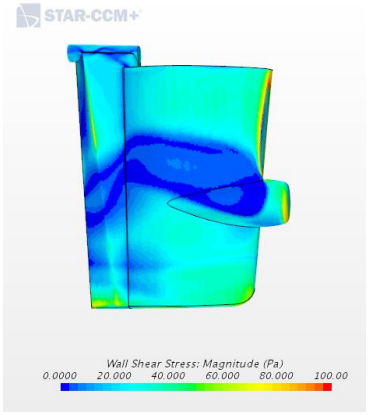

Reduced water depth (20m)

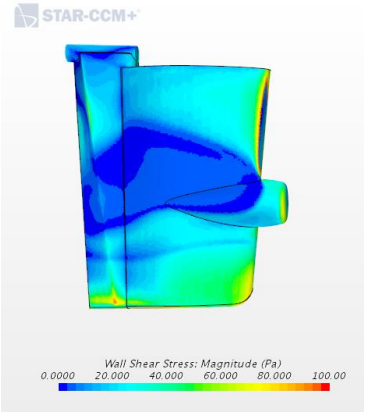

Increased water depth (600m)

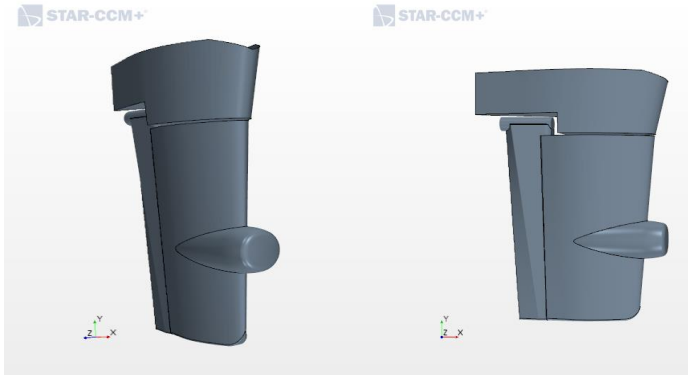

Figure 73-symmetric rudder with bulb

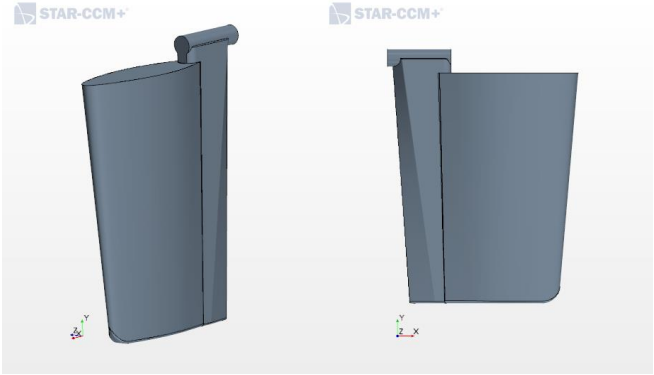

Figure 74-Symmetric rudder without bulb

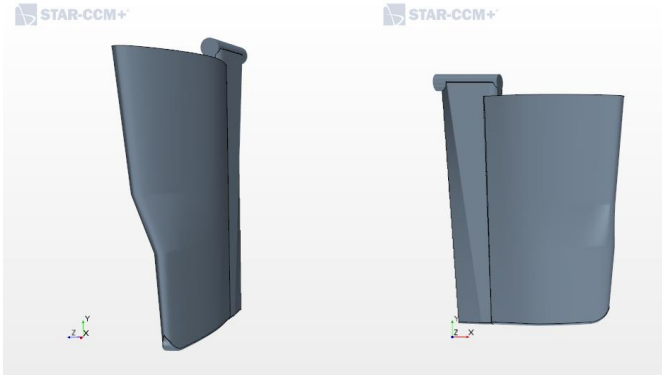

Figure 75-Twist blended rudder

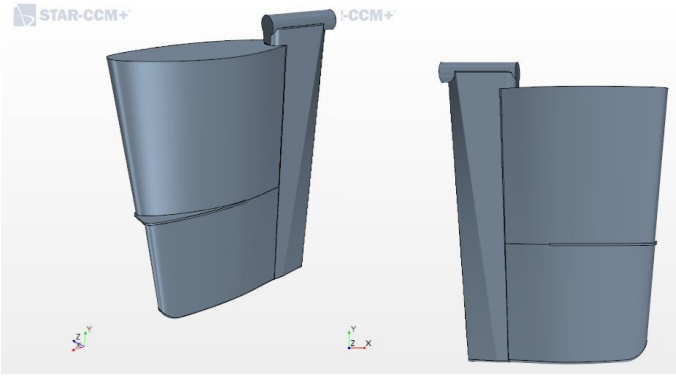

Figure 76- Twist plate rudder

Figure 77-shear stress distribution of existing rudder with slow speed

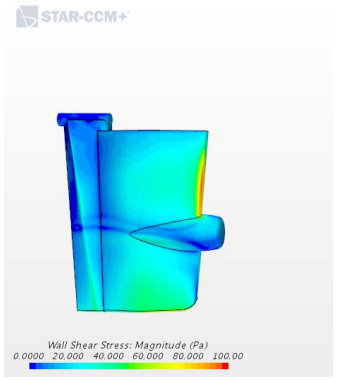 0 degRudder angle	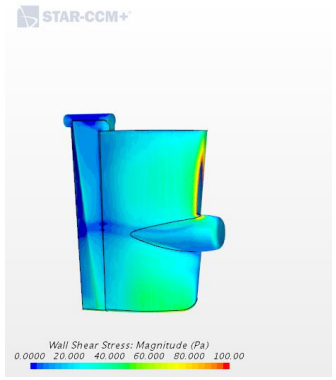 5 deg Rudder angle	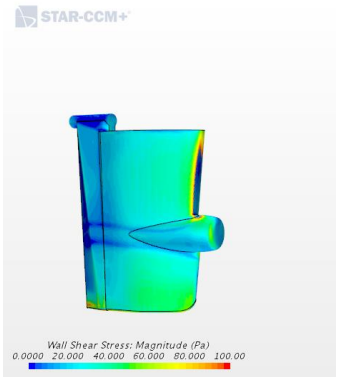 10 deg Rudder angle	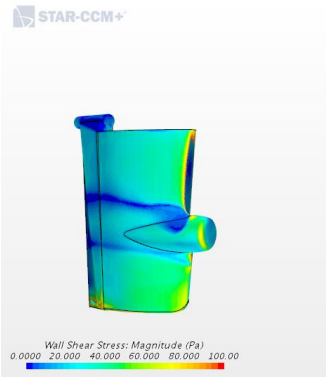 15 deg Rudder angle
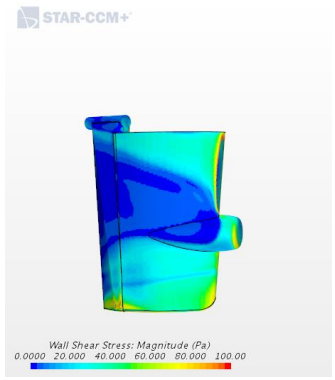 20 deg Rudder angle	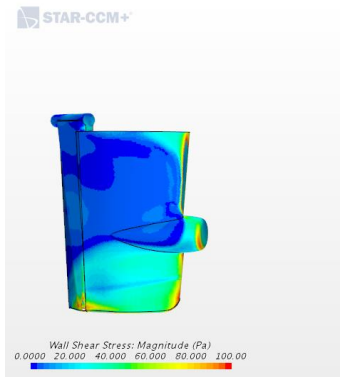 25 deg Rudder angle	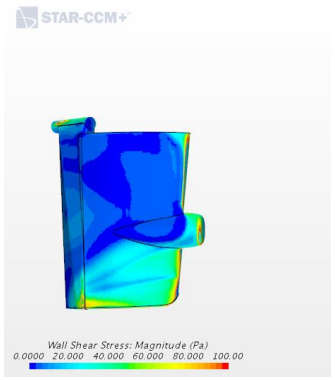 30 deg Rudder angle	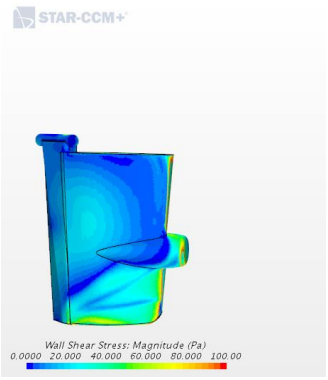 35 deg Rudder angle

Figure 78-Shear stress distribution for newly developed symmetrical rudder (rotating toward port side–slow speed)

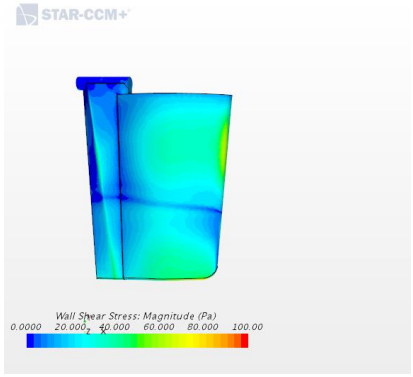

0 deg rudder angle

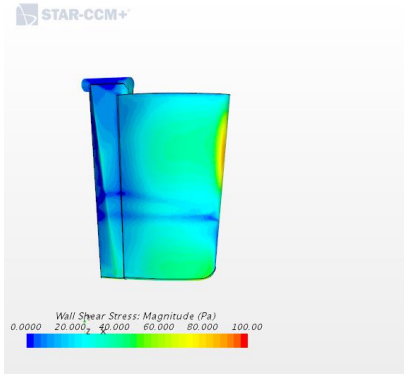

5 deg rudder angle

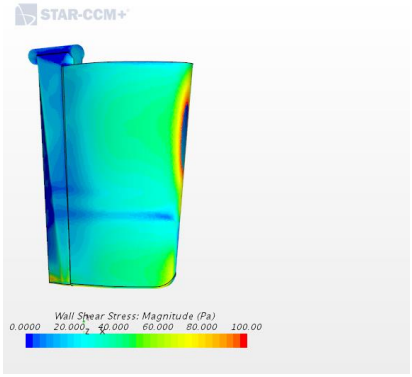

10 deg rudder angle

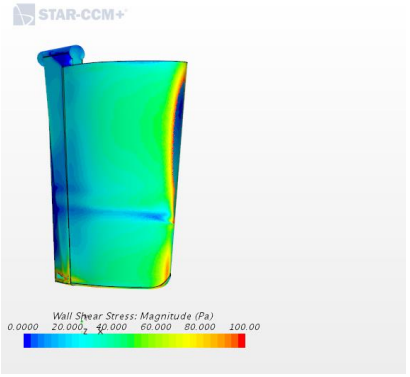

15 deg rudder angle

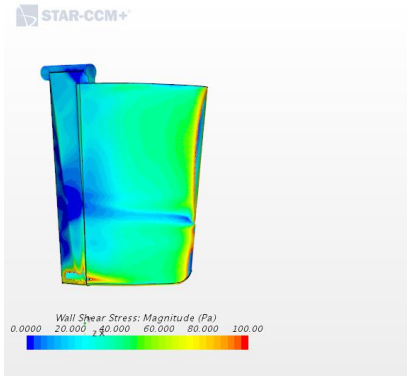

20 deg rudder angle

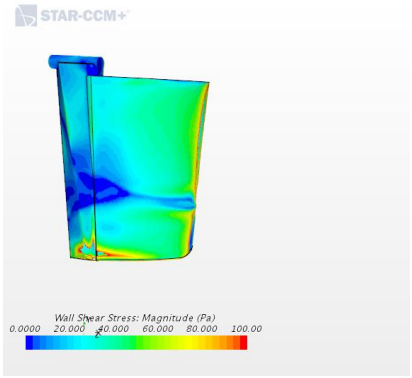

25 deg rudder angle

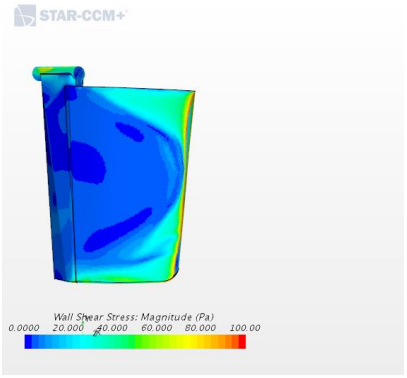

30 deg Rudder angle

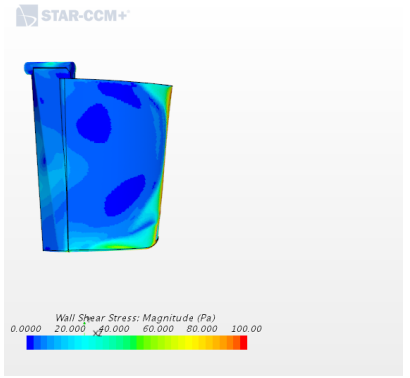

35 deg rudder angle

Appendix II

Table 18-Flap angle calculations

Distance between flap& Rudder rotation axis (a)	**2.07**																		
Distance between Rudder axis and fixed pivoted point (b)	**1.38**																		
a/b ratio	**1.5**																		
Existing Ratio																			
Rudder Angle	**0**	**2**	**4**	**6**	**8**	**10**	**12**	**14**	**16**	**18**	**20**	**22**	**24**	**26**	**28**	**30**	**32**	**34**	**35**
Rudder Angle (radian)	**0.00**	0.03	0.07	0.10	0.14	0.17	0.21	0.24	0.28	0.31	0.35	0.38	0.42	0.45	0.49	0.52	0.56	0.59	0.61
unknown distance ©	**0.69**	0.69	0.70	0.71	0.73	0.75	0.78	0.80	0.84	0.87	0.91	0.94	0.98	1.03	1.07	1.11	1.16	1.21	1.23
sin β	**0.00**	0.07	0.14	0.20	0.26	0.32	0.37	0.42	0.46	0.49	0.52	0.55	0.57	0.59	0.61	0.62	0.63	0.64	0.64
Flap angle, β (Radian)	**0.00**	0.07	0.14	0.20	0.27	0.33	0.38	0.43	0.47	0.51	0.55	0.58	0.61	0.63	0.65	0.67	0.68	0.69	0.70
Flap angle, β (Degree)	**0.00**	**3.99**	**7.90**	**11.68**	**15.27**	**18.63**	**21.72**	**24.55**	**27.10**	**29.38**	**31.40**	**33.18**	**34.74**	**36.10**	**37.26**	**38.26**	**39.10**	**39.81**	**40.11**

Distance between flap& Rudder rotation axis (a)	**2.07**																		
Distance between Rudder axis and fixed pivoted point (b)	**1.34**																		
a/b ratio	**1.55**																		
Ratio A																			
Rudder Angle	**0**	**2**	**4**	**6**	**8**	**10**	**12**	**14**	**16**	**18**	**20**	**22**	**24**	**26**	**28**	**30**	**32**	**34**	**35**
Rudder Angle (radian)	**0.00**	0.03	0.07	0.10	0.14	0.17	0.21	0.24	0.28	0.31	0.35	0.38	0.42	0.45	0.49	0.52	0.56	0.59	0.61
unknown distance ©	**0.73**	0.74	0.74	0.75	0.77	0.79	0.81	0.84	0.87	0.90	0.93	0.97	1.01	1.05	1.09	1.13	1.17	1.22	1.24
sin β	**0.00**	0.06	0.13	0.18	0.24	0.29	0.34	0.39	0.42	0.46	0.49	0.52	0.54	0.56	0.58	0.59	0.60	0.61	0.62
Flap angle, β (Radian)	**0.00**	0.06	0.13	0.19	0.24	0.30	0.35	0.40	0.44	0.48	0.51	0.54	0.57	0.59	0.61	0.63	0.65	0.66	0.67

Flap angle, β (Degree)	**0.00**	**3.63**	**7.20**	**10.66**	**13.96**	**17.08**	**19.98**	**22.65**	**25.09**	**27.29**	**29.27**	**31.03**	**32.58**	**33.95**	**35.14**	**36.17**	**37.05**	**37.80**	**38.13**

Distance between flap& Rudder rotation axis (a)	**2.07**
Distance between Rudder axis and fixed pivoted point (b)	**1.29**
a/b ratio	**1.60**
Ratio B	

Rudder Angle	**0**	**2**	**4**	**6**	**8**	**10**	**12**	**14**	**16**	**18**	**20**	**22**	**24**	**26**	**28**	**30**	**32**	**34**	**35**
Rudder Angle (radian)	0.00	0.03	0.07	0.10	0.14	0.17	0.21	0.24	0.28	0.31	0.35	0.38	0.42	0.45	0.49	0.52	0.56	0.59	0.61
unknown distance ©	0.78	0.78	0.78	0.79	0.81	0.83	0.85	0.87	0.90	0.93	0.96	1.00	1.03	1.07	1.11	1.15	1.19	1.23	1.25
sin β	0.00	0.06	0.12	0.17	0.22	0.27	0.32	0.36	0.40	0.43	0.46	0.49	0.51	0.53	0.55	0.56	0.58	0.59	0.59
Flap angle, β (Radian)	0.00	0.06	0.12	0.17	0.22	0.28	0.32	0.37	0.41	0.44	0.48	0.51	0.53	0.56	0.58	0.60	0.61	0.63	0.63
Flap angle, β (Degree)	0.00	3.33	6.60	9.79	12.86	15.76	18.49	21.02	23.34	25.46	27.38	29.11	30.65	32.01	33.21	34.26	35.17	35.95	36.30

Distance between flap& Rudder rotation axis (a)	**2.07**
Distance betwwen Rudder axis and fixed pivoted point (b)	**1.25**
a/b ratio a/b	**1.65**
Ratio C	

Rudder Angle	**0**	**2**	**4**	**6**	**8**	**10**	**12**	**14**	**16**	**18**	**20**	**22**	**24**	**26**	**28**	**30**	**32**	**34**	**35**
Rudder Angle (radian)	0.00	0.03	0.07	0.10	0.14	0.17	0.21	0.24	0.28	0.31	0.35	0.38	0.42	0.45	0.49	0.52	0.56	0.59	0.61
unknown distance ©	0.82	0.82	0.82	0.83	0.85	0.86	0.88	0.91	0.93	0.96	0.99	1.02	1.06	1.09	1.13	1.17	1.21	1.25	1.27
sin β	0.00	0.05	0.11	0.16	0.21	0.25	0.30	0.34	0.37	0.40	0.43	0.46	0.48	0.50	0.52	0.54	0.55	0.56	0.57
Flap angle, β (Radian)	0.00	0.05	0.11	0.16	0.21	0.26	0.30	0.34	0.38	0.42	0.45	0.48	0.50	0.53	0.55	0.57	0.58	0.60	0.60
Flap angle, β (Degree)	0.00	3.07	6.10	9.06	11.91	14.63	17.20	19.59	21.81	23.85	25.71	27.40	28.91	30.27	31.47	32.53	33.46	34.26	34.62

Distance between flap& Rudder rotation axis (a)	**2.07**																		
Distance between Rudder axis and fixed pivoted point (b)	**1.22**																		
a/b ratio	**1.70**																		
Ratio D																			
Rudder Angle	**0**	**2**	**4**	**6**	**8**	**10**	**12**	**14**	**16**	**18**	**20**	**22**	**24**	**26**	**28**	**30**	**32**	**34**	**35**
Rudder Angle (radian)	0.00	0.03	0.07	0.10	0.14	0.17	0.21	0.24	0.28	0.31	0.35	0.38	0.42	0.45	0.49	0.52	0.56	0.59	0.61
unknown distance ©	0.85	0.85	0.86	0.87	0.88	0.90	0.91	0.94	0.96	0.99	1.02	1.05	1.08	1.11	1.15	1.18	1.22	1.26	1.28
sin β	0.00	0.05	0.10	0.15	0.19	0.24	0.28	0.31	0.35	0.38	0.41	0.44	0.46	0.48	0.50	0.51	0.53	0.54	0.55
Flap angle, β (Radian)	0.00	0.05	0.10	0.15	0.19	0.24	0.28	0.32	0.36	0.39	0.42	0.45	0.48	0.50	0.52	0.54	0.56	0.57	0.58
Flap angle, β (Degree)	0.00	2.85	5.67	8.43	11.09	13.65	16.07	18.34	20.46	22.42	24.22	25.86	27.35	28.68	29.88	30.94	31.88	32.70	33.07

Table 19-2D rudder performance calculation at +0.7 R section (port side with slow speed)

Rudder Angle (Deg)	Lift Force					Drag Force				
	EXISTING	RATIO A	RATIO B	RATIO C	RATIO D	EXISTING	RATIO A	RATIO B	RATIO C	RATIO D
0	20601.65	20601.65	20601.65	20601.65	20601.65	604.04	604.04	604.04	604.04	604.04
2	31465.44	30651.96	30030.17	29635.98	29231.68	770.61	764.89	756.83	751.42	746.84
4	42825.03	41848.03	41096.21	39931.31	40166.06	1567.21	1350.24	1288.03	1211.89	1021.26
6	49630.10	52157.02	48779.86	46898.45	48507.58	2080.71	2527.60	2011.88	1892.48	2036.48
8	54052.27	53175.03	52562.54	49930.02	51288.25	2713.11	2535.52	2558.91	2063.37	2411.72
10	57397.67	56645.86	57247.20	55951.59	55845.77	3942.39	3648.51	2987.22	3341.41	3278.24
12	64518.45	59937.46	60144.33	58890.65	56747.59	4576.33	4292.00	4395.20	3992.17	3623.91
14	46901.41	64991.73	64730.88	60965.21	57614.01	6247.88	5353.89	5273.41	5190.07	4465.63
16	64584.23	65083.03	63688.52	62019.06	60434.67	7064.73	7407.80	6707.38	6611.41	6298.47
18	66134.33	65825.26	65680.81	62105.89	63843.96	8153.13	7843.88	8301.81	7638.60	7291.84
20	61774.37	66125.38	59627.54	55574.34	63390.66	10320.58	9730.15	12085.42	8939.05	9310.49
22	56769.84	51372.54	64724.44	52114.22	54347.42	16064.96	14516.89	10677.46	13484.11	13506.48
24	44335.59	44744.62	38823.39	43732.94	42669.26	29478.15	27820.00	36464.16	24717.38	26780.97
26	44232.12	42796.73	40614.32	43929.47	41991.79	34589.91	31249.24	31243.96	30853.44	32726.39
28	41626.26	42564.61	43728.00	44308.58	42769.64	35659.09	35411.50	33958.41	34817.18	32414.95
30	44873.87	46494.97	42868.04	42947.16	40491.08	41453.78	41483.13	37573.11	37619.67	39442.67
32	44923.21	45874.73	45335.67	42336.44	43860.76	44363.26	44644.85	43309.24	41069.00	43276.66
34	42520.15	40274.13	41561.21	43139.81	42708.27	45261.25	44021.66	43400.76	44371.60	45254.06
35	44672.45	41000.99	44105.54	44005.01	41511.43	48674.44	45621.98	47394.46	44393.01	43894.09

Table 20-2D rudder performance calculation at -0.7 R section (stb side with slow speed)

Rudder Angle (Deg)	Lift Force					Drag Force				
	EXISTING	RATIO A	RATIO B	RATIO C	RATIO D	EXISTING	RATIO A	RATIO B	RATIO C	RATIO D
0	1169.01	1169.01	1169.01	1169.01	1169.01	433.01	433.01	433.01	433.01	433.00
2	2500.17	2430.92	2262.50	2233.39	2164.90	271.83	268.97	258.74	285.47	273.42
4	3264.35	3135.20	3046.42	2932.15	2848.07	191.88	244.33	155.54	188.88	156.95
6	3867.61	3643.79	3489.83	3416.91	3292.26	106.79	88.64	84.55	75.62	89.50
8	4497.71	4356.42	4232.47	4005.42	3870.44	235.01	153.57	121.61	118.66	54.57
10	5185.82	4880.83	4812.93	4399.74	4368.71	189.80	131.10	189.11	78.69	71.06
12	4823.27	4954.91	5573.12	5551.38	5164.53	450.43	317.23	47.93	0.74	21.00
14	5370.48	6150.10	5319.76	5467.46	4948.87	1552.44	1203.52	732.69	768.43	481.81
16	4796.29	6276.86	5084.22	5773.24	5167.16	2080.45	1874.42	1432.21	892.48	910.01
18	5500.50	5859.03	5773.36	5983.57	5854.66	1770.74	1629.91	2277.97	2380.45	1853.69
20	6024.06	6040.52	5785.38	5581.48	6215.33	3228.74	3205.92	2607.10	1774.36	2428.40
22	3707.74	5630.87	5398.83	5888.87	5833.46	4011.83	3038.35	3631.08	2385.76	2352.64
24	3469.06	5180.11	4923.68	5902.88	5568.90	3669.26	5277.16	4153.94	3613.03	2751.10
26	4455.68	4887.14	5253.19	4809.12	5207.55	4396.12	4419.26	4204.75	5078.72	2334.84
28	5354.81	4129.23	4694.34	4585.89	3769.88	6479.23	4513.08	6199.51	3752.20	3633.80
30	4240.98	6853.93	5744.02	5210.47	4727.94	5516.14	737.73	5907.01	5514.18	5561.04
32	3710.97	5256.26	4158.66	4768.07	4690.71	6455.15	2176.72	6394.31	6342.04	5174.854
34	3547.28	4150.60	4477.81	4557.99	5079.18	6834.36	3922.12	6478.32	5561.41	6339.35
35	3810.04	5605.92	4278.82	4595.71	4479.31	7355.29	2248.98	6207.25	5730.82	6530.84

Table 21-2D rudder performance calculation at -0.7 R section (port side with slow speed)

Rudder Angle (Deg)	Lift Force					Drag Force				
	EXISTING	RATIO A	RATIO B	RATIO C	RATIO D	EXISTING	RATIO A	RATIO B	RATIO C	RATIO D
0	1169.01	1169.01	1169.01	1169.01	1169.01	433.01	433.01	433.01	433.01	433.00
2	370.67	245.91	128.33	47.10	26.79	390.20	411.13	424.91	429.72	436.11
4	2029.17	1768.21	1566.69	1385.92	1244.95	119.04	157.21	217.48	244.69	273.14
6	3561.58	3197.26	2975.95	2696.83	2492.47	133.21	102.70	26.20	13.33	57.68
8	4874.28	4533.24	4216.47	3910.22	3684.86	197.71	159.25	139.13	90.81	35.63
10	5773.47	5461.87	5249.05	4939.61	4694.80	40.85	12.86	56.43	77.89	66.30
12	6103.95	5961.20	5748.80	5607.15	5406.77	334.16	296.49	107.90	122.24	50.72
14	6698.61	6319.51	5986.85	5907.68	5777.96	727.55	532.86	311.79	299.38	296.48
16	7066.59	6725.37	6509.65	6224.27	5944.37	1051.82	943.14	711.38	741.48	430.64
18	7078.16	7055.33	6804.48	6361.14	6257.41	1319.51	1178.62	1056.82	900.65	778.46
20	6864.03	7240.07	6886.04	6827.93	6456.31	1444.38	1444.26	1300.45	1280.51	1112.99
22	6907.16	6888.86	6768.28	6682.93	6829.60	1853.24	1632.01	1494.81	1299.05	1489.97
24	6975.10	6831.40	6849.69	6548.48	6761.01	2423.50	1990.62	1746.19	1536.38	1485.29
26	6390.54	6995.78	6691.48	6649.31	6466.48	2107.70	2145.19	1763.32	1616.53	1594.44
28	4651.92	6191.17	6657.95	6629.54	6450.25	2918.51	2457.47	2088.53	1660.30	1381.53
30	4170.04	6853.94	6949.70	6625.45	6396.37	3137.42	737.74	1860.67	1764.41	1522.75
32	4859.25	5256.27	5692.53	5915.29	6183.15	3144.05	2176.72	1966.027	1566.91	984.19
34	3647.07	4150.61	5744.04	4449.19	4227.01	3625.49	3922.13	2578.47	3446.33	2756.65
35	5101.31	5605.92	6261.97	4077.87	5831.37	1907.71	2248.98	995.41	3479.16	1163.84

Table 22-2D rudder performance calculation at +0.7 R upper section (port side with cruise speed)

Rudder Angle (Deg)	Lift Force					Drag Force				
	EXISTING	RATIO A	RATIO B	RATIO C	RATIO D	EXISTING	RATIO A	RATIO B	RATIO C	RATIO D
0	189587.89	189587.89	189587.89	189587.89	189587.89	4861.90	4861.90	4861.90	4861.90	4861.90
2	294808.57	287504.52	282215.10	278488.03	273797.19	6360.53	6294.74	6187.57	6267.30	6156.00
4	441044.68	426199.41	413629.02	405575.66	396248.79	8210.98	7991.41	7777.78	7830.78	7653.29
6	488650.67	475330.11	541074.22	458040.17	477897.70	19489.70	19162.89	9861.57	15106.49	11226.26
8	524879.45	518702.52	542078.33	514453.31	501992.43	22643.12	22673.17	22326.37	23171.76	19223.75
10	553773.73	550555.35	547534.06	538453.41	526755.15	31378.17	30101.76	24874.89	26346.44	25219.83
12	599019.97	600083.46	593039.64	576639.48	564798.53	37374.18	37027.11	35011.84	33154.32	33644.19
14	628485.93	624680.27	606888.79	610978.22	589444.68	51074.36	44537.58	42717.56	41843.01	42226.31
16	656774.05	633546.27	455840.14	488778.47	433667.04	58149.03	59760.63	49248.60	47729.98	56370.69
18	648210.42	655001.82	650766.57	642987.66	631592.67	71707.82	69090.22	62749.99	63483.55	59292.84
20	656897.61	653702.21	646051.11	642935.11	631547.57	86897.81	81032.98	81306.48	75912.62	73898.94
22	380043.135	674873.60	362003.95	648684.37	630274.51	162875.787	91484.77	185592.88	94430.979	85811.10
24	611019.227	371868.73	383315.13	368862.56	533315.20	129146.565	192288.27	192731.42	199388.56	138637.60
26	418061.293	347244.75	353852.14	381608.483	402774.11	188640.504	249919.71	217708.83	246942.14	280197.73
28	386818.076	407465.05	399954.92	410220.737	360240.85	307954.95	310283.95	317413.212	319604.19	252181.49
30	394418.611	385757.35	399517.92	379075.183	370288.82	374017.233	334821.68	331380.46	332113.71	282440.07
32	414268.348	405453.75	392929.00	399165.441	383782.40	403912.04	374906.83	364271.39	363069.713	357016.93
34	382250.448	387540.52	411201.80	398137.775	394390.95	384961.567	401223.55	436714.94	408412.6	389667.29
35	378635.028	359343.31	409201.69	385500.124	381095.58	431636.06	388832.06	412065.97	415490.103	384499.17

Table 23-2D rudder performance calculation at -0.7 R lower section (port side with cruise speed)

Rudder Angle (Deg)	Lift Force					Drag Force				
	EXISTING	RATIO A	RATIO B	RATIO C	RATIO D	EXISTING	RATIO A	RATIO B	RATIO C	RATIO D
0	11255.26	11255.26	11255.26	11255.26	11255.26	3854.05	3854.05	3854.05	3854.05	3854.05
2	23207.06	22806.94	22041.65	21179.01	20348.41	1785.35	1949.33	1985.76	1986.10	2087.90
4	30687.78	29766.23	28678.05	27821.35	26822.28	689.00	541.97	431.74	818.83	305.29
6	36303.30	34704.14	33353.49	32358.41	31169.02	67.22	43.38	725.70	17.08	499.64
8	43609.20	40795.54	39289.86	36827.83	35601.87	1613.68	803.91	302.22	1017.92	70.41
10	47476.24	44717.27	44690.36	42675.99	41097.80	602.31	1706.55	221.31	541.78	512.69
12	51508.71	54648.57	49714.71	49638.47	44651.82	2465.17	3958.40	1698.24	1132.80	2355.23
14	55048.97	52329.95	50806.89	48527.97	52077.17	731.80	13222.31	11593.04	5317.03	1711.44
16	49608.98	53912.87	58153.04	54863.87	51360.34	11691.15	16586.69	19482.06	8520.07	8792.23
18	56398.36	53316.69	49074.07	56497.15	49844.43	26849.56	20529.61	12670.45	21075.92	10956.67
20	50868.18	52191.43	55603.81	52837.29	51776.95	26397.35	25171.37	25661.41	22702.34	20311.62
22	50961.60	51156.06	51152.20	52307.44	53443.83	31114.34	29165.41	27338.37	25018.46	24384.08
24	50036.76	50804.65	51927.80	52348.69	52537.57	35360.96	33359.55	30882.90	29823.67	29132.83
26	48978.66	49111.81	51034.66	51081.95	52259.46	39036.58	37426.89	36166.46	34179.83	32825.11
28	48088.41	49181.98	53810.10	50690.40	52588.20	51433.86	35632.17	35970.55	37671.49	36950.33
30	46764.71	58153.48	55357.76	49839.77	50559.57	51130.77	49347.55	42232.37	38564.46	39149.85
32	49730.54	52605.28	58020.31	61600.66	58908.98	52945.32	52305.93	49162.20	52342.71	44145.93
34	38491.56	49939.77	47920.42	50947.40	53099.20	65764.73	60329.84	50869.63	52191.05	46956.44
35	44411.50	53523.37	43531.45	59936.56	59849.73	61971.70	64675.69	66503.62	57163.30	57498.33

Table 24-2D rudder performance calculation at +0.7 R lower section (stb side with cruise speed)

Rudder Angle (Deg)	Lift Force					Drag Force				
	EXISTING	RATIO A	RATIO B	RATIO C	RATIO D	EXISTING	RATIO A	RATIO B	RATIO C	RATIO D
0	11255.26	11255.26	11255.26	11255.26	11255.26	3854.05	3854.05	3854.05	3854.05	3854.05
2	3345.12	2168.21	1151.51	184.64	403.39	3473.04	3678.73	3809.04	3876.96	3921.11
4	18720.41	16133.55	14533.66	12905.90	11547.50	850.05	1311.87	1821.99	2252.61	2478.00
6	33320.35	30270.44	27505.18	25119.25	23236.17	1412.06	1208.44	672.28	86.19	343.05
8	45799.69	42517.80	38913.80	36519.66	34478.14	1659.48	1802.92	1697.34	965.94	831.69
10	55528.16	51891.51	48932.03	46634.24	43699.03	50.51	263.15	1245.29	1006.72	901.15
12	59622.11	57569.23	55321.42	53562.74	51260.41	2837.56	1391.56	612.49	916.50	551.36
14	62369.34	59808.64	57831.74	57157.71	55721.15	5686.66	3719.10	2471.91	2183.78	2383.67
16	65563.40	63759.23	61129.25	58499.74	56904.86	8084.30	8214.73	5532.94	5702.37	4199.43
18	69545.16	63286.04	61949.89	61213.37	60129.92	12740.92	9054.25	8270.14	7490.38	7354.20
20	65369.05	67533.90	64607.60	62946.36	62290.13	14130.66	13339.20	11450.38	10785.17	9663.29
22	63038.23	66983.10	61586.86	64479.14	62781.57	16542.09	16859.65	12129.81	12364.01	12224.17
24	62486.74	62984.29	61996.14	59792.08	63098.64	17050.34	15287.52	14156.28	12003.65	12531.73
26	65380.61	64112.29	59501.94	62781.69	58293.84	18779.40	17634.59	16332.61	12762.06	11597.03
28	64687.37	62523.28	59635.03	59564.53	58397.15	20034.75	19405.17	15646.70	15588.30	12973.41
30	59536.03	65526.10	62589.94	59348.16	58699.99	18821.64	7898.87	16907.72	15597.89	14291.74
32	54122.00	57478.95	58868.52	60272.59	59705.73	17337.40	15393.74	14176.92	14374.32	12806.64
34	50887.83	50049.99	56830.01	56493.64	57823.96	17646.43	13330.79	13459.05	10480.87	11042.65
35	49535.20	50813.27	61914.58	52691.46	57765.78	23295.12	15095.86	10186.77	27468.23	13740.81

Table 25-Turbulnce model comparison study

k -epsilon							
Rudder Angle	**Continuity**	**X-momentum**	**Y-momentum**	**Tke**	**Tdr**	**Drag Monitor**	**Lift Monitor**
0	4.72E-03	2.95E-02	6.34E-03	3.21E-02	1.82E-02	-6.13E+02	-2.11E+04
5	1.73E-03	5.93E-03	1.61E-03	2.06E-03	2.27E-03	-9.58E+02	-3.76E+04
10	7.30E-03	2.21E-02	7.72E-03	4.72E-02	1.55E-02	-1.46E+03	-4.31E+04
15	1.44E-02	6.69E-02	2.45E-02	2.92E-01	4.35E-02	-2.03E+03	-4.19E+04
20	2.21E-02	9.95E-02	4.80E-02	5.46E-01	1.03E-01	-2.83E+03	-4.12E+04
25	4.34E-01	7.51E-01	3.42E-01	3.69E+00	1.49E+00	-5.63E+03	3.25E+03
k-omega							
Rudder Angle	**Continuity**	**X-momentum**	**Y-momentum**	**Tke**	**Tdr**	**Drag Monitor**	**Lift Monitor**
0	2.36E-04	1.48E-03	1.31E-03	1.06E-02	1.18E-05	-6.18E+02	-1.87E+04
5	4.74E-03	2.04E-02	1.72E-02	2.04E-01	1.33E-04	-1.16E+03	-3.44E+04
10	9.61E-04	3.01E-03	2.63E-03	3.94E-02	1.87E-05	-1.70E+03	-3.43E+04
15	1.46E-02	6.56E-02	5.58E-02	1.25E+00	3.52E-04	-2.38E+03	-3.77E+04
20	5.70E-02	2.26E-01	2.00E-01	4.85E+00	1.19E-03	-4.74E+03	-3.90E+04
25	4.04E-01	6.60E-01	7.50E-01	1.38E+01	4.33E-03	-4.87E+03	2.23E+03
spalart almaras							
Rudder Angle	**Continuity**	**X-momentum**	**Y-momentum**	**Sa_nut**	**Drag Monitor**	**Lift Monitor**	
0	3.80E-03	2.63E-02	2.60E-02	8.40E+02	-4.97E+02	-1.96E+04	
5	1.69E-03	8.22E-03	6.98E-03	4.40E+02	-7.98E+02	-4.15E+04	
10	1.44E-03	4.40E-03	3.65E-03	2.69E+02	-8.62E+02	-5.11E+04	
15	4.37E-01	7.06E-01	6.96E-01	9.29E+04	-3.39E+03	1.92E+03	
25	4.85E-01	6.68E-01	8.54E-01	1.37E+05	-2.57E+03	3.47E+02	

RST Turbulent model										
Rudder Angle	**Continuity**	**X-momentum**	**Y-momentum**	**Tdr**	**uu-stress**	**vv-stress**	**ww-stress**	**uv-stress**	**Drag Monitor**	**Lift Monitor**
0	8.45E-04	1.36E-03	1.27E-03	1.93E-03	3.08E-02	1.30E-02	1.18E-02	6.96E-01	-6.29E+02	-2.29E+04
5	5.86E-04	1.28E-03	1.14E-03	2.81E-03	4.21E-02	2.42E-02	1.87E-02	8.62E-01	-8.47E+02	-3.78E+04

10	5.95E-04	1.12E-03	8.71E-04	3.64E-03	5.11E-02	2.71E-02	1.92E-02	1.09E+00	-1.19E+03	-4.57E+04
15	1.60E-02	7.80E-02	7.06E-02	1.97E-01	2.83E+00	2.02E+00	1.74E+00	4.68E+01	-1.73E+03	-4.47E+04
20	4.46E-02	1.74E-01	1.85E-01	3.18E-01	4.72E+00	3.35E+00	2.68E+00	9.10E+01	-2.27E+03	-4.71E+04
25	4.45E-01	7.69E-01	8.72E-01	1.93E+00	2.00E+01	1.18E+01	1.05E+01	3.98E+02	-4.72E+03	2.05E+03

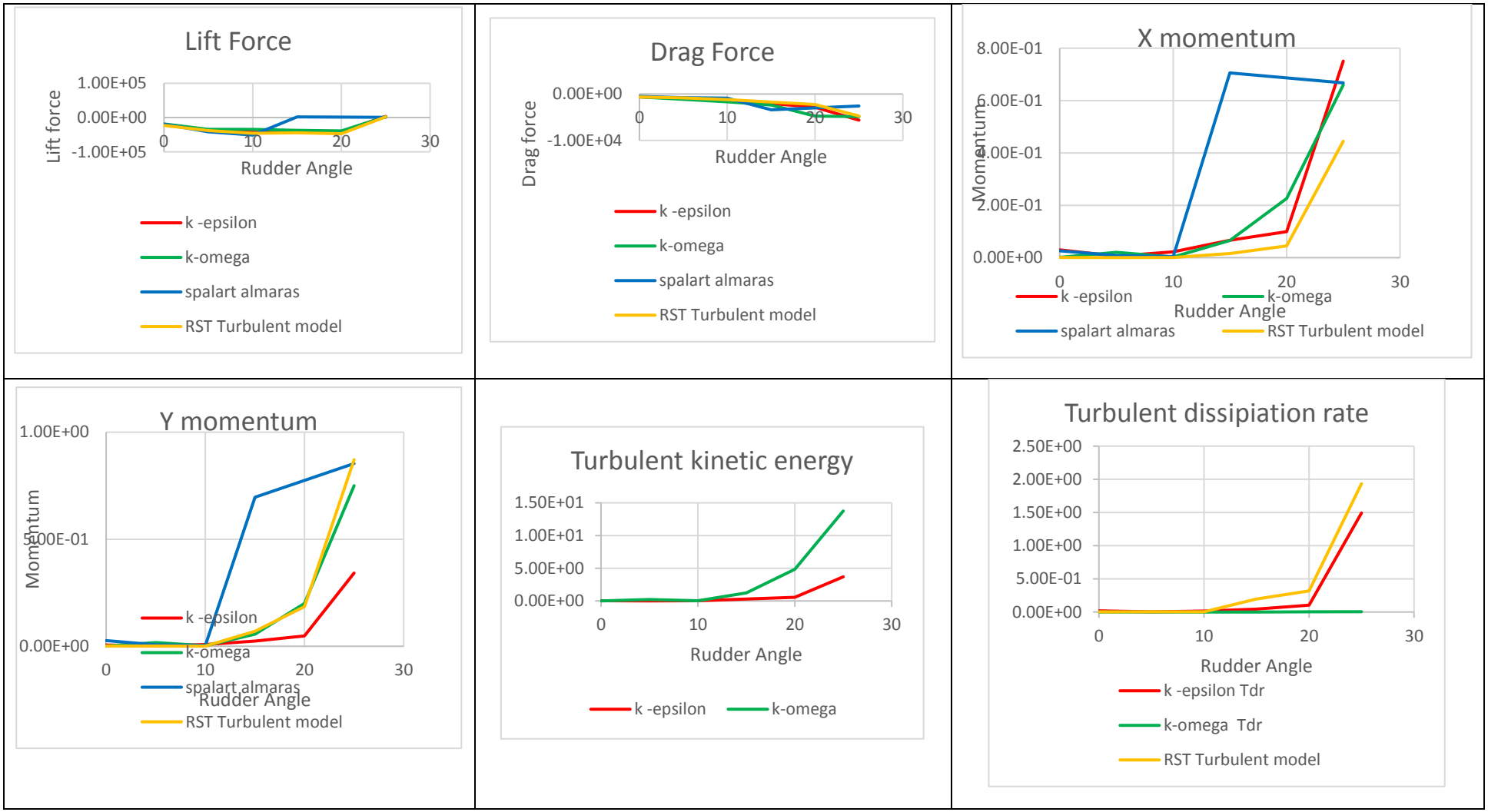

Figure 79-Turbulence models comparison

Table 26-3D CFD result for New geometries

Rudder Angle	Symmetric rudder			Symmeric rudder without bulb			Twisted blended Rudder			Twisted holding plate rudder		
	Torque	Drag	Lift	Torque	Drag	Lift	Torque	Drag	Lift	Torque	Drag	Lift
-35	-4.06E+05	-4.08E+05	5.81E+05	-2.30E+05	-3.85E+05	5.16E+05	-1.87E+05	-4.14E+05	4.89E+05	-1.70E+05	-4.19E+05	4.82E+05
-30	-4.26E+05	-3.50E+05	5.94E+05	-3.35E+05	-3.18E+05	5.60E+05	-2.44E+05	-3.29E+05	4.62E+05	-2.20E+05	-3.34E+05	4.56E+05
-25	-4.20E+05	-2.93E+05	5.85E+05	-6.93E+05	-3.04E+05	8.70E+05	-2.68E+05	-2.70E+05	4.64E+05	-2.33E+05	-2.80E+05	4.65E+05
-20	-6.90E+05	-2.41E+05	7.56E+05	-6.36E+05	-2.19E+05	7.79E+05	-3.35E+05	-2.05E+05	4.76E+05	-3.57E+05	-2.11E+05	4.89E+05
-19	-6.78E+05	-2.20E+05	7.28E+05	-6.18E+05	-2.01E+05	7.50E+05	-3.42E+05	-1.91E+05	4.66E+05	-4.50E+05	-1.93E+05	5.28E+05
-18	-6.57E+05	-2.00E+05	6.96E+05	-5.96E+05	-1.85E+05	7.18E+05	-6.52E+05	-1.82E+05	7.07E+05	-4.42E+05	-1.80E+05	5.08E+05
-17	-6.33E+05	-1.81E+05	6.61E+05	-5.79E+05	-1.67E+05	6.87E+05	-6.30E+05	-1.66E+05	6.73E+05	-4.38E+05	-1.67E+05	4.95E+05
-16	-6.37E+05	-1.52E+05	6.24E+05	-5.61E+05	-1.50E+05	6.51E+05	-6.08E+05	-1.51E+05	6.43E+05	-4.43E+05	-1.54E+05	4.88E+05
-15	-6.12E+05	-1.38E+05	5.95E+05	-5.40E+05	-1.34E+05	6.14E+05	-5.84E+05	-1.36E+05	6.07E+05	-5.01E+05	-1.46E+05	5.56E+05
-10	-4.89E+05	-7.16E+04	4.11E+05	-4.30E+05	-6.69E+04	4.04E+05	-4.67E+05	-7.19E+04	4.06E+05	-4.58E+05	-7.36E+04	3.90E+05
-5	-3.40E+05	-2.98E+04	1.69E+05	-3.11E+05	-2.81E+04	1.67E+05	-3.43E+05	-3.17E+04	1.76E+05	-3.53E+05	-3.26E+04	1.80E+05
0	-1.51E+05	-1.99E+04	-4.29E+04	-1.48E+05	-1.84E+04	-4.11E+04	-1.90E+05	-2.16E+04	-3.58E+04	-1.97E+05	-2.25E+04	-2.54E+04
5	9.29E+04	-3.59E+04	-2.00E+05	6.93E+04	-3.25E+04	-1.92E+05	1.49E+04	-3.67E+04	-2.05E+05	9.60E+03	-3.65E+04	-1.88E+05
10	2.55E+05	-8.74E+04	-4.05E+05	1.96E+05	-7.79E+04	-3.82E+05	1.33E+05	-8.55E+04	-4.04E+05	1.17E+05	-8.59E+04	-3.94E+05
15	3.80E+05	-1.70E+05	-5.72E+05	3.10E+05	-1.55E+05	-5.83E+05	2.34E+05	-1.55E+05	-5.73E+05	1.62E+05	-1.59E+05	-5.32E+05
20	4.84E+05	-2.71E+05	-7.15E+05	4.27E+05	-2.52E+05	-7.62E+05	3.46E+05	-2.60E+05	-7.66E+05	2.23E+05	-2.72E+05	-6.84E+05
25	5.75E+05	-3.99E+05	-8.60E+05	5.10E+05	-3.76E+05	-8.76E+05	4.03E+05	-3.88E+05	-8.76E+05	3.57E+05	-3.78E+05	-8.33E+05
30	6.44E+05	-5.42E+05	-9.75E+05	4.67E+05	-4.80E+05	-8.75E+05	2.22E+05	-4.75E+05	-7.75E+05	2.36E+05	-4.50E+05	-7.44E+05
35	5.05E+05	-6.13E+05	-8.69E+05	3.28E+05	-5.34E+05	-7.52E+05	1.90E+05	-5.17E+05	-7.01E+05	2.09E+05	-5.21E+05	-7.20E+05

Table 27-Hull force and turning moment at different water depth and drift angles

Drift angle	Radius/Lpp	water depth 20.5 m				water depth = vessel length			
beta	R/L=	Hull-FX	Hull-FY	Hull-FZ	Hull-MZ	Hull-FX	Hull-FY	Hull-FZ	Hull-MZ
0	100	-509748	12578	30935150	-4845155	-404467	7987	6996818	-3865096
5	100	-576341	1710887	35571057	376350721	-425638	562409	8028794	129013043
10	100	-600592	5858862	48112715	855380727	-449319	1607172	10762088	258231648
0	10	-514718	115062	31149078	-51573193	-408216	142966	7079785	-48168794
5	10	-714249	1784112	36129652	281688503	-457854	707163	8064177	73731086
10	10	-924573	5820177	50169701	636791610	-521517	1683496	10857608	178075282
0	5	-529010	182913	31907630	-136107644	-421142	307928	7342711	-114392375
5	5	-873833	2201179	37089763	187162763	-496134	926777	8267036	15435744
10	5	-1280301	6033988	52521876	418431629	-597287	1867338	11089283	94758975
0	5	-529010	182913	31907630	-136107644	-421142	307928	7342711	-114392375
0	10	-514718	115062	31149078	-51573193	-408216	142966	7079785	-48168794
0	100	-509748	12578	30935150	-4845155	-404467	7987	6996818	-3865096